Dynamics close to Bifurcations: From Spins to Granular Media

Inaugural-Dissertation
zur Erlangung des Doktorgrades
der Mathematischen-Naturwissenschaftlichen
Fakultät
der Universität zu Köln

vorgelegt von

Koray Önder

aus Lohne (Oldb)

Köln, 2019

Berichterstatter: -apl. Prof. Dr. Ralf Bulla

(Gutachter) :   -Prof. Dr. Matthias Sperl

Tag der mündlichen Prüfung: 20. September 2019

Ich widme diese Arbeit meinen Eltern
Leyla Önder und Mustafa Önder

Kurzfassung

Die meisten Flüssigkeiten erstarren beim Abkühlen zu einem geordneten und kristallinen Festkörper. Diese Festkörper weisen eine langreichweitige Ordnung auf, die mit Streuexperimenten gemessen werden kann. Im Gegensatz dazu erstarren die sogenannten Glasbildner in einen amorphen Festkörper, welcher keine langreichweitige Ordnung besitzt und sich in Streuexperimenten nicht von einer Flüssigkeit unterscheidet. Mit der Modenkopplungstheorie werden solche Flüssig-Glas Übergänge mit Hilfe von Dichtekorrelatoren erklärt. Die Bewegungsgleichungen der Dichtekorrelatoren weisen für lange Zeiten eine Bifurkation auf. Die Modenkopplung beschreibt mit diesen Bifurkationen die Dynamik von glasbildenden Systemen.

Solche Bifurkationen erscheinen in verschiedensten Systemen wie z.B. in granularen Medien oder in Spin-Modellen. Das Ziel dieser Arbeit ist die Analyse solcher Bifurkationen in verschiedensten Systemen und die Anwendung der Modenkopplungstheorie, um die Dynamik solcher Systeme zu erklären. Dazu wird unter anderem für den Glasübergang in dissipativen granularen Medien mit Hilfe der Modenkopplungstheorie eine geschlossene Bewegungsgleichung hergeleitet. Auch in sogenannten Spin-Modellen mit eingeschränkter Dynamik (kinetically constraint models), wo die Dynamik hauptsächlich von der Nachbarschaft eines Spins bestimmt ist, treten Übergänge von einem ergodischen Zustand in einen nicht-ergodischen auf. Solche Übergänge sind mit dem Flüssig-Glas Übergang gleichzusetzen und generieren ebenfalls eine Bifurkation, die in dieser Arbeit mit der Modenkopplungstheorie untersucht wird. Hier wird die mit der Modenkopplung hergeleitete Dynamik mit Simulationen verglichen.

Abstract

Most liquids solidify into an ordered crystalline solid during cooling. These solids have a long-range order which can be measured by scattering experiments. In contrast, the so-called glass formers solidify into an amorphous solid, which does not have a long-range order and does not differ from a liquid in scattering experiments. Mode coupling theory is used to explain such liquid-glass transitions using density correlators. The equations of motion of the density correlators show a bifurcation in the long time limit. Mode coupling uses these bifurcations to describe the dynamics of glass-forming systems.

Such bifurcations appear in various systems such as granular media or spin models. The aim of this thesis is to analyze bifurcations in different systems and to apply mode coupling theory to explain the dynamics of such systems. For the glass transition in dissipative granular media a closed equation of motion is derived with the help of the mode coupling theory. Also in kinetically constraint spin models, where the dynamics are mainly determined by the neighborhood of a spin, transitions from an ergodic state to non-ergodic one occur. Such transitions can be identified with the liquid-glass transition and also generate a bifurcation, which is investigated in this thesis with the mode coupling theory. Here, the dynamics derived from mode coupling theory are compared with simulations.

Contents

Part I
Introduction

1 Motivation

The liquid-solid transition for crystals is well understood. Since a crystal solid has long-range order, one obtains Bragg peaks in scattering experiments. In liquids the structure factor is not sharp, so that the transition from a liquid to a solid state can be measured from the static structure factor. But not all solids are crystals, with the most prominent example being glasses. The physics behind glassy systems differs, to handle glassy systems we first need a definition for a glass. In simple words and from a physical point of view a glass is an amorphous solid. It can sustain static shear stress, that is why we call them solids, but they do not have a spatial long-range order so they are amorphous and not crystalline solids. If one only considers the static structure, it is not clear whether the system is in a liquid or a glass state.

Since the static structure of glasses and liquids is similar, one needs dynamical measurements to see the different nature of normal liquids and glass-forming liquids, which are showing nontrivial behavior over many orders of magnitude in time. Therefore, we will use dynamical variables to study the liquid-glass transition. An effective way to analyze the dynamics is to use correlation functions. The theoretical framework of correlation functions is well established, there are a lot of simulations around correlation functions for different systems, and one can also measure them in experiments, e.g., dynamic lightscattering. In a liquid, where we use density autocorrelation functions, the correlation function decays exponentially to zero. Here the relaxation time depends sensitively on the control parameters and changes by orders of magnitude in time when the system gets close to the transition point. At the liquid-glass transition the relaxation time diverges which is an indication for an arrested system.

We will use the mode-coupling theory (MCT) for ideal glass transitions to capture the glassy dynamics [1–3]. Mode-coupling theory deals with density-autocorrelation functions, $\Phi_{\vec{q}}(t) = \langle \rho_{\vec{q}}^*(t) \rho_{\vec{q}}(0) \rangle$, here $\vec{q}$ denotes the wave vector, and describes its slow dynamics close to the transition. The long time limit, $t \to \infty$, of $\Phi_{\vec{q}}(t)$ is an indicator for the state of the system. In a liquid, the autocorrelation function of the density fluctuations will vanish independent of the wave vector, $\Phi_{\vec{q}}^{\text{Liq}}(t \to \infty) = 0$. In contrast to the liquid state, the autocorrelation function in the glassy state converges to a finite value, $\Phi_{\vec{q}}^{\text{Glass}}(t \to \infty) = f_q$, where f_q is the so-called glass form factor.

The equation of motion (EOM) for the density-autocorrelation function can be derived

within the Mori-Zwanzig formalism

$$\ddot{\Phi}_{\vec{q}}(t) + \nu_q \dot{\Phi}_{\vec{q}}(t) + \Omega_q^2 \Phi_{\vec{q}}(t) + \Omega_q^2 \int_0^t \mathrm{d}\tau\, m_{\vec{q}}(t-\tau) \dot{\Phi}_{\vec{q}}(\tau) = 0 \ ,$$

where ν_q is the characteristic frequency and Ω_q is the microscopic frequency of the system. Because of the memory kernel, $m_q(t)$, the EOM is not closed. In mode-coupling theory the memory kernel is approximated as a function of the density autocorrelation functions, $m_q(t) = \mathcal{F}_q[\Phi_k(t)]$, and within this approximation the equation of motion for $t \to \infty$ yields a bifurcation equation.

In this thesis, the bifurcations will be classified according to Arnol'd [4]. The simplest singularity is the fold bifurcation, where the long time limit changes discontinuously by a smooth variation of only one control parameter. This sensitive dependence on a control parameter and the drastic change of the long time limit can be identified with the liquid-glass transition, where the long time limit of $\Phi(t)$ goes from zero, in the liquid state, to a finite value, in the glass state.

To simplify the memory kernel the so-called schematic mode-coupling theory will be used. The memory kernel will be expressed as a polynomial of the autocorrelation function. With an asymptotic expansion of the equation of motion near the glass transition one gets an analytical expression to describe the two step decay with power laws [5]. One can thus calculate the exponents of the two step decay for a given memory kernel. Schematic MCT can be used to match the exponents to some experimental or simulation data in order to describe a microscopic theory with simple analytical models and predict the liquid-glass transitions.

An ergodic to non-ergodic transition is also obtained in some spin models [6, 7]. In 1975, Edwards and Anderson introduced the so-called Edwards-Anderson parameter, q_{EA}, which gives the long time limit of the spin-autocorrelation function. For $q_{EA} \neq 0$ there are, induced by couplings between the spins, some frozen spin clusters. A frozen spin can not be flipped, which leads to the system being in a non ergodic state, like the glassy state. On the other hand, for $q_{EA} = 0$, there are no frozen spins and all the spins can be flipped, just like in paramagnets, and the system is in a ergodic state.

In contrast to the spin models with interactions between the spins there are kinetically constrained spin models. In such models the dynamics depends on the neighborhood of a spin. A spin can be flipped, if the spin has at least more than f down-spin neighbors.

Starting in non-equilibrium with an initial up-spin concentration and a non vanishing temperature $T \neq 0$, the system relaxes to equilibrium. When the initial up-spin concentration of such models is high enough, there will be some up-spin clusters in the ground state of the system, otherwise all the up-spins will be flipped to down-spins. Such models thus also have an ergodic to non-ergodic transition.

The aim of this thesis is to describe different systems with an ergodic to non-ergodic transition through the use of a memory kernel. It is divided into two parts, the introduction part and the application part. The first part will introduce theoretical aspects which will be relevant later. I structured the first part into three sections:

In the first section I will motivate the mode-coupling theory and I will derive the basic formulas. Starting from the correlation function I will derive the equation of motion and discuss it for different systems, e.g., Newtonian or Brownian. After introducing the mode-coupling approximation and getting the bifurcation equation, I will perform the asymptotic expansion and discuss the different timescales of the correlation function. This section will be finished after introducing the schematic mode-coupling theory and a brief summary.

The second section is about glass transitions in granular media. Starting with the collision rules in dissipative systems I introduce the Liouville dynamic which is relevant for describing the microscopic dynamics of granular media. Here, we use the hard core potential to get the Liouville operators for elastic and inelastic hard sphere systems. With the explicit expression of the Liouville operators the memory kernel for granular media will be calculated and the glass-liquid transition will be discussed. A generalization of the memory kernel to binary mixtures will be presented.

The third section is about the Fredrickson-Andersen model (FA), which is a kinetically constrained lattice model. I will show that the FA-model on the Bethe lattice exhibits a bifurcation scenario, which I will identify with the mode-coupling bifurcations. With those bifurcations the dynamics of the model will be generated and the power laws of the decays will be calculated. I will also introduce a microscopic derivation of the spin model, where all the variables, like system frequency and transition probability, will be computed.

The second part of the thesis is the application part where I will use the theory which I derived in the first part and use it for different applications. In the first section of the second part I will talk about the Fredrickson-Andersen model, and here I will compare

the theoretically calculated dynamics with simulations done by Sellitto [8]. In the last
two sections I will talk about schematic mode-coupling theory and its applications. In
the second section of the second part, I compare schematic MCT with hard sphere
data and try to match the microscopic model to a simple schematic model. In the last
section I fit the simulation data for the FA model with schematic MCT, and compare
the results with the theoretically calculated model.

2   Mode Coupling Theory

The main result of mode coupling theory (MCT) is the description of the glass-transition as a dynamic ergodic to non-ergodic transition. In liquids the particles can move nearly without any restrictions, the density fluctuations become uncorrelated for long times, which means that the system is in an ergodic state. In contrast to that, in glassy systems, the particles are arrested in a cage formed by their neighbors: This is called the cage-effect. Consequently, the density correlations are tending for long times to a finite value, f, and the system reaches a non-ergodic state.

The MCT deals with density autocorrelation functions, whose long time limit are the non-ergodicity parameters, f, which are a kind of order parameter, which does not depend on any free energy function. It vanishes for liquid systems and goes to a finite value in the glassy state.

We use the Mori-Zwanzig (MZ) formalism to get an exact equation for the density correlation function. Here projection operators will be introduced to separate the variables of interest from all the other variables and to derive the equation of motion (EOM).

Within the MZ-formalism a memory kernel, $m(t)$, appears in the EOM. Since the memory kernel is not known exactly one can not find an exact solution for the density correlation function. The mode coupling approximation (MCA) will be used to factorize the memory kernel in terms of the correlation function of the density fluctuations. With this approximation the Mori-Zwanzig derived EOM is not exact anymore but solvable for a given MCT kernel.

In the microscopic regime the time evolution of the density autocorrelation function is dominated by a power law, the critical decay, to a plateau. For glassy system the correlation function stays at the plateau for a diverging time scale. For liquids the correlation function has a second decay, following the von Schweidler law, from the plateau to zero.

The long-time limit of the EOM generates a bifurcation equation. With such bifurcations the MCT connects the critical decay with an exponent a and the von Schweidler decay with an exponent b.

These bifurcation equations for glassy systems are a function of the non-ergodicity

parameter, f, and the memory kernel:

$$\frac{f}{1-f} = m[f] \ .$$

Within the mode coupling approximation the memory kernel is a bilinear function of the density correlation function, so the equation above is an algebraic one and the bifurcations can be identified as glass-transition singularities.

A detailed derivation of the MCT is given in [9], this chapter just gives a general overview of the mode coupling theory.

2.2 Observables of the System

To describe the macroscopic behavior of a system with N particles in a volume V, we introduce two observables, the particle density $\rho(\vec{r})$ and the current density $\vec{j}(\vec{r})$:

$$\rho(\vec{r}) = \frac{1}{\sqrt{N}} \sum_{j=1}^{N} \delta(\vec{r} - \vec{r}_j) \qquad \underline{\mathbf{FT}} \quad \rho(\vec{q}) = \frac{1}{\sqrt{N}} \sum_{j=1}^{N} e^{i\vec{q}\cdot\vec{r}_j} \ , \qquad (2.2.1)$$

$$\vec{j}(\vec{r}) = \frac{1}{\sqrt{N}} \sum_{j=1}^{N} \vec{v}_j \delta(\vec{r} - \vec{r}_j) \quad \underline{\mathbf{FT}} \quad \vec{j}(\vec{q}) = \frac{1}{\sqrt{N}} \sum_{j=1}^{N} \vec{v}_j e^{i\vec{q}\cdot\vec{r}_j} \ . \qquad (2.2.2)$$

Here, the $\sqrt{N}$ is the normalization and $\mathbf{FT}$ is the Fourier transformation with $\mathbf{FT}[f(\vec{r})](\vec{q}) = \int f(\vec{r}) e^{-i\vec{q}\vec{r}} \mathrm{d}^D r$.

The current $\vec{j}(\vec{q})$ can be split into a longitudinal part $j^{\mathrm{L}}(\vec{q}) = \hat{e}_{\vec{q}}\vec{j}(\vec{q})$, where $\hat{e}_{\vec{q}} = \vec{q}/q$ is the unit vector parallel to $\vec{q}$, and a transverse part $j^{\mathrm{T}}(\vec{q}) = \hat{e}_{\vec{q}}^{\mathrm{T}}\vec{j}(\vec{q})$, where $\hat{e}_{\vec{q}}^{\mathrm{T}}$ is the unit vector perpendicular to $\vec{q}$. In contrast to the transverse current $j^{\mathrm{T}}(\vec{q})$, the longitudinal part $j^{\mathrm{L}}(\vec{q})$ couples to the density fluctuation. This can be shown with the time derivative of the density which is proportional to the longitudinal current, $\dot{\rho}(q) = qj^{\mathrm{L}}(\vec{q})$.

The time evolution of an observable, A, is given by the Liouville equation

$$\frac{\partial A(t)}{\partial t} = i\mathcal{L}A(t) \quad \Rightarrow \quad A(t) = A(0)\, e^{-i\mathcal{L}t} \ , \qquad (2.2.3)$$

with the Liouville operator $\mathcal{L}$:

$$\mathcal{L} = -i \sum_l \left(\frac{\partial H}{\partial \vec{p}_l} \frac{\partial}{\partial \vec{r}_l} - \frac{\partial H}{\partial \vec{r}_l} \frac{\partial}{\partial \vec{p}_l} \right) = \{H, \cdot\} \; , \tag{2.2.4}$$

here H is the Hamiltonian of the system, $\vec{p}$ the momentum and $\{.,.\}$ are the Poisson brackets. The Liouville operator applied to the observables yields

$$\mathcal{L}\rho(\vec{q},t) = qj^{\mathrm{L}}(\vec{q},t) \; , \tag{2.2.5}$$

$$\mathcal{L}j^{\mathrm{L}}(\vec{q},t) = -\hat{e}_{\vec{q}} \sum_j \dot{\vec{v}}_j(t) \mathrm{e}^{i\vec{q}\vec{r}_j(t)} + q \sum_j \vec{v}_j^2(t) \mathrm{e}^{i\vec{q}\vec{r}_j(t)} \; . \tag{2.2.6}$$

In MCT the EOM will be expressed in terms of density fluctuations, which are given by correlation functions. An advantage of correlation functions is that one can determine them experimentally. To describe such correlations mathematically, we introduce canonical averages, $\langle \bullet \rangle$, and define on the space of fluctuating dynamical variables the so-called Kubo scalar product

$$\langle A | B \rangle := \langle \delta A^* \delta B \rangle \; , \tag{2.2.7}$$

where we define $\delta A = A - \langle A \rangle$ and the star denotes the complex conjugation.

With these averages we introduce for describing the dynamical structure of liquids the density-autocorrelation function $F(q,t) = \langle \rho(\vec{q},0) | \rho(\vec{q},t) \rangle$. For static structures one also introduces the structure factor $S(q) = \langle \rho(\vec{q}) | \rho(\vec{q}) \rangle$, which can be calculated from the interaction potential.

The correlation functions will be normalized by the static structure factor to normalized density-autocorrelation functions [1]

$$\phi(q,t) = \frac{\langle \rho(\vec{q},0) | \rho(\vec{q},t) \rangle}{\langle \rho(\vec{q}) | \rho(\vec{q}) \rangle} \; . \tag{2.2.8}$$

2.3   Mori-Zwanzig Formalism

As we know from Eq. (2.2.5), $\dot{\rho}(\vec{q},t) = qj^{\mathrm{L}}(\vec{q},t)$, the change of the density $\rho(\vec{q},t)$ decreases for $\vec{q} \to 0$ and gets conserved at $\vec{q} = 0$.

We introduce here the so-called Mori-Zwanzig projector $\mathcal{P}$ to separate the slow modes,

$q \to 0$, and the fast modes, so we get an exact reformulation of the Liouville equation [10–12]. We also introduce the orthogonal projector $\mathcal{Q} = 1 - \mathcal{P}$ for the fast modes. Note, the significant identities $\mathcal{P}^2 = \mathcal{P}$, $\mathcal{P}^\dagger = \mathcal{P}$, $\mathcal{Q}^2 = \mathcal{Q}$, $\mathcal{Q}^\dagger = \mathcal{Q}$ and $\mathcal{Q}\mathcal{P} = \mathcal{P}\mathcal{Q} = 0$. Since we are interested in the glass transition, which can be described with the densities and currents, we define the projector $\mathcal{P}$ as

$$\mathcal{P} := |\rho(\vec{q})\rangle \langle \rho(\vec{q})|\rho(\vec{q})\rangle^{-1} \langle \rho(\vec{q})| + |j^{\mathrm{L}}(\vec{q})\rangle \langle j^{\mathrm{L}}(\vec{q})|j^{\mathrm{L}}(\vec{q})\rangle^{-1} \langle j^{\mathrm{L}}(\vec{q})| \ , \tag{2.3.1}$$

with the static structure factor $\langle \rho(\vec{q})|\rho(\vec{q})\rangle = S(q)$ and the velocity $\langle j^{\mathrm{L}}(\vec{q})|j^{\mathrm{L}}(\vec{q})\rangle = v_0^2$, $v_0 = \sqrt{k_{\mathrm{B}}T/m}$, as normalization.

With the Laplace transformation $\mathbf{LT}[f(t)](z) = i \int_0^\infty f(t)\mathrm{e}^{izt}\mathrm{d}t$ one can rewrite the density-autocorrelation function as

$$\langle \phi(\vec{q},0)|\mathrm{e}^{-i\mathcal{L}t}|\phi(\vec{q},0)\rangle \quad \underrightarrow{\mathbf{LT}} \quad \langle \phi(\vec{q},0)|(z - \mathcal{L})^{-1}|\phi(\vec{q},0)\rangle \ . \tag{2.3.2}$$

From appendix A we know

$$\mathcal{P}\frac{1}{z - \mathcal{L}}\mathcal{P} = \left[z - \mathcal{P}\mathcal{L}\mathcal{P} - \mathcal{P}\mathcal{L}\mathcal{Q}(z - \mathcal{Q}\mathcal{L}\mathcal{Q})^{-1}\mathcal{Q}\mathcal{L}\mathcal{P}\right]^{-1} \ . \tag{2.3.3}$$

With the state vector, $|a\rangle = S(q)^{-1/2}|\rho(\vec{q})\rangle + (m/k_{\mathrm{B}}T)^{-1/2}|j^{\mathrm{L}}(\vec{q})\rangle$, the correlation matrix reads

$$\underline{\underline{\Phi}}(q,z)^{-1} = \langle a|z - \mathcal{P}\mathcal{L}\mathcal{P} - \mathcal{P}\mathcal{L}\mathcal{Q}(z - \mathcal{Q}\mathcal{L}\mathcal{Q})^{-1}\mathcal{Q}\mathcal{L}\mathcal{P}|a\rangle \ , \tag{2.3.4}$$

$$= \begin{pmatrix} z & -\Omega_{\rho j}(q)[1 + L(q)] \\ -\Omega_{j\rho}(q) & z - \Omega_{jj}(q) - M(q) \end{pmatrix} ,$$

with the frequencies $\Omega_{\rho\rho}(q) \propto \langle \rho(\vec{q})|\mathcal{L}|\rho(\vec{q})\rangle = 0$, $\Omega_{\rho j}(q) \propto \langle \rho(\vec{q})|\mathcal{L}|j^{\mathrm{L}}(\vec{q})\rangle$, $\Omega_{j\rho}(q) \propto \langle j^{\mathrm{L}}(\vec{q})|\mathcal{L}|\rho(\vec{q})\rangle$ and $\Omega_{jj}(q) \propto \langle j^{\mathrm{L}}(\vec{q})|\mathcal{L}|j^{\mathrm{L}}(\vec{q})\rangle := i\nu(\vec{q})$ and the two memory functions

$$M(q,z) = \frac{m}{k_{\mathrm{B}}T} \langle j^{\mathrm{L}}(\vec{q})|\mathcal{L}\mathcal{Q}(z - \mathcal{Q}\mathcal{L}\mathcal{Q})^{-1}\mathcal{Q}\mathcal{L}|j^{\mathrm{L}}(\vec{q})\rangle \ , \tag{2.3.5}$$

$$L(q,z) = \frac{\langle \rho(\vec{q})|\mathcal{L}\mathcal{Q}(z - \mathcal{Q}\mathcal{L}\mathcal{Q})^{-1}\mathcal{Q}\mathcal{L}|j^{\mathrm{L}}(\vec{q})\rangle}{\langle \rho(\vec{q})|\mathcal{L}|j^{\mathrm{L}}(\vec{q})\rangle} \ . \tag{2.3.6}$$

The Matrix $\underline{\underline{\Phi}}(q,z)$ therefore is:

$$\underline{\underline{\Phi}}(q,z) = \frac{1}{z(z-\Omega_{jj}(q)-M(q))-\Omega^2[1+L(q)]} \begin{pmatrix} z-\Omega_{jj}(q)-M(q) & \Omega_{\rho j}(q)[1+L(q)] \\ \Omega_{j\rho}(q) & z \end{pmatrix} \; .$$

The density-autocorrelation function is given as a matrix element

$$\phi(q) = \frac{1}{z - \frac{\Omega(q)^2[1+L(q)]}{z-i\nu(q)-M(q)}} \; . \tag{2.3.7}$$

Note that $\mathcal{QL}\,|\rho(\vec{q})\rangle = q(1-\mathcal{P})\,|j^{\mathrm{L}}(\vec{q})\rangle = 0$ so the memory function $L(q)$ vanishes in equilibrium and the frequencies $\Omega_{\rho j}(q) = \Omega_{j\rho}(q) = qv_0/\sqrt{S(q)}$ are equal.

2.4   Mode Coupling Approximation

The Eq. (2.3.7) can be written in the time domain as

$$\ddot{\phi}(q,t) + \nu(q)\dot{\phi}(q,t) + \Omega(q)^2\phi(q,t)$$
$$+ \Omega(q)^2 \int_0^t \mathrm{d}\tau\, m(q,t-\tau)\dot{\phi}(q,\tau)$$
$$+ \Omega(q)^2 \int_0^t \mathrm{d}\tau\, L(q,t-\tau)\phi(q,\tau) = 0 \; , \tag{2.4.1}$$

with the memory kernel $m(q,t) = M(q,t)/\Omega(q)^2$ and the initial conditions $\phi(q,0)=1$ and $\dot{\phi}(q,0)=0$. One can show that Eq. (2.4.1) has exactly one analytical solution with these conditions [13].

The Eq. (2.4.1) is exact but useless since we do not know the memory kernels. Here the memory kernel $M(q,t) \propto \langle \vec{F}(\vec{q})^\dagger|\mathrm{e}^{it\mathcal{QLC}}|\vec{F}(\vec{q})\rangle$ is a correlation function of forces driven by the projected operator $\mathcal{QLQ}$.

The idea behind the mode coupling approximation (MCA) is to connect the memory kernels with the density relaxations. Therefore we define a second projection operator

$$\mathcal{P}^{\mathrm{MCT}} = \sum_{\vec{k}<\vec{p}} |\rho(\vec{k})\rho(\vec{p})\rangle \, \langle\rho(\vec{k})\rho(\vec{p})|\rho(\vec{k})\rho(\vec{p})\rangle^{-1} \, \langle\rho(\vec{k})\rho(\vec{p})| \tag{2.4.2}$$

and get

$$
\begin{aligned}
M(q,t)^{\mathrm{MCT}} &= \frac{m}{k_{\mathrm{B}}T} \langle j^{\mathrm{L}}(\vec{q})|\mathcal{L}\mathcal{Q}\mathcal{P}^{\mathrm{MCT}}\mathrm{e}^{-i\mathcal{Q}\mathcal{L}\mathcal{Q}t}\mathcal{P}^{\mathrm{MCT}}\mathcal{Q}\mathcal{L}|j^{\mathrm{L}}(\vec{q})\rangle \\
&= \sum_{\vec{k}<\vec{p}} \frac{m}{k_{\mathrm{B}}T}\mathcal{V}(\vec{q},\vec{k},\vec{p}) \langle \rho(\vec{k})\rho(\vec{p})|\mathrm{e}^{-i\mathcal{Q}\mathcal{L}\mathcal{Q}t}|\rho(\vec{k})\rho(\vec{p})\rangle \, \mathcal{W}(\vec{q},\vec{k},\vec{p}) \\
&\approx \sum_{\vec{k}<\vec{p}} \frac{m}{k_{\mathrm{B}}T}\mathcal{V}(\vec{q},\vec{k},\vec{p}) \langle \rho(\vec{k})|\mathrm{e}^{-i\mathcal{Q}\mathcal{L}\mathcal{Q}t}|\rho(\vec{k})\rangle \, \rho(\vec{k}) \, \langle \rho(\vec{p})|\mathrm{e}^{-i\mathcal{Q}\mathcal{L}\mathcal{Q}t}|\rho(\vec{p})\rangle \, \mathcal{W}(\vec{q},\vec{k},\vec{p}) \\
&= \sum_{\vec{k}<\vec{p}} \frac{m}{k_{\mathrm{B}}T}\mathcal{V}(\vec{q},\vec{k},\vec{p})\phi(k,t)\phi(p,t)\mathcal{W}(\vec{q},\vec{k},\vec{p}) \;,
\end{aligned}
\tag{2.4.3}
$$

with the vertices defined as $\mathcal{V}(\vec{q},\vec{k},\vec{p}) = \langle j^{\mathrm{L}}(\vec{q})|\mathcal{L}\mathcal{Q}\rho(\vec{k})\rho(\vec{p})\rangle S(k)^{-1}$ and $\mathcal{W}(\vec{q},\vec{k},\vec{p}) = \langle \rho(\vec{k})\rho(\vec{p})|\mathcal{Q}\mathcal{L}j^{\mathrm{L}}(\vec{q})\rangle S(p)^{-1}$, which are equal in equilibrium. From the literature [14] the left vertex is known analytically

$$
\mathcal{V}(\vec{q},\vec{k},\vec{p}) = \frac{m}{k_{\mathrm{B}}T}\delta_{\vec{q},\vec{k}+\vec{p}} \left[(\hat{q}\cdot\vec{k})S(p) + (\hat{q}\cdot\vec{p})S(k) - qS^{(3)}(\vec{k},\vec{p})S(q)^{-1} \right] S(k)^{-1} \;. \tag{2.4.4}
$$

With the convolution approximation [15] $S^{(3)}(\vec{k},\vec{p}) \approx S(\vec{q})S(\vec{k})S(\vec{p})$ and the direct correlation function, $c(\vec{q})$, which is related to the structure factor in the Ornstein-Zernike relation [11], one can rewrite the vertex to

$$
\mathcal{V}(\vec{q},\vec{k},\vec{p}) = \frac{m}{k_{\mathrm{B}}T}n\delta_{\vec{q},\vec{k}+\vec{p}} \left[(\hat{q}\cdot\vec{k})c(k) + (\hat{q}\cdot\vec{p})c(p) \right] S(p) \;, \tag{2.4.5}
$$

where $n = N/V$ is the particle density. Barrat et al. [14] show that the convolution approximation does not affect much the MCT results. For hard spheres the change in the critical point is only 2%.

The second memory kernel $L(q,t) \approx \frac{m}{qk_{\mathrm{B}}T}\sum_{\vec{k}>\vec{p}}\mathcal{U}(\vec{q},\vec{k},\vec{p})\mathcal{W}(\vec{q},\vec{k},\vec{p})\phi(k,t)\phi(p,t)$ vanishes because of the vertex $\mathcal{U}(\vec{q},\vec{k},\vec{p}) = \langle \rho(\vec{q})|\mathcal{L}\mathcal{Q}\rho(\vec{k})\rho(\vec{p})\rangle S(k)^{-1} = 0$ due to parity.

Since real systems are not monodisperse, the EOM will be be derived for polydisperse systems, too. In the simplest case, which is the binary mixture, all the physical quantities will be decorated with greek indices for the species, e.g., the structure factor $S(q)$ which is a scalar in monodisperse systems becomes a matrix $S_{\alpha\beta}(q)$. The particles differ in their masses and diameter, in general they can differ in more quantities like temperature. The different species have a different concentration, $x_\alpha = N_\alpha/N$, where

α denotes the species. The calculation for binary mixture is more involved, so the longitudinal current correlation, which is in monodisperse case the thermal velocity, is now given by $\langle j_\alpha^{\mathrm{L}}(\vec{q}) | j_\beta^{\mathrm{L}}(\vec{q}) \rangle = \delta_{\alpha\beta} x_\alpha v_\alpha^2$.

In appendix B the calculation of the memory kernel via the MCA for binary mixtures is shown.

2.5   The Density Correlation Function $\phi(t)$

The EOM in equilibrium is a closed integro-differential equation of the form

$$\ddot{\phi}(q,t) + \nu(q)\dot{\phi}(q,t) + \Omega(q)^2\phi(q,t) + \Omega(q)^2 \int_0^t m(q,t-\tau)\dot{\phi}(q,\tau)\mathrm{d}\tau = 0 \ . \qquad (2.5.1)$$

At this point two special cases should be introduced:

- **Brownian Equation of Motion** [16, 17]

  For colloids, where the particle have momentum transfers with the solvent, one can ignore, for timescales which are larger than the microscopic timescale of the solvent, the inertia term and Eq. (2.4.1) becomes

  $$\tau(q)\dot{\phi}(q,t) + \phi(q,t) + \int_0^t m(q,t-\tau)\dot{\phi}(q,\tau)\mathrm{d}\tau = 0 \ . \qquad (2.5.2)$$

  Here we only need the condition $\phi(q,0) = 1$ and we further define a microscopic time scale $\tau(q) = S(q)/(D_0 q^2)$, with the short-time diffusion D_0.

  Note that the dynamics of Eq. (2.5.2) has no hydrodynamic interaction [18].

- **Newtonian Equation of Motion** [1, 2]

  In contrast to the Brownian EOM we introduce here the Newtonian EOM, where the inertia term gets relevant and we rewrite the Eq. (2.4.1) to

  $$\ddot{\phi}(q,t) + \Omega(q)^2\phi(q,t) + \Omega(q)^2 \int_0^t m(q,t-\tau)\dot{\phi}(q,\tau)\mathrm{d}\tau = 0 \ . \qquad (2.5.3)$$

  Notice, the inertia term produces some oscillations for small time scales, therefore it is also called the oscillating dynamics.

To determine if the system goes into a liquid regime, or if it is in an arrested glassy state, we introduce the glass-form factor f_q, which is the long-time limit of the correlation function

$$\phi(q, t \to \infty) = \begin{cases} 0, & \text{for a liquid ,} \\ 0 < f_q \leq 1, & \text{for a glass .} \end{cases} \tag{2.5.4}$$

In literature one finds several names for f_q such as Debye-Waller factor and Edwards-Anderson order parameter [14]. From a physical point of view, the system relaxes to a liquid state if the density correlations vanishes. This means that the particle can escape the surrounding cage, which means $f_q = 0$. When the correlations do not vanish but reach a finite value, $f_q \neq 0$ the particles are arrested in the cage made by the surrounding particles, the system is then in the glass state.

For the long-time limit, where the correlation function changes slowly, one can neglect the first derivative of the correlation function in the EOM. For the MCA we also assume that the memory kernel is a bilinear function of the correlation functions, $m(q, t) = \mathcal{F}_q[\mathbf{V}, \phi(k, t)]$ [1]. It can be shown that the EOM yields to the so-called bifurcation equation

$$\frac{f_q}{1 - f_q} = \mathcal{F}_q[\mathbf{V}, f_k] \; . \tag{2.5.5}$$

The bifurcation equation (2.5.5) may have more than one solution, $\tilde{f}_q$, but with the maximum property [2] one can show that the glass form factor f_q is given by

$$\tilde{f}_q \leq f_q \; , \qquad \text{for all } q. \tag{2.5.6}$$

One can see, that f_q is independent of the microscopic details and only depends on the coupling parameters $\mathbf{V}$, the vertices. Of special interest is the glass form factor, f_q^c, at the singularity, which is given by the critical coupling parameter $\mathbf{V}^c$. At that point a discontinuous jump occurs in the $(f, \mathbf{V})$-plane.

2.6   Asymptotic Expansion

As already explained in the section above, the MCA assumes that the memory kernel can be expanded as a polynomial of $\phi(t)$. For long times, $t \to \infty$, respectively, $z \to 0$ in the Laplace domain, the frequencies are $|(z + i\nu(q))/\Omega(q)^2| \ll |\text{LT}[\mathcal{F}_q[\mathbf{V}, \phi(k,t)]](z)|$ negligible, so Eq. (2.3.7) is [3]

$$\frac{\phi(q,z)}{1 + z\phi(q,z)} = \text{LT}[\mathcal{F}_q[\mathbf{V}, \phi(k,t)]](z) \ . \tag{2.6.1}$$

Notice, Eq. (2.6.1) is scale invariant in time, so with a solution $\phi(q,t)$ the function $\phi^y(q,t) = \phi(q, t/y)$ is also a solution.

To eliminate the non-ergodicity pole, f^c, we introduce the master function $G(t)$ for the analysis of the glass state according to

$$\phi(q,t) = f_q^c + G(q,t) \qquad \text{or} \qquad z\phi(q,z) = -f_q^c + zG(q,z) \ . \tag{2.6.2}$$

For $G(t)$ we know that $|zG(t)|$ is small for $z \to 0$ so we can assume $|zG(t)/1-f^c| \ll 1$. In addition to that, $G(t)^{n+1}$ decreases faster than $G(t)^n$ so the ratio is also small for $z \to 0$.

With both assumptions above we can expand Eq. (2.6.1) in terms of $G(t)$ [2]

$$\begin{aligned}
-\frac{\delta_0}{z} &+ \delta_1 G(z) \\
&+ (1 + \delta_2)\text{LT}[G(t)^2](z) + zG(z)^2 \\
&+ (1 + \delta_3)\text{LT}[G(t)^3](z) + \gamma_3 z^2 G(z)^3 \\
&+ (1 + \delta_4)\text{LT}[G(t)^4](z) + \gamma_4 z^3 G(z)^4 \\
&+ \dots = 0 \ .
\end{aligned} \tag{2.6.3}$$

with

$$\delta_k = \frac{\partial^k \Delta\mathcal{F}_q}{\partial f^k} \frac{(1-f)^3}{k!} \qquad \text{and} \qquad \gamma_k = \frac{1}{(1-f)^{k-2}} \ , \tag{2.6.4}$$

and $\Delta\mathcal{F}_q = f_q/(1 - f_q) - \mathcal{F}_q[\mathbf{V}, \phi(k,t)]$. A detailed derivation is found in appendix C, there we set $\phi(0) \neq 1$ which is relevant for section 5.

2.6.1 Bifurcation Singularities

The only solution in the liquid state of the bifurcation equation is $f_q = 0$ and a non zero value for glassy systems. With model dependent coupling parameters, $\mathbf{V}$, such as temperature and particle density one can change from a liquid to a glassy state. So the non-ergodicity parameter jumps discontinuously at the critical point from zero to a finite value. The phenomenon in which the solution of $\Delta \mathcal{F}_q$, which is a function of f, does no longer depends smoothly on the parameter but changes dramatically is called a bifurcation.

In this thesis we will use the definition of V.I. Arnol'd to classify bifurcations [4, 19, 20]. In this sense we introduce A_l-Singularities with

$$A_l: \qquad \left.\frac{\partial^k \Delta \mathcal{F}[\mathbf{V}, f]}{\partial f^k}\right|_{f=f^c} = 0 \quad \text{for } k < l \ ,$$

$$\left.\frac{\partial^k \Delta \mathcal{F}[\mathbf{V}, f]}{\partial f^k}\right|_{f=f^c} \neq 0 \quad \text{for } k = l \ . \qquad (2.6.5)$$

Notice, we use q-independent variables to simplify the problem. A q-dependent derivation can be found in [21]. For an A_2-singularity at the critical point, also called Whitney fold singularity, Eq. (2.6.3) can be written as

$$\begin{aligned}
&\lambda \mathrm{LT}[G(t)^2](z) + zG(z)^2 \\
&+ (1 + \delta_3)\mathrm{LT}[G(t)^3](z) + \gamma_3 z^2 G(z)^3 \\
&+ (1 + \delta_4)\mathrm{LT}[G(t)^4](z) + \gamma_4 z^3 G(z)^4 \\
&+ ... = 0 \ ,
\end{aligned} \qquad (2.6.6)$$

with $\lambda = 1 + \delta_2^c$.

Further works on higher order singularities and glass-glass transitions can be found in [22–26]. Since we are analyzing the glass-liquid transition we are mainly interested into the A_2-Singularities. The leading order contribution is dominated by the first line of Eq. (2.6.6). In general we get

$$\lambda \mathrm{LT}[G(t)^2](z) + zG(z)^2 = \frac{\sigma}{z} \ . \qquad (2.6.7)$$

Here, $\delta_0 = \sigma$ is the distance parameter, which give us the information how far we are from the critical point. For $\sigma = 0$, Eq. (2.6.7) can be solved with the ansatz $G_0(t) \propto t^{-a}$. The prefactor λ has to fulfill the condition

$$\lambda = \frac{\Gamma(1-a)^2}{\Gamma(1-2a)} \ , \tag{2.6.8}$$

for $0 < a < 1/2$ with the Euler Gamma-function Γ.

Furthermore, for non vanishing σ, the correlator $G_0(t)$ remains the same. The distance parameter σ merely enters as a rescaled time $\hat{t} = t/t_\sigma$, where t_σ is the plateau crossing time. So we have [3]

$$G_\sigma(\hat{t}) = c_\sigma g_\pm(\hat{t}) \ , \qquad c_\sigma = \sqrt{|\sigma|} \ , \qquad t_\sigma = t_0 |\sigma|^{-\frac{1}{2a}} \ . \tag{2.6.9}$$

Here $g_\pm(\hat{t})$ is the master function which is independent of σ but depends only on λ and is the solution of

$$\mp \hat{z}^{-1} + \lambda \mathrm{LT}[g_\pm(\hat{t})^2] + \hat{z} g_\pm(\hat{z})^2 = 0 \ . \tag{2.6.10}$$

At the critical point, $\sigma \to 0$, the prefactor c_σ vanishes and the plateau crossing time, t_σ, diverges. So the time is scaled to $G_0(\hat{t}) \propto (t/t_0)^{-a}$, where t_0 is the microscopic time scale.

On the glass side, $\sigma > 0$, in order to get an expression for the glass form factor, $f \neq f^c$, we introduce $\delta f = f - f^c$ as a solution for the long-time limit of Eq. (2.6.7)

$$\delta f^2 = \frac{\sigma}{1-\lambda} \qquad \Rightarrow \qquad f = f^c + \sqrt{\frac{|\sigma|}{1-\lambda}} \ . \tag{2.6.11}$$

So the correlator on the glass side is [3]

$$g_+(\hat{t}) = \frac{1}{\sqrt{1-\lambda}} + 2\sqrt{1-\lambda} g(\hat{t}) \ , \tag{2.6.12}$$

where $g(\hat{t})$ fulfills the following equation

$$-g(\hat{z}) + \lambda \mathrm{LT}[g(\hat{t})^2](\hat{z}) + \hat{z} g(\hat{z})^2 = 0 \ . \tag{2.6.13}$$

On the liquid side, for negative σ, there is a decay away from the plateau, which is governed by the von Schweidler law $g_-(\hat{t}) \propto -\hat{t}^b$, with $0 < b \leq 1$. The exponent b can also be expressed via λ

$$\lambda = \frac{\Gamma(1+b)^2}{\Gamma(1+2a)} \ . \tag{2.6.14}$$

For the so-called α relaxation process [2, 17], where the correlation function has an asymptotic relaxation to zero $\phi(t \to 0)$, the correlation function at leading order can be written as

$$\phi(\tilde{t}) = f^c - h\,\tilde{t}^b \ , \tag{2.6.15}$$

with the time scale $\tilde{t} = t/t_{\sigma'}$, $t_{\sigma'} \propto |\sigma|^{-\gamma}$ and $\gamma = 1/(2a) + 1/(2b)$ and the amplitude h. In Fig. 2.6.1 one can see the dynamic of the correlation function for a liquid and glass.
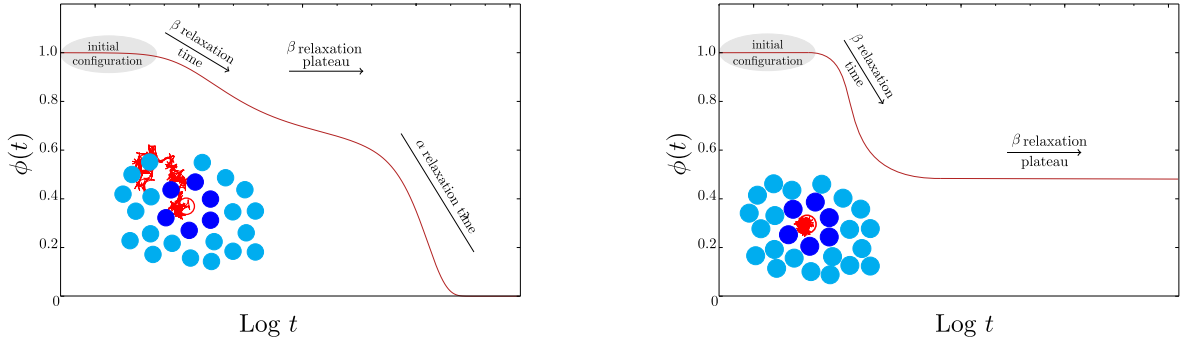
Figure 2.6.1: *Left:* The correlation function $\phi(t)$ decays for a liquid to zero. The decay to the plateau can be described by the critical law $g(t) \propto \hat{t}^{-a}$ and the decay from the plateau with the von Schweidler law $g(\tilde{t}) \propto -\tilde{t}^b$. *Right:* One can see the critical decay to the plateau and a non vanishing value for $\phi(t \to \infty)$ [27].

2.6.2   Schematic Models

Next to the general MCT, where we set the memory function to a functional of a bilinear polynomial, there is a so-called schematic MCT. Here the memory function is a

sum of different powers of the correlation function $\phi(t)$

$$\mathcal{F}[\mathbf{V}, \phi(t)] = \sum_n v_n \phi(t)^n \ . \tag{2.6.16}$$

For long times, when the correlation function becomes the non-ergodicity parameter, we put the schematic memory kernel into the bifurcation equation (2.5.5)

$$\frac{f}{1-f} = \sum_n v_n f^n \ . \tag{2.6.17}$$

For different kinds of schematic kernels one can solve this equation, where the critical point can be calculated exactly. The simplest model, $F_1 = v_1 f$, is a trivial one. For $F_2 = v_2 f^2$ a bifurcation occurs and will therefore be calculated here in detail to get an intuition. From the bifurcation equation we directly get

$$\frac{f}{1-f} = v_2 f^2 \quad \Rightarrow \quad f_\pm = \frac{1}{2} \left(1 \pm \sqrt{\frac{v_2 - 4}{v_2}} \right) \ , \tag{2.6.18}$$

with the critical values $(f^c, v_2^c) = (1/2, 4)$. The solution can be seen in Fig. 2.6.2. One can see that the solution jumps at the critical point, which is a feature of the bifurcation. From the maximum theorem, Eq. (2.5.6), the solution is unambiguous, f_+. Now the exponent parameter can be calculated

$$\lambda = 1 + (1 - f^c)^3 \left. \frac{\partial^2 \Delta \mathcal{F}[v_2, f]}{\partial f^2} \right|_{f=f^c, v_2=v_2^c} = \frac{1}{2} \ . \tag{2.6.19}$$

With $\lambda = 1/2$ there is no stretching for α relaxation and therefore the model is not realistic to describe glassy systems [1, 28].

We need one more parameter to vary the exponent parameter, therefore the two parameter model $F_{12} = v_1 f + v_2 f^2$ is the simplest case of interest. In this model an A_2 singularity occurs and we can generate the dynamics of the system via Eq. (2.6.6). One can find this model in several works [5, 29, 30]. In [31] the F_{12}-model is discussed in connection with the Pott's model.
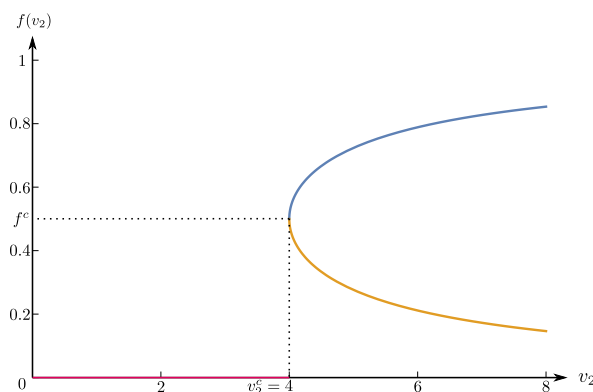
Figure 2.6.2: The non-ergodicity parameter as a function of the control parameter v_2. For $v_2 < 4$ the non-ergodicity parameter is always zero (red line on the x-axis), which means that the system is in the liquid state. At the critical point $(f^c, v_2^c) = (1/2, 4)$ there is a discontinuous jump from zero to the critical value, f^c, which is a common behavior of bifurcations. For $v_2 > 4$ there are two different paths, which also can be seen in Eq. (2.6.18). With the maximum theorem the blue line, f_+, describes the glassy state.

In analogy to the calculation of the F_2-model, we also start with the bifurcation equation $f^c/(1 - f^c) = v_1 f^c + v_2 f^{c2}$. In addition we also use the derivative with respect to f, $1/(1 - f^c)^2 = v_1 + 2v_2 f^c$ as a second condition and get for the control parameters $v_1^c = (1 - 2f^c)/(1 - f^c)^2$ and $v_2 = 1/(1 - f^c)^2$. For this model the exponent parameter is not given as a single number anymore but is given by $\lambda = 1 - f^c$. Rewriting the control parameter as a function of λ one gets

$$v_1^c = \frac{2\lambda - 1}{\lambda^2} \quad \text{and} \quad v_2^c = \frac{1}{\lambda^2} \; . \tag{2.6.20}$$

By plotting v_1 as a function of v_2, one can see the liquid-glass transition line shown in Fig. 2.6.3. In contrast to the F_2-model, the exponent parameter varies between 1 and $\frac{1}{2}$.

One can find higher order singularities like an A_3-singularity in the $F_{13} = v_1 f + v_3 f^3$ model which is discussed in [32] and an A_4-singularity which occurs for the $F_{123} = v_1 f + v_2 f^2 + v_3 f^3$ model. A technical approach to the higher order singularities one can find in [26].

The one component model can be extended into more component models like the
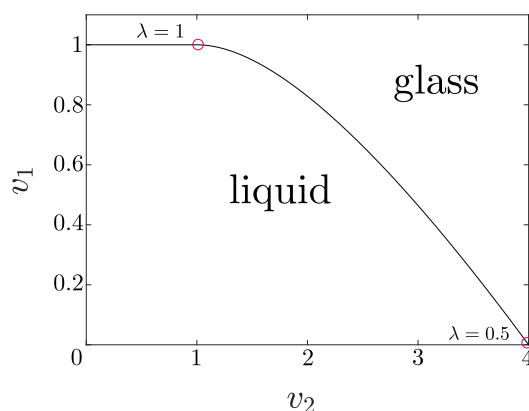
Figure 2.6.3: The (v_1, v_2)-plane with the liquid-glass transition line. Along the line the non-ergodicity parameter has its critical value, which is given by the control parameter, and the exponent parameter, λ, can be calculated exactly. Under the transition line the system is in the liquid state, while above the transition line a glassy state dominates. The interval $v_2 \in \{0, 1\}$, where $v_1 = 1$, is constant is the so-called Type-A line.

Bosse-Krieger model where you have two correlators, $\phi_1(t)$ and $\phi_2(t)$ [33] :

$$m_1 = v_1 \phi_1(t)^2 + v_2 \phi_2(t)^2 \; ,$$
$$m_2 = v_3 \phi_1(t) \phi_2(t) \; , \tag{2.6.21}$$

with the control parameters $v_n \geq 0$. In the Bosse-Krieger model a swallowtail-bifurcation in Arnold's definition appears. In the F_{12}- and F_{13}-model it is difficult to handle high exponent parameters close to unity since a type-A line occurs. The advantage of the Bosse-Krieger model is, that here a type-B line appears, which depends on f_1. Since all parameters can be calculated analytically one can fit all the parameters of microscopic systems with the parameters of the schematic model to compare theoretical accuracy [34].

Conclusion

The starting point for describing liquids and glassy systems is the normalized density autocorrelation function, $\phi_q(t)$. Within the Mori-Zwanzig formalism one derives the equation of motion for $\phi_q(t)$, which is exact. In the equation of motion a memory kernel,

$m_q(t)$, occurs as a part of a convolution and since the memory kernel is not known the equation is not closed. Here, I outlined the mode coupling approximation that expresses the memory kernel as a bilinear functional of the density autocorrelation function. In subsequent chapters I am going to apply the mode coupling approximation to close equations of motion and to make them amenable to numerical solutions. In general this kind of approximation can be used for a variety of systems with Brownian or Newtonian dynamics like hard sphere systems, or some stochastic dynamics like some spin models. In early works E. Frey and F. Schwabel used the mode coupling theory to describe the critical dynamics of ferromagnets [35].

In this thesis I will use mode coupling theory to describe the glass transition in dissipative systems like granular matter, and for the Fredrickson-Andersen model, which is a lattice model for glassy dynamics.

In these sections I am going to introduce extensions of mode coupling theory: For the hard sphere system I will fix the parameters of schematic mode coupling models to reproduce the essential features of a fully microscopic solution. For the Fredrickson-Andersen model the memory kernel is known exactly in the limit $t \to \infty$ and I am going to propose a mode coupling like extension to finite times.

3   Microscopic Dynamics of Granular Matter

With a simple view on sand one can see all the difficulties of describing the interactions of granular particles. The grains are not spherical, each of them has a different irregular shape. Because of some off-center collisions, the particles rotate and dissipate different amounts of energy. Nevertheless, granular systems are deterministic, one can describe their dynamics with mechanical collisions of the particles and the effect of external forces. Notice, the free streaming of the particles also affects the dynamics.

Now, we have to make some assumptions, which are justified for ideal systems of granular matter:

- All the particles are spherical, so that they are described by their masses, m, and their radii, a.

- The dissipation of the particles is equal and given by the coefficient of restitution, $\epsilon \in [0, 1]$ [36]. The coefficient of restitution can expressed as:

$$\epsilon = \left| \frac{\hat{r}_{12} \cdot \vec{v}'_{12}}{\hat{r}_{12} \cdot \vec{v}_{12}} \right| \tag{3.0.1}$$

  where $\vec{v}_{12} = \vec{v}_1 - \vec{v}_2$ is the relative velocity, $\hat{r}_{12} = \vec{r}_{12}/|\vec{r}_{12}|$ is the unit vector which specifies the geometry of the collision and the prime denotes the velocity after the collision.

In several studies [37–40] the effect of dissipation on granular media is shown. Systems with dissipation do not conserve the kinetic energy of the particles, which breaks the time reversal symmetry and renders the system out of equilibrium. With the restitution coefficient one can control the dissipativity of the system, so for $\epsilon = 1$, the elastic limit, the kinetic energy is fully conserved and for $\epsilon = 0$, the particles lose their kinetic energy fully. A discussion on whether the coefficient of restitution can describe granular dynamics with dissipation can be found in [41].

With the rules of momentum conservation and the kinetic energy of the particle before and after the collision, with respect to ϵ, one expresses the postcollisional velocities as

a function of the precollisional ones [41]

$$\vec{v}_1' = \vec{v}_1 - \frac{m_2}{m_1 + m_2}(1 + \epsilon)(\vec{v}_{12} \cdot \hat{r}_{12})\hat{r}_{12} \ , \tag{3.0.2}$$

$$\vec{v}_2' = \vec{v}_1 + \frac{m_1}{m_1 + m_2}(1 + \epsilon)(\vec{v}_{12} \cdot \hat{r}_{12})\hat{r}_{12} \ . \tag{3.0.3}$$

For rough spheres one has to extend Eq. (3.0.2) with the tangential restitution, which describes the surface roughness [42].

One can define, in analogy to the temperature of a molecular gas, the granular kinetic temperature, $T = m \langle v^2 \rangle / D$, where D is the dimension, as a function of the average square of the particle velocities. In dissipative systems, where the kinetic energy reduces after a collision, a free cooling of a granular system can be observed. For a system which remains homogeneous this effect is called the homogeneous cooling state [41]. The time evolution of the temperature with an initial temperature, T_0, is given by Haff's law [36]

$$T(t) = \frac{T_0}{(1 + {}^t/_{\tau_0})^2} \ , \tag{3.0.4}$$

where $\tau_0 \propto D/(1 - \epsilon^2)$ is the relaxation time scale for measuring the time as the number of collisions.

3.1   Microscopic Dynamics

The particles' interaction is deterministic, the postcollisional velocities of the particles are given by the precollisional ones, which is shown above. For most of those systems one can introduce a Hamiltonian to get the equation of motion. In general the Hamiltonian is defined by

$$H = \frac{\vec{p}^2}{2m} + \frac{1}{2}\sum_{i<j}^{N} V(\vec{q}) \ , \tag{3.1.1}$$

with the positions $\vec{q} = (\vec{r}_1, ..., \vec{r}_N)$, the momenta $\vec{p} = (\vec{p}_1, ..., \vec{p}_N)$ of a system with N interacting particles, and the interacting potential V.

A point in the phase space, Γ, is now given by the pair $(\vec{q}, \vec{p})$. With the interaction potential, $V(\vec{q}) = \sum_{i<j} V(|\vec{r}_i - \vec{r}_j|)$, the dynamics is given by the Hamilton equations

$\dot{\vec{q}} = \partial H/\partial \vec{p}$ and $\dot{\vec{p}} = -\partial H/\partial \vec{q}$, uniquely.

In section 2.2 we introduce the Liouville operator $\mathcal{L}$ for the time evolution of the microscopic variables. With Eq. (2.2.4) and the Hamiltonian one can write the Liouville-operator as

$$i\hat{\mathcal{L}} = i\hat{\mathcal{L}}_0 + \sum_{i<j} i\hat{\mathcal{L}}'_{ij}$$
$$= \vec{v} \cdot \frac{\partial}{\partial \vec{r}} - \frac{1}{m} \sum_{i<j} \frac{\partial V(\vec{r}_{ij})}{\partial \vec{r}_{ij}} \cdot \left(\frac{\partial}{\partial \vec{v}_i} - \frac{\partial}{\partial \vec{v}_j} \right) \ . \tag{3.1.2}$$

An ensemble average $\langle A \rangle$ for a time t should be introduced as an average over the distribution ρ at time $t = 0$

$$\langle A \rangle = \int \mathrm{d}\Gamma \rho(\Gamma, 0) A(\Gamma, t) \ . \tag{3.1.3}$$

In analogy to quantum mechanics, we can transfer the time evolution from the Heisenberg representation to the Schrödinger representation whilst we introduce the adjoint operator $\bar{\mathcal{L}}$ [43]. So the Liouville equation for the distribution function is given by

$$\frac{\partial \rho(\Gamma, t)}{\partial t} = -i\bar{\mathcal{L}}\rho(\Gamma, t) \ . \tag{3.1.4}$$

The Eq. (3.1.4) is well defined but for most of the problems not useful since it can not be solved explicitly.

One tool to rewrite the distribution function is the BBGKY-hierarchy [11].

The full phase space probability density is unnecessarily detailed for the description of a system and only the behavior of a subset of particles is sufficient. So we integrate over the irrelevant parameters and introduce the reduced phase space distribution function

$$f_n(x_1, ..., x_n) = \frac{N!}{(N-n)!} \int \mathrm{d}x_{n+1}...\mathrm{d}x_N f_N(x_1, ..., x_N) \ . \tag{3.1.5}$$

With the definition of the Liouville operator and Eq. (3.1.4) one gets

$$\left(\frac{\partial}{\partial t} + \sum_{i=1}^{n} \vec{v}_i \frac{\partial}{\partial \vec{r}_i} \right) f_n + \sum_{i=1}^{n} \int \mathrm{d}x_{n+1} i\hat{\mathcal{L}}'_{i,n+1} f_{n+1} = 0 \ . \tag{3.1.6}$$

This identity is at the beginning not so useful, it expresses the unknown n-particle distribution function , f_n, in terms of the $(n+1)$-particle distribution function f_{n+1}. For $n = 1$ the single particle distribution, f_1, is a function of the two particle distribution f_2. Here we assume, that the one particle distribution depends less on the higher order functions of the hierarchy, and so we can truncate the hierarchy without severe restrictions.

Further assumptions are (i) the collision time τ_c is much smaller than the mean time τ between two collisions, which is realistic for systems with low density. So we are only interested in collisions of two particles but not more. (ii) We use the so-called molecular chaos assumption, which supposes that the correlation between two collisions is negligible. It lets us factorize the two particle distribution function with respect to the velocities. With these approximation, the Eq. (3.1.6) for $n = 1$ becomes the Boltzmann equation [11]

$$\left(\frac{\partial}{\partial t} - \vec{v}_1 \frac{\partial}{\partial \vec{v}_1}\right) f_1 = \int \mathrm{d}^d v_2 \int d\Omega \frac{\partial \sigma}{\partial \Omega} v_{12} \left[f_1(\vec{v}_1') f_1(\vec{v}_2') - f_1(\vec{v}_1) f_1(\vec{v}_2)\right] \qquad (3.1.7)$$

with the scattering cross section σ and the solid angle Ω. With the Boltzmann equation the hydrodynamic transport coefficients can be calculated [44]. In this thesis we will use the YBG-relation (Yvon-Born-Green) [45] as a special case of the BBGKY hierarchy. The YBG theorem for the pair correlation function $g(r)$ is given by

$$\nabla_1 g(\vec{r}_{12}) = -n\beta g(\vec{r}_{12})\nabla_1 V(\vec{r}_{12}) - n\beta \int \mathrm{d}r_3 g_3(\vec{r}_1, \vec{r}_2, \vec{r}_3)\nabla_1 V(\vec{r}_{13}) . \qquad (3.1.8)$$

The pair correlation function, $g(r)$, is defined as

$$g(r_{12}) = \frac{V^2}{Z} \int \mathrm{d}^3 r_3 ... \mathrm{d}^3 r_N \exp\left(-\beta \sum_{i<j} V(r_{ij})\right) , \qquad (3.1.9)$$

here $Z = \int \mathrm{d}^3 r_1 ... \mathrm{d}^3 r_N \exp\left(-\beta \sum_{i<j} V(r_{ij})\right)$ is the partition function and $\beta = 1/(k_\mathrm{B} T)$ the inverse temperature.

So with the YBG theorem we write the pair correlation function for two particles, $g_2(\vec{r}_1, \vec{r}_2)$, as a function of the triplet correlation function, $g_3(\vec{r}_1, \vec{r}_2, \vec{r}_3)$. A full derivation of the YBG-relation for binary systems is given in appendix E.

3.2   Hard Sphere Systems

Since the hard spheres have a simple potential, infinity at the contact point and zero elsewhere, we will use the hard sphere potential to approximate the interaction between granular media. First a we derive Liouville operator for the elastic case, where the energy is conserved, and after that we introduce the coefficient of restitution for dissipative systems, like the inelastic hard spheres.

3.2.1   Elastic Hard Spheres

The interaction potential V for hard sphere systems (HSS) is given by

$$V(r) = \begin{cases} 0 & \text{if } r > d \\ \infty & \text{if } r \leq d \,, \end{cases} \tag{3.2.1}$$

where d is the diameter of the sphere, so at contact the interaction potential diverges. So, for HSS the interaction part, $i\mathcal{L}'$, of the Liouville operator is not defined due the discontinuity. Nevertheless, the HSS is a deterministic system so that the velocities after the collision can be described by the collision rules, a propagator $U(t, t')$ must exist.

The free streaming, $U_0(t, 0) = \exp(it\mathcal{L}_0)$, is independent on external forces. For the hard core interaction we use the ansatz that we can write the instantaneous collisions as the following recursive equation [46, 47]

$$U(t, 0) = U_0(t, 0) + \sum_{kl} \int_0^t \mathrm{d}\tau U(t, \tau) i\mathcal{T}_{kl}^+ U_0(\tau, 0) \tag{3.2.2}$$

with the free streaming propagator $U_0(t, 0) = \mathrm{e}^{i\mathcal{L}_0 t}$ and the binary collision operator $i\mathcal{T}_{ij}^+$. Now, with expanding Eq. (3.2.2) to second order in time we get

$$\begin{aligned} U(t, 0) = {} & 1 + it\hat{\mathcal{L}}_0(0) - \frac{1}{2}t^2\hat{\mathcal{L}}_0^2(0) \\ & + \sum_{j<k} \int_0^t \mathrm{d}\tau [1 + i(t-\tau)\hat{\mathcal{L}}_0(\tau)]i\hat{\mathcal{T}}_{jk}^+(\tau)[1 + i\tau\hat{\mathcal{L}}_0(0)] \\ & + \sum_{j,k,l,m} \int_0^t \mathrm{d}\tau \int_\tau^t \mathrm{d}\tau' i\hat{\mathcal{T}}_{jk}^+(\tau')i\hat{\mathcal{T}}_{lm}^+(\tau) + \mathcal{O}(t^3) \,. \end{aligned} \tag{3.2.3}$$

From the expansion one can show the relation $\hat{\mathcal{L}}^2 \neq \hat{\mathcal{L}}\hat{\mathcal{L}}$ [48]. This relation is important to understand the propagator, $\mathrm{e}^{i\mathcal{L}t}$, as a modified product

$$\hat{\mathcal{L}}^2 = \hat{\mathcal{L}}_0^2 + \sum_{j<k}[\hat{\mathcal{L}}_0\hat{\mathcal{T}}_{jk}^+ + \hat{\mathcal{T}}_{jk}^+\hat{\mathcal{L}}_0] + \sum_{j,k,l,m}\hat{\mathcal{T}}_{jk}^+\hat{\mathcal{T}}_{lm}^+ , \qquad (3.2.4)$$

where the summations are only over all disjoint particles. Notice, the interaction operator $\mathcal{L}'$ is given by the collision operator, $\hat{\mathcal{T}}^+$, which can be used forward and backward in time, and is defined as [41]

$$i\hat{\mathcal{T}}_{kl}^{\pm} = -\Theta(\mp\hat{r}_{kl}\cdot\vec{v}_{kl})(\hat{r}_{kl}\cdot\vec{v}_{kl})\delta(\vec{r}_{kl}-d)(\hat{b}_{kl}^{\pm}-1) . \qquad (3.2.5)$$

Now, to understand the collision operator $\hat{\mathcal{T}}_{kl}^{\pm}$ we look at its components. The Heaviside function $\Theta(\hat{r}\cdot\vec{v})$ selects the direction of the velocity before the collision and the delta function $\delta(\vec{r}-d)$ assures that the collision takes place when two particle are in contact. The operator $\hat{b}^+$ implements the collision rules with $\hat{b}_{ij}^+f(v_1,...,v_i,v_j,...) = f(v_1,...,v_i',v_j',...)$, so that $(\hat{b}^+-1)$ gives the change of a variable x due to the collision. Since the elastic HSS is in thermal equilibrium, the hermitian Liouville operator is related to the time reversed operator and only differs in the direction of the time, which is given by the theta function, $\hat{\mathcal{L}}_{\pm}^{\dagger} = \hat{\mathcal{L}}_{\mp}$. The adjoint of the free streaming operator can be calculated with operator identities and is given by $i\hat{\mathcal{L}}_0^{\dagger} = i\hat{\mathcal{L}}_0 + \sum_{k<l}(\hat{r}_{kl}\cdot\vec{v}_{kl})\delta(r_{kl}-d)$. For HSS systems in general we assume that we can factorize the distribution function, $\rho(\Gamma)$, into a product of a velocity distribution function $\rho_v(\Gamma)$ and a spatial distribution function $\rho_r(\Gamma)$. For the velocity distribution function we assume a gaussian with $\rho_v(\vec{v}) \propto \mathrm{e}^{-\frac{m\vec{v}^2}{2k_{\mathrm{B}}T}}$. The spatial distribution function is a Boltzmann factor given by $\rho_r(\vec{r}) = \lim_{\beta V\to\infty}\mathrm{e}^{-\beta\sum_{k<l}\Theta(d-r_{kl})} = \prod_{k<l}\Theta(r_{kl}-d)$. so we have

$$\rho(\Gamma) \propto \prod_{k<l}\Theta(r_{kl}-d)\mathrm{e}^{-\frac{m\vec{v}^2}{2k_{\mathrm{B}}T}} . \qquad (3.2.6)$$

With the spatial distribution function, $\rho_r(\vec{r})$, we directly can calculate the YBG relation for HSS. As we know that $\nabla_1\exp(-\beta U(r_{1i})) = \hat{r}\delta(r_{1i}-d)$ the YBG relation is

$$\nabla_1 g(\vec{r}_1,\vec{r}_2) = \hat{r}_{12}\delta(\hat{r}_{12}-d)g_2(\vec{r}_1,\vec{r}_2) + n\int \mathrm{d}r_3\hat{r}_{13}\delta(\hat{r}_{13}-d)g_3(\vec{r}_1,\vec{r}_2,\vec{r}_3) . \qquad (3.2.7)$$

3.2.2   Inelastic Hard Spheres

For the dissipative inelastic HSS we also have a pseudo Liouville operator which is given by

$$i\hat{\mathcal{L}} = i\hat{\mathcal{L}}_0 + \sum_{j<k} i\hat{\mathcal{T}}_{jk}^+ + i\hat{\mathcal{L}}_D \ . \tag{3.2.8}$$

Since the time reversal symmetry is broken for inelastic systems the collision operator, $\hat{\mathcal{T}}_{jk}^+$, is only defined for one time direction. Here $\hat{b}_{jk}^+$ is the operator for inelastic collisions. The Liouville operator for the driving force, $\hat{\mathcal{L}}_D$, which is necessary for the limit of infinite driving frequency, can be written as [49]

$$\langle \hat{\mathcal{L}}_D \rangle_\xi = \frac{P_D}{m} \frac{\partial^2}{\partial \vec{v}_i^2} \ , \tag{3.2.9}$$

with the driving power P_D and the gaussian random variable $\xi_i(t)$, which has zero mean $\langle \vec{\xi}_i(t) \rangle = 0$ and variance $\langle \vec{\xi}_i^\alpha(t) \vec{\xi}_j^\beta(t) \rangle = \delta_{ij}\delta^{\alpha\beta}$.

Since nothing is known about the canonical distribution function for the driven inelastic hard sphere fluids, we assume that we can factorize the distribution function (see [50] for an analysis of the molecular chaos assumption), $\rho(\Gamma) = \rho_v(\vec{v})\rho_r(\vec{r})$. According to the elastic hard spheres we make the assumption that the velocity distribution function is also a Gaussian.

The spatial distribution function for homogeneous and isotropic systems only depends on the distance between the particles, $\rho_r(\vec{r}) = \rho_r(\vec{r}_{ij})$. So we assume [47, 51]

$$\rho_r(\vec{r}_{ij}) \propto \prod_{i<j} \Theta(r_{ij} - d)\chi(r_{ij}) \ , \tag{3.2.10}$$

with $\chi(r)$ as an unknown function. Furthermore, we will assume that the pair correlation function of an elastic hard sphere system is approximately the same as for inelastic hard sphere fluids. In [51] it is shown that the structure factor of an elastic hard sphere fluid is not the same as for an inelastic hard sphere fluid. Nevertheless, we set $\chi(r_{ij}) = 1$ and get the same spatial distribution function as for a fluid of elastic hard spheres in thermal equilibrium. Note, that for systems out of equilibrium the adjoint pseudo Liouville operator has to be calculated, which is possible with $\hat{\mathcal{L}}^\dagger A = \rho(\Gamma)^{-1} \hat{\bar{\mathcal{L}}} \rho(\Gamma) A$.

3.3 The Granular MCT

Now, the knowledge of the Liouville operator should be used to calculate the memory kernel in Eq. (2.4.3) in section 2.4

$$M(q,t)^{\mathrm{MCT}} = \sum_{\vec{k}<\vec{p}} \frac{m}{k_{\mathrm{B}}T} \mathcal{V}(\vec{q},\vec{k},\vec{p})\phi(k,t)\phi(p,t)\mathcal{W}(\vec{q},\vec{k},\vec{p}) \ . \tag{3.3.1}$$

Here, we need to calculate the two vertices $\mathcal{V}$ and $\mathcal{W}$ to get an expression for the kernel. After getting the memory kernel we will discuss the problems of the extension into binary mixtures. Nevertheless, in appendix D is the calculation of the vertices for binary mixtures under some simplifications.

The Liouville operator, which is introduced above, shall be recalled here again

$$\mathcal{L} = \mathcal{L}_0 + \sum_{j<k} \mathcal{T}_{jk}^+ + \mathcal{L}_D \ . \tag{3.3.2}$$

The three terms, the free streaming operator, $\mathcal{L}_0$, the interaction operator, $\mathcal{T}_{ij}^+$, and the driving operator, $\mathcal{L}_D$ are derived in the section above.

3.3.1 Calculation of the Vertex $\mathcal{V}$

The left vertex is known from literature [14] and given in Eq. (2.4.4). Nevertheless, its calculation should be motivated here:

$$\mathcal{V}(\vec{q},\vec{k},\vec{p}) = \langle j^{\mathrm{L}}(\vec{q})|\mathcal{L}\mathcal{Q}\rho(\vec{k})\rho(\vec{p})\rangle \frac{1}{S(k)S(p)}$$

$$= \left[\langle j^{\mathrm{L}}(\vec{q})|\mathcal{L}\rho(\vec{k})\rho(\vec{p})\rangle - \langle j^{\mathrm{L}}(\vec{q})|\mathcal{L}\mathcal{P}\rho(\vec{k})\rho(\vec{p})\rangle \right] \frac{1}{S(k)S(p)} \ . \tag{3.3.3}$$

In the first term, the Liouville operator acts on both of the densities and in the second term only the $|\rho(\vec{q})\rangle$ part of the projection operator gives a non-vanishing contribution:

$$\mathcal{V}(\vec{q},\vec{k},\vec{p}) = \left[(\hat{q}\cdot\vec{k})\,\langle j^{\mathrm{L}}(\vec{q})|j^{\mathrm{L}}(\vec{k})\rho(\vec{p})\rangle + (\hat{q}\cdot\vec{p})\,\langle j^{\mathrm{L}}(\vec{q})|\rho(\vec{k})j^{\mathrm{L}}(\vec{p})\rangle \right.$$

$$\left. - \langle j^{\mathrm{L}}(\vec{q})|\mathcal{L}\rho(\vec{q})\rangle \frac{1}{S(\vec{q})}\,\langle\rho(\vec{q})|\rho(\vec{k})\rho(\vec{p})\rangle \right] \frac{1}{S(k)S(p)} \ . \tag{3.3.4}$$

The brackets in the first line are given by $\langle j^{\mathrm{L}}(\vec{q})|j^{\mathrm{L}}(\vec{k})\rho(\vec{p})\rangle = \frac{\delta(\vec{k}+\vec{p},\vec{q})}{V}\frac{k_{\mathrm{B}}T}{m}S(p)$, a full derivation is in appendix D. Since one knows the time derivative of the density, the matrix element in the second line is easy to calculate, $\langle j^{\mathrm{L}}(\vec{q})|\mathcal{L}\rho(\vec{q})\rangle = qv^2$. Last but not least the last term is known in the literature as the triplet correlation function, $\frac{\delta(\vec{k}+\vec{p},\vec{q})}{V}S^{(3)}(\vec{k},\vec{p}) = \langle\rho(\vec{q})|\rho(\vec{k})\rho(\vec{p})\rangle$. Only less is known about the triplet correlation function, see e.g. the following reference for theoretical and some numerical works [52, 53].

Here, we also introduce the direct correlation functions, $nc(q) = 1 - S^{-1}(q)$ and $S^{(3)} = S(q)S(k)S(p) - n^2 c^{(3)}(\vec{k},\vec{p})$ so the vertex as a function of c is

$$\mathcal{V}(\vec{q},\vec{k},\vec{p}) = -\frac{\delta(\vec{k}+\vec{p},\vec{q})}{V}\frac{k_{\mathrm{B}}T}{m}n\left[(\hat{q}\cdot\vec{k})c(k) + (\hat{q}\cdot\vec{p})c(p) + nc^{(3)}(\vec{k},\vec{p})\right] \ . \qquad (3.3.5)$$

The Kirkwood approximation [54, 55], $c^{(3)} = 0$, which fails for large length scales but is in a good agreement for smaller length scales [56], can be used to simplify the vertex. This approximation can be seen as a maximization of an entropy functional [57]. Finally, one has

$$\mathcal{V}(\vec{q},\vec{k},\vec{p}) = -\frac{\delta(\vec{k}+\vec{p},\vec{q})}{V}\frac{k_{\mathrm{B}}T}{m}n\left[(\hat{q}\cdot\vec{k})c(k) + (\hat{q}\cdot\vec{p})c(p)\right] \ . \qquad (3.3.6)$$

Notice, in equilibrium the left and the right vertices are equal and the memory kernel is given by

$$m(\phi(t),q) = \frac{k_{\mathrm{B}}T}{m}n^2\sum_{\vec{k}+\vec{p}=\vec{q}}S(k)S(p)\left[(\hat{q}\cdot\vec{k})c(k) + (\hat{q}\cdot\vec{p})c(p)\right]^2\phi(k,t)\phi(p,t) \ . \qquad (3.3.7)$$

3.3.2 Calculation of the Vertex $\mathcal{W}$

Since dissipation plays a key role in granular systems, the left and the right vertices differ by at least the restitution coefficient ϵ, which is a degree of the dissipativity of the system.

A full calculation of the right vertex for monodisperse granular matter can be found in [47, 51] and in appendix D a long detailed and very technical calculation for a binary mixture.

Now, we want to motivate the calculation of the right vertex here. The explicit form of

the right vertex is

$$\mathcal{W} = \langle \rho(\vec{k})\rho(\vec{p})|\mathcal{Q}\mathcal{L}j^{\mathrm{L}}(\vec{q})\rangle \frac{1}{S(k)S(p)}$$

$$= \left[\langle \rho(\vec{k})\rho(\vec{p})|\mathcal{L}j^{\mathrm{L}}(\vec{q})\rangle - \langle \rho(\vec{k})\rho(\vec{p})|\mathcal{P}\mathcal{L}j^{\mathrm{L}}(\vec{q})\rangle\right] \frac{1}{S(k)S(p)} \ . \tag{3.3.8}$$

For the righthand term in the second line, one uses the definition of the projection operator, $\mathcal{P}$, and gets the triplet correlation function and a frequence Ω again. The frequence is not easy to calculate like in section 3.3.1, where we have to apply the Liouville-operator explicitly:

$$\Omega_{\rho j} \propto \langle \rho(\vec{q})|\mathcal{L}j^{\mathrm{L}}(\vec{q})\rangle = \langle \rho(\vec{q})|(\mathcal{L}_0 + \sum_{ij} \mathcal{T}_{ij}^+ + \mathcal{L}_D)j^{\mathrm{L}}(\vec{q})\rangle \ . \tag{3.3.9}$$

Since the driving operator is proportional to the second derivative of the velocity, $\mathcal{L}_D \propto \frac{\partial^2}{\partial \vec{v}^2}$, but the longitudinal current is only linear in $\vec{v}$, it vanishes. The calculation of the free streaming part is mostly given by the velocity average, which can be seen in appendix F. So the only interesting term is the interacting one, $\mathcal{T}_{ij}^+$. Since none of the particles are privileged, one can fix a particle and let it collide with the others. So the sum over all particles becomes to a prefactor $N(N-1)/2$.

$$\langle \rho(\vec{q})|\sum_{ij} \mathcal{T}_{ij}^+ j^{\mathrm{L}}(\vec{q})\rangle = \frac{N(N-1)}{2} \langle \rho(\vec{q})|\Theta(\hat{r}_{12}\cdot\vec{v}_{12})(\hat{r}_{12}\cdot\vec{v}_{12})\delta(r_{12}-d)(\hat{b}_{12}^+ - 1)j^{\mathrm{L}}(\vec{q})\rangle \ . \tag{3.3.10}$$

The collision operator, b_{12}^+, used on the longitudinal current transforms the velocity to the postcollisional one, where the coefficient of restitution, ϵ appears. The $(\hat{r}_{12}\cdot\vec{v}_{12})$-term can be calculated independently from the spatial part with the velocity average. After respecting those facts one gets

$$\langle \rho(\vec{q})|\sum_{ij} \mathcal{T}_{ij}^+ j^{\mathrm{L}}(\vec{q})\rangle = \frac{(N-1)}{2}\frac{1+\epsilon}{2}\frac{k_{\mathrm{B}}T}{m}\hat{q}\langle \hat{r}_{12}\delta(r_{12}-d)(\mathrm{e}^{i\vec{q}\vec{r}_2} - \mathrm{e}^{i\vec{q}\vec{r}_1})\sum_j \mathrm{e}^{-i\vec{q}\vec{r}}\rangle \ . \tag{3.3.11}$$

Now, the summation in the spatial average can be described by three cases, $\sum_j \mathrm{e}^{-i\vec{q}\vec{r}_j} = \mathrm{e}^{-i\vec{q}\vec{r}_1} + \mathrm{e}^{-i\vec{q}\vec{r}_2} + (N-2)\mathrm{e}^{-i\vec{q}\vec{r}_3}$. With relabeling the integration variables, the four averages can be collapsed to two terms:

$$\langle \hat{r}_{12}\delta(r_{12} - d)(\mathrm{e}^{i\vec{q}\vec{r}_2} - \mathrm{e}^{i\vec{q}\vec{r}_1}) \sum_j \mathrm{e}^{-i\vec{q}\vec{r}}\rangle = 2\langle \hat{r}_{12}\delta(r_{12} - d)\mathrm{e}^{-i\vec{q}\vec{r}_1}\mathrm{e}^{i\vec{q}\vec{r}_2}\rangle$$
$$+ 2(N-2)\langle \hat{r}_{12}\delta(r_{12} - d)\mathrm{e}^{-i\vec{q}\vec{r}_3}\mathrm{e}^{i\vec{q}\vec{r}_2}\rangle. \quad (3.3.12)$$

For the last term the YBG-relation will be used to rewrite the term as a function of $\vec{r}_1$ and $\vec{r}_2$. From the YBG-relation one gets the right hand side of the first line of Eq. (3.3.12) and a term which depends on the structure factor. Now, with collecting all the terms one gets

$$\frac{\langle \rho(\vec{k})\rho(\vec{p})|\mathcal{P}\mathcal{L}j^{\mathrm{L}}(\vec{q})\rangle}{S(k)S(p)} = \frac{\delta(\vec{k} + \vec{p}, \vec{q})}{V}\frac{k_{\mathrm{B}}T}{2m}q\left[(1-\epsilon)S(q) + (1+\epsilon)\right] \quad (3.3.13)$$

The calculation of the first term in Eq. (3.3.8), $\langle \rho(\vec{k})\rho(\vec{p})|\mathcal{L}j^{\mathrm{L}}(\vec{q})\rangle$, is from a theoretical point of view equal to the calculation above, but because three different observables are interacting with each other one has to do more steps in the calculations and use the YBG-relation more than one time. A full derivation can be found in [47] and in appendix D for binary mixtures:

$$\langle \rho(\vec{k})\rho(\vec{p})|\mathcal{L}j^{\mathrm{L}}(\vec{q})\rangle = \frac{k_{\mathrm{B}}T}{m}\frac{\delta(\vec{k} + \vec{p}, \vec{q})}{V}\left[\frac{1+\epsilon}{2}\left((\hat{q}\cdot\vec{p})S^{-1}(\vec{p}) + (\hat{q}\cdot\vec{k})S^{-1}(\vec{k})\right) + \frac{1-\epsilon}{2}qS(\vec{q})\right].$$
$$(3.3.14)$$

Notice, in both equations, (3.3.13) and (3.3.14), we used the convolution-approximation. Sum over all results and use the direct correlation function, $c(\vec{q})$, the right vertex becomes

$$\mathcal{W} = -\frac{1+\epsilon}{2}\frac{\delta(\vec{k} + \vec{p}, \vec{q})}{V}\frac{k_{\mathrm{B}}T}{m}n\left[(\hat{q}\cdot\vec{k})c(\vec{k}) + (\hat{q}\cdot\vec{p})c(\vec{p})\right]. \quad (3.3.15)$$

For the elastic limit of $\epsilon \to 1$ the right and the left vertex are equal, $\mathcal{V} = \mathcal{W}$.
The memory kernel with dissipation is given by

$$m(\phi(t), q) = \frac{1 + \epsilon}{2} \frac{k_B T}{m} n^2 \sum_{\vec{k} + \vec{p} = \vec{q}} S(k) S(p) \left[(\hat{q} \cdot \vec{k}) c(k) + (\hat{q} \cdot \vec{p}) c(p) \right]^2 \phi(k, t) \phi(p, t) \; .$$

(3.3.16)

Now, we go to the limit of continuous wave vectors, where the sum is replaced by an integral

$$m(\phi(t), q) = A(q, \epsilon) \frac{n}{q^2 S(q)}$$

$$\int \mathrm{d}^3 k S(k) S(|\vec{q} - \vec{k}|) \left\{ [\hat{q} \cdot \vec{k}] c(k) + [\hat{q} \cdot (\vec{q} - \vec{k})] c(|\vec{q} - \vec{k}|) \right\}^2 \phi(k, t) \phi(|\vec{q} - \vec{k}|, t) \; .$$

(3.3.17)

The prefactor $A(q, \epsilon) = [1 + (1 - \epsilon) S(q)/(1 + \epsilon)]^{-1} > 0$ guarantees that the memory kernel remains positive definite. In the elastic case, $\epsilon = 1$, the prefactor also equals unity. Since the structure factor, $S(q)$, exhibits some oscillations, the prefactor also oscillates for $\epsilon < 1$. In Fig. 3.3.1 one can see the behavior of the prefactor, it is dominated by the Percus-Yevick structure factor [58]. One can see in Fig. 3.3.1 that $A(q, \epsilon)$ has a local
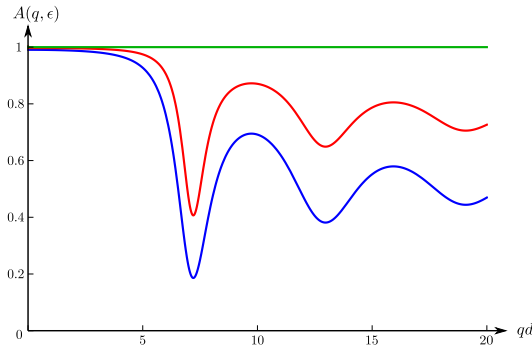
Figure 3.3.1: The prefactor, $A(q, \epsilon)$, as a function of the wave number qd for different coefficients of restitution in 3D. The diameter is set to one, $d = 1$. In the elastic case, $\epsilon = 1$, the prefactor is a constant (green line). The deviation from the unity gets larger for decreasing ϵ. The red curve is for $\epsilon = 0.5$ and the blue one is for the total inelastic case, where the coefficient vanishes, $\epsilon = 0$.

minimum at the first peak of the structure factor. The weakness of the memory kernel
or the cage effect is related to the dissipation, for increasing dissipation the memory
kernel decreases and the cage effect becomes weaker. To compare the inelastic case
with the elastic case, one has to go to higher densities. For increasing dissipation or
decreasing ϵ the critical density, where the liquid-glass transition takes place, increases.
This makes insofar sense as the memory kernel decreases for a given density with
increasing dissipation.
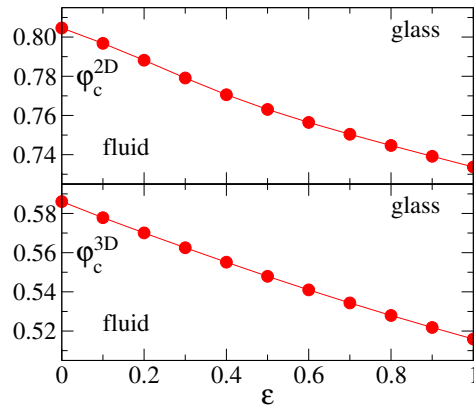
Figure 3.3.2: The critical packing fraction, φ_c, for different coefficients of restitution.
One can see a decreasing φ_c for decreasing dissipation [51].

With the granular mode coupling in this chapter it can be shown, that the mode
coupling theory can be used for systems out of the equilibrium, too.

3.3.3   Granular Mode Coupling Theory for Binary Mixtures

The memory kernel for a binary mixture is similar to the monodisperse case, a full
motivation is given in the PhD of A. Latz [59] and T. Voigtmann [60]. In appendix B
the memory kernel is derived as

$$
\begin{aligned}
M_{\alpha\beta}(\vec{q}) &\approx J_{\alpha\beta}^{-1} \langle j_\beta^{\mathrm{L}}(\vec{q}) | \mathcal{L}\mathcal{Q}\mathcal{P}^{\mathrm{MCT}}\mathcal{R}\mathcal{P}^{\mathrm{MCT}}\mathcal{Q}\mathcal{L} | j_\alpha^{\mathrm{L}}(\vec{q}) \rangle \ , \\
&= J_{\alpha\beta}^{-1} \sum_{\substack{\gamma'\delta'\epsilon\psi, \\ \vec{k}>\vec{p},\vec{k}'>\vec{p}'}} \mathcal{V}_{\beta\gamma\delta}(\vec{q}\vec{k}\vec{p}) \mathcal{Z}_{\epsilon\psi}^{\gamma'\delta'}(\vec{k}'\vec{p}',\vec{k}\,\vec{p}) \mathcal{W}_{\epsilon'\psi'\alpha}(\vec{k}'\vec{p}'\vec{q}) \ ,
\end{aligned}
\tag{3.3.18}
$$

with

$$\mathcal{V}_{\beta\gamma\delta}(\vec{q}\vec{k}\vec{p}) = \sum_{\substack{\gamma''\delta'' \\ \vec{k}''\vec{p}''}} \langle j_{\beta}^{\mathrm{L}}(\vec{q})|\mathcal{L}\mathcal{Q}\rho_{\gamma''}(\vec{k}'')\rho_{\delta''}(\vec{p}'')\rangle \, g_{\gamma\delta}^{\gamma''\delta''}(\vec{k}''\vec{p}'', \vec{k}\,\vec{p}) \ ,$$

$$\mathcal{W}_{\epsilon'\psi'\alpha}(\vec{k}'\vec{p}'\vec{q}) = \sum_{\substack{\epsilon''\psi'' \\ \vec{k}''\vec{p}''}} \langle \rho_{\epsilon''}(\vec{k}'')\rho_{\psi''}(\vec{p}'')\mathcal{L}\mathcal{Q}|j_{\alpha}^{\mathrm{L}}(\vec{q}))\rangle \, g_{\epsilon'\psi'}^{\epsilon''\psi''}(\vec{k}''\vec{p}'', \vec{k}'\,\vec{p}') \ ,$$

$$\mathcal{Z}_{\epsilon\psi}^{\gamma'\delta'}(\vec{k}'\vec{p}', \vec{k}\,\vec{p}) = \langle \rho_{\gamma'}(\vec{k}')\rho_{\delta'}(\vec{p}')|\mathcal{R}|\rho_{\epsilon}(\vec{k})\rho_{\psi}(\vec{p})\rangle \ ,$$

$$\approx \Phi_{\gamma'\epsilon}(k, t)\Phi_{\delta'\psi}(p, t)\delta_{\vec{k}\vec{k}'}\delta_{\vec{p}\vec{p}'} \ . \tag{3.3.19}$$

Where the greek indices denote different species of particles and $g_{\alpha'\beta'}^{\alpha\beta}(\vec{k}'\vec{p}', \vec{k}\vec{p}) = S_{\alpha\alpha'}(\vec{k})S_{\beta\beta'}(\vec{p})\delta_{\vec{k},\vec{k}'}\delta_{\vec{p},\vec{p}'}$ is the normalization of the vertex. Now, one only has to calculate the averages like in the section above and the memory kernel for binary mixture is ready for some applications. The left vertex, $\mathcal{V}$, can be calculated easily like in the monodisperse case without further restrictions and is given by (full calculation in appendix D):

$$\mathcal{V}_{\beta\gamma\delta}(\vec{q}\vec{k}\vec{p}) = -\frac{\delta(\vec{k}+p, \vec{q})}{V}\frac{k_{\mathrm{B}}T_{\beta}}{m_{\beta}}n\left[(\hat{q}\cdot\vec{k})c_{\beta\gamma}(\vec{k})\delta_{\beta\delta} + (\hat{q}\cdot\vec{p})c_{\beta\delta}(\vec{p})\delta_{\beta\gamma} + qx_{\beta}nc_{\beta\gamma\delta}^{(3)}(\vec{k}\,\vec{p})\right] \ . \tag{3.3.20}$$

One can see that in the monodisperse limit, where the concentration x goes to one and the indices disappear, the left vertex is equal to Eq. (3.3.6).

The calculation of the right vertex, $\mathcal{W}$, is much more complicated than in the monodisperse case. Since we have to calculate the averages explicitly with the Liouville operator, we have to know the impact of the different particles on the averages.

In general the different species of particles interact differently, which changes the coefficient of restitution for each species. The coefficient becomes a matrix, $\epsilon_{\alpha\beta}$. The effect of the temperature on the different particles is in general also varying. So particle α has a thermal velocity of $v_{\alpha}^2 \propto T_{\alpha}$.

The problem we get with different temperatures is that the spatial averages, which we use inter alia for the YBG-relation, is depending on the interacting part of the Hamiltonian, $\langle ... \rangle_{\chi} \propto \mathrm{e}^{-\beta\sum_{ij}V(r_{ij})}$, here χ denotes the spatial average. β is the inverse temperature, and there is no analog definition for β for more than one temperature. So

in our calculations we use two assumptions: 1) the coefficient of restitution is a constant like in the monodisperse case and 2) the temperatures are equal for all particles. Under those assumptions we can calculate the right vertex (a very technical derivation is given in appendix D)

$$\mathcal{W}_{\alpha\beta\gamma} = -\frac{\delta(\vec{k}+\vec{p},\vec{q})}{V}\frac{k_\mathrm{B}T_\gamma}{m_\gamma}n\frac{1+\epsilon}{2}\left[(\hat{q}\cdot\vec{k})\delta_{\gamma\beta}c_{\gamma\alpha}(\vec{k}) + (\hat{q}\cdot\vec{p})\delta_{\gamma\alpha}c_{\gamma\beta}(\vec{p}) + qnx_\gamma c^{(3)}_{\gamma\alpha\beta}(\vec{k},\vec{p})\right] \ . \tag{3.3.21}$$

Here we have both limits: i) for $\epsilon = 1$, the elastic limit, the right vertex equals the left one and ii) for vanishing indices, the monodisperse limit, the right vertex equals Eq. (3.3.15).

In analogy to the monodisperse case we will write the memory kernel as a function of the prefactor $A(\vec{q},\epsilon)$

$$m_{\alpha\beta}(\vec{q}) = A^\epsilon_{\alpha\beta}(\vec{q})\frac{n^2}{q^2V^2}\frac{1}{\delta_{\beta\alpha}x_\beta}\sum_{\substack{\gamma,\delta\\\epsilon',\psi'}}\sum_{\vec{k}>\vec{p}}V_{\beta\gamma\delta}\Phi(\vec{k},t)_{\gamma,\epsilon'}\Phi(\vec{p},t)_{\delta,\psi'}V_{\epsilon'\psi'\alpha} \ , \tag{3.3.22}$$

where the prefactor is given by $A^\epsilon_{\alpha\beta}(\vec{q}) = \left[x_\alpha\delta_{\alpha\beta} + \frac{1-\epsilon}{1+\epsilon}S_{\alpha\beta}(\vec{q})\right]^{-1}$.

The next step is to calculate the right vertex for different coefficients of restitution and after that to generalize the YBG-relation to the BBGKY hierarchy [45, 61] to calculate the spatial average for different temperatures.

Lebowitz solved the Ornstein-Zernike equation with the Percus-Yevick closure analytically [62]. For the analysis of binary mixtures we will use the Lebowitz structure factor for the memory kernel, $m_{\alpha,\beta}(\vec{q})$, and for the dynamics of binary mixtures.

Conclusion

In this section I introduced the physics around granular matter. A particularity of granular matter is that the dynamics is ruled by some dissipative interactions. The degree of dissipation is given by the coefficient of restitution, $\epsilon \in [0,1]$.

We used the Liouville operators to calculate the mode coupling memory kernel, $m_q(t)$, of such systems analytically. Here we assume that the particles energy is given by their translation and ignore the rotational energy. Since the calculation of $m_q(t)$ is done in

the work of T. Kranz [47] we extend the theory for binary mixtures. Here I assumed that the species' temperatures, T_α, are all equal and obtained the microscopic memory kernel in this approximation.

The next steps in this section would be the numerical implementation of the theoretical framework to get the density autocorrelation function for binary mixtures. The next step is to generalize the theory by allowing for different species dependent temperatures, T_α.

4   Spin Glass Theory

The definition of a spin glass is an arbitrary distribution of spins on a lattice in which a part of the spins are frozen. One way to realize such states is to have some bonds with ferromagnetic interaction and some with antiferromagnetic interaction. So, for all temperatures the spin orientation is not uniform in space and some of the spins become frozen [63]. In Fig. 4.1.1 we have a square lattice with a ferromagnetic interaction with the nearest neighbors and an antiferromagnetic interaction with the next to nearest neighbors. For this system it is not possible to satisfy both kind of interactions. One can see in the green circles that some spins can fulfill the interaction. But for the whole lattice it is not possible to fulfill always all interactions at the same time. The spin in the center is highly frustrated, on the one hand it needs to be a down-spin to satisfy some of its interactions but on the other hand as a down-spin it will be in opposition with the remaining interactions. The phenomenon of frustration is a feature of spin glasses. The ground state of such systems is highly degenerate [6].
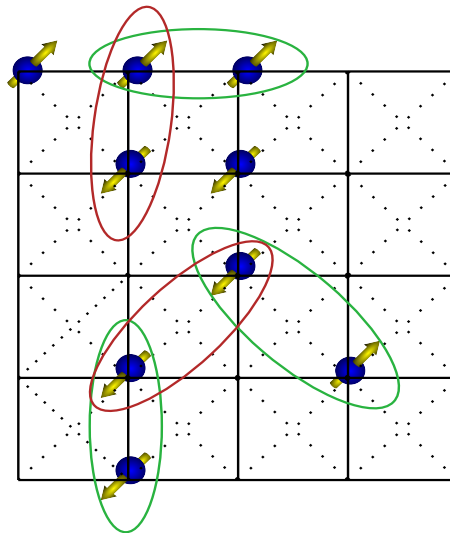
Figure 4.1.1: A square lattice with some up- and down-spins. Here the nearest neighbor interaction is a ferromagnetic one (straight lines), and the next to nearest neighbor interaction is antiferromagnetic (dotted line). In the green circles the spins are in a happily connected environment, whereas the spins in the red circles are against the given interaction.

In 1975 Edwards and Andersen [64] introduced a model that features a spin glass phase. The main idea of the Edwards-Anderson (EA) model is given by the Hamiltonian

$$H = -\sum_{i \neq j} J_{ij}(\vec{S}_i \cdot \vec{S}_j) - h\sum_i S_i^z, \tag{4.1.1}$$

where $\vec{S}_i$ is the spin on site i, J_{ij} the interaction between the spins $\vec{S}_i$ and $\vec{S}_j$, and h the external magnetic field. For a suitable distribution of the interactions, $P[J_{ij}]$, like in Fig 4.1.1 the system is in highly frustrated. The distribution of the couplings, J_{ij}, is a gaussian with [63]

$$P[J_{ij}] = \frac{1}{(2\pi\Delta^2)^{1/2}}\exp\left(-\frac{J_{ij}^2}{2\Delta^2}\right) , \tag{4.1.2}$$

where Δ is the variance.

The glassy phase does not have long-range order and therefore an order parameter which is used in thermodynamics can not be used here [63]. So in the Edwards-Anderson model we are interested into the dynamics. Frozen spins should not change their orientation over time, this motivates the introduction of a spin autocorrelation function

$$q = \lim_{t \to \infty} \left\langle \left\langle \vec{S}(0) \cdot \vec{S}(t) \right\rangle_T \right\rangle_C . \tag{4.1.3}$$

The inner bracket is the thermal average and the outer bracket the average over all bound configurations [63]. If the spin orientation remains the same, the Edwards-Anderson parameter will go to a finite value, $q \neq 0$. Otherwise, when the spins are not frozen but changing their orientation the correlation function goes to zero. The Edwards-Anderson parameter is the order parameter for spin glasses, in analogy to the non-ergodicity parameter, f, in the mode coupling theory

In the same year Sherrington and Kirkpatrick used a mean-field theory to get an exact solution of the infinite-range EA model [65, 66]. They assumed that every spin $\sigma_i \in \{-1, +1\}$ couples, independently of the distance between the spins, to all the other spins equally. Notice, the definition σ for a spin will only used for Ising spins, which means that the spin only has two possible states, up and down, for all the other spin orientations the spin will defined as a vector, $\vec{S}$. A generalization of the SK model is

the p-spin model which describes the interaction of p spins

$$H = - \sum_{1 \leq i_1 < ... < i_p \leq N} J_{i_1, i_2, ..., i_p} \sigma_{i_1} \sigma_{i_2} ... \sigma_{i_p} \qquad (4.1.4)$$

with the Ising spin σ_i (for $p = 2$ one gets the SK model) [67, 68].

In both models, the Edwards-Anderson model and the p-spin model (which also includes the Sherrington-Kirkpatrick model), we need to evaluate the free energy $\langle F \rangle = -k_B T \langle \ln Z\{J_{ij}\} \rangle$ [7]. For the calculation of the partition function one uses the replica trick [6] which rewrites the logarithm of the partition function as a derivative of the partition function, $\langle \ln Z \rangle = \lim_{n \to 0} \partial_n \langle Z^n \rangle$. Nevertheless, the calculation of $\langle Z^n \rangle$ is also problematic, one can approximate n being an integer and can rewrite the average over the partition function as $\langle Z^n \rangle = \int \mathcal{D}\sigma_1 ... \int \mathcal{D}\sigma_n \langle \exp(-\beta H(\sigma_1, J)... - \beta H(\sigma_n, J)) \rangle$. Solving of such integrals is not the topic of this thesis, for interested people I can suggest to read the work of Castellani and Cavagna [69].

The difficulties of these models are calculating integrals to get the partition function and calculate the free energy of the system. Inspired by the theory of liquids [70, 71] one has introduced lattice models to analyze glass-forming liquids without any knowledge about the partition function or free energy. One of the promising models are the kinetic constrained models (KCM). Here the spins are not interacting which each other, $J_{ij} = 0$, and the dynamic of the system is only based on the neighborhood of a spin. Depending on the model, the flipping of a spin is constrained and depends only on the nearest neighbors. Two prominent models are the Kob-Andersen (KA) model [72] and the Fredrickson-Andersen (FA) model which is the main part of this chapter and will be explained in detail. So at this point I want to introduce the main idea of the KA model: At the beginning the lattice is occupied with an initial probability, p, and particle can only move if they fulfill some conditions. The first condition is intuitive, the particle can only move, when the target site is empty. In addition the particle must have less than f nearest neighbors before and after it moved. So the particle number is conserved. In the work of Sellitto [73] the model shows some properties which it has in common with real glass-forming systems.

4.2   Fredrickson-Andersen Model

The other prominent kinetic constraint model is the Fredrickson-Andersen model [74], in which features of glass-forming systems also occur [8, 75–77].

The FA model is a Ising like model [78] with non interacting up- and down-spins and an external magnetic field which favors one spin direction [79, 80]. So the Hamiltonian of the system is simple, $H = h \sum_i \sigma_i$, and $h < 0$ favors down spins. The dynamics is constrained, each time step a chosen spin will be flipped with a rate $\omega(\sigma_i \to -\sigma_i)$, only when the number of nearest neighbor down-spins is larger or equal to the facilitation parameter, f [74, 81]. The kinetic constraint is an analogy to the cage effect in super-cooled liquids, where the neighbors of a particle form a cage so that the particle is arrested between the neighbors till it finds a way to escape from the surrounding particles.

If the up-spin concentration is equal to one, it is trivial to say, that none of the spins will be flipped and the ground state remains the same. The opposite case, an up-spin concentration of zero, is also trivial, since the systems favors down-spins the lattice will be filled in the ground state with only down spins. Now, the question is, can we find a non trivial initial up-spin concentration, $p_c < 1$, for the emergence of some up-spin clusters in the ground state. For $f = 1$ it is shown that the critical concentration is always one, otherwise it is always possible to flip all up spins in each lattice in a finite time to a down-spin [81, 82]. The critical up-spin concentration in hypercubic lattices $\mathbb{Z}^d$ is, independent of the facilitation parameter, also $p_c = 1$ [81, 82]. On a random graph, like the Bethe lattice, one can show that for $1 < f < k$, where k is the connectivity, a non trivial concentration $p_c < 1$ exists [83, 84].

Motivated by the numerical result of Sellitto [8] we have the Bethe lattice decorated with up-spins, with the concentration p, and down-spins, with $1 - p$. The Bethe lattice is a regular tree graph with a fixed connectivity, k [85]. One can see in Fig. 4.2.1, that the number of sites inside the lattice is smaller than the number of sites on the surface of the lattice. The Bethe lattice also has no loops, so once you started walking from one point, you will never reach this point again.

The bootstrap percolation [86–88] is the ground state, where $T = 0$, of the FA model from an initial up-spin concentration, p. The probability for an up-spin in the ground
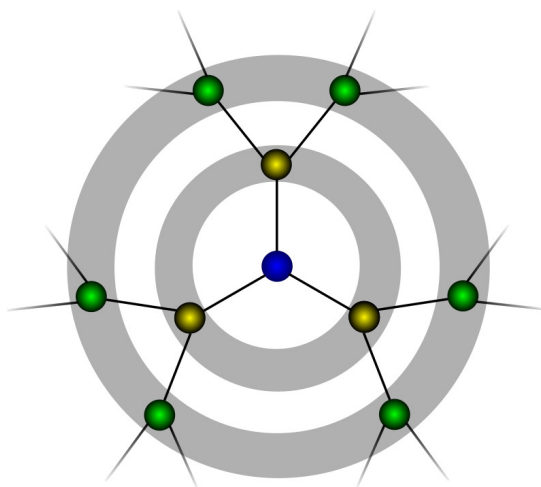
Figure 4.2.1: The Bethe lattice with a coordination number $z = 3$ and a connectivity $k = 2$. One can see that there are no closed loops, so once you started, let's say, from the blue site, you will never come back to this blue site again. The different colors mark the different shells (the grey circles) around a chosen point.

state, q, is given implicitly as [86]

$$q = p \sum_{i=0}^{f-1} \binom{k}{i} q^{k-i} (1-q)^i \ , \tag{4.2.1}$$

with the initial up-spin concentration p. The Hamiltonian, $\mathcal{H} = -\frac{1}{2} \sum_i \sigma_i$, is so simple that the up spin concentration can be calculated explicitly

$$p = \frac{e^{\frac{1}{2}\beta}}{e^{\frac{1}{2}\beta} + e^{-\frac{1}{2}\beta}} = \frac{1}{1 + e^{-\beta}} \ , \tag{4.2.2}$$

where β is the inverse temperature. The Eq. (4.2.1) can be illustrated as follows, for an frozen up-spin in the groundstate one needs more than f up-spin neighbors. The sum in the equation is over all down-spin neighbors. It starts at zero, which means you only have up-spin neighbors, and goes till $f - 1$, where you also have less than f down spin-neighbors and the spin is frozen. The binomial coefficient gives you all possible configurations for your down-spin. So for $i = 0$, when all of your neighbors are up-spins and are indistinguishable, the coefficient is equal to one, and for $i = 1$, one has only

one down-spin and could put this down-spin to k sites and so on.

Since the numerical calculations [8, 77] are not in terms of a correlation function but a persistence function, $\psi(t)$, it should be introduced as an observable. The persistence function is the fraction of the spins, which are never flipped till a time t. The long-time limit, $\psi^\infty \equiv \psi(t \to \infty)$, so the fraction of the spins which are permanently frozen, can be calculated with the probability of the spins in the ground state, q [77]

$$\psi^\infty = p \sum_{i=0}^{f-1} \binom{k+1}{i} q^{k+1-i}(1-q)^i + (1-p) \sum_{i=0}^{f-1} \binom{k+1}{i} (p\chi_{k,f})^{k+1-i}(1-p\chi_{k,f})^i \ ,$$

$$(4.2.3)$$

with $\chi_{k,f} = \sum_{i=0}^{f-2} \binom{k}{i} q^{k-i}(1-q)^i$. The first term gives the probability that an up-spin is frozen, because its neighborhood don't fulfill the conditions. The second term is the probability that the down-spin becomes frozen after the down-spin neighbors of it gets frozen.

Since the persistence function is an unusual observable in MCT, we are interested in finding a spin correlation function, $\phi(t)$. The aim is to understand the microscopic dynamics of the FA-model with the correlation function, $\phi(t)$. With Eq. (4.2.3) we can compute from the spin autocorrelation function the persistence function and can compare the numerical data with the theoretical calculation.

4.3   Equation of Motion for the FA-Model

The time evolution of a probability distribution function of Brownian motion, $P(\{\sigma\}, t)$, is given by the Fokker-Planck Eq. ([89])

$$\frac{\partial P(\{\sigma\}, t)}{\partial t} = \sum_\alpha \left[\omega_\alpha(\{-\sigma\}_\alpha) P(\{-\sigma\}_\alpha, t) - \omega_\alpha(\{\sigma\}_\alpha) P(\{\sigma\}_\alpha, t) \right]$$

$$= \underline{\Omega} P(\{\sigma\}_\alpha, t) \ , \tag{4.3.1}$$

where $\{\sigma\}$ is a set of Ising spins and ω_α is the the transition probability. We are interested in a group of spins $\{\sigma\}_\alpha$ which are flipped into $\{-\sigma\}_\alpha$ with the transition probability of ω_α. The stochastic operator, $\underline{\Omega}$, can be expressed with the spinflip

operator, $\hat{S}_\alpha$, as

$$\underline{\Omega} = \sum_\alpha \left(\hat{S}_\alpha - 1\right) \omega_\alpha(\{\sigma\}_\alpha) \ . \tag{4.3.2}$$

where the spinflip operator is defined as $\hat{S}_\alpha X(\{\sigma\}_\alpha) = X(\{-\sigma\}_\alpha)$ and the transition probability ω_α is given for the FA model as

$$\omega_\alpha = \frac{\omega_0}{N}\left(\delta_{1,n_\alpha} + \delta_{0,n_\alpha}\mathrm{e}^{-1/T}\right)\left[1 - \Theta\left(\sum_{j\in\mathcal{K}}n_j - k + f - 1\right)\right] \ . \tag{4.3.3}$$

Here $\mathcal{K}$ denotes the set of children of site i. Since the time derivative of the equilibrium distribution vanishes, $\partial_t P_\mathrm{eq}(\{\sigma\},t) = 0$, one can derive the detailed balance condition

$$\omega_\alpha(\{-\sigma\}_\alpha)P_\mathrm{eq}(\{-\sigma\}_\alpha,t) = \omega_\alpha(\{\sigma\}_\alpha)P_\mathrm{eq}(\{\sigma\}_\alpha,t) \ . \tag{4.3.4}$$

With the detailed balance one can create a self-adjoint operator, $\hat{H}$, for the time evolution [90]

$$\begin{aligned}
\hat{H} &= P_\mathrm{eq}^{-1/2}(\{\sigma\}_\alpha)\underline{\Omega}P_\mathrm{eq}^{1/2}(\{\sigma\}_\alpha) \ , \\
&= \sum_\alpha \omega_\alpha^{1/2}(\{\sigma\}_\alpha)(\hat{S}_\alpha - 1)\omega_\alpha^{1/2}(\{\sigma\}_\alpha) \ .
\end{aligned} \tag{4.3.5}$$

With the identity, $\hat{S}_\alpha - 1 = -\frac{1}{2}\left(\hat{S}_\alpha - 1\right)^2$, one can write the self-adjoint operator, $\hat{H}$, as

$$\begin{aligned}
\hat{H} &= -\sum_\alpha \frac{1}{\sqrt{2}}\omega_\alpha^{1/2}(\hat{S}_\alpha - 1)(\hat{S}_\alpha - 1)\omega_\alpha^{1/2}\frac{1}{\sqrt{2}} \ , \\
&= -\sum_\alpha \hat{U}_\alpha^\dagger \hat{U}_\alpha \ , \\
&= -\hat{\boldsymbol{U}}^\dagger\hat{\boldsymbol{U}} \ .
\end{aligned} \tag{4.3.6}$$

This representation of the self-adjoint Hamiltonian will be useful in the next section, when we derive the Brownian of motion for the Fredrickson-Andersen model.

4.3.1   Microscopic Dynamics of FA-Model

To get an EOM like 2.5.2 we need an appropriate variable for an autocorrelation function. As we know both the initial and the end concentrations of the up-spins in the FA model the following microscopic variable is suitable

$$\eta_{\sigma_i(t)} = \delta_{1,\sigma_i(t)} \ , \tag{4.3.7}$$

which is one for an up-spin on site i and zero for a down-spin.
Motivated by the bootstrap percolation a spin correlation function, $\phi(t)$, with the long-time limit $\phi(t \to \infty) = q$ in the non-ergodic phase is needed to describe the microscopic behavior of the FA model. Such a correlation function is given by

$$\phi(t) = \langle \eta_i(0)\eta_i(t) \rangle \ , \tag{4.3.8}$$

the brackets are an average over all initial spin configurations. The initial value, $\phi(0) = p$ is not normalized to one but to the initial concentration of the up-spins, p. Notice, the initial concentration p is a given up-spin concentration, so the systems is at time $t = 0$ out of equilibrium and it relaxes to equilibrium. The probability q is also not the equilibrium concentration of up-spins. It is only the fraction of the frozen up-spins, ignoring the unfrozen up-spins which comes from thermal fluctuations. Since the correlation between the unfrozen and frozen up-spins vanishes, we are not interested in the equilibrium concentration.
The Fredrickson-Andersen model has an ergodic-nonergodic transition, which can be described by the Mode-Coupling theory [1, 2, 28]. In both theories, correlation functions will be used, the spin autocorrelation function for the FA model and the particle density autocorrelation function in the MCT, to describe such transitions. Nevertheless, it is not easy to match both theories, the Fredrickson-Andersen model has a stochastic irreversible dynamics for spins, whereas, the MCT deals with deterministic reversible dynamics for liquids. The extended mode coupling theory deals with second order memory kernels, which is the memory function of the memory function, [91]. In analogy to that first applications of the MCT on a spin model was with introducing a second memory kernel [92]. However, the correlation functions resulting from this approximation were unphysical. Kawasaki introduces the so-called irreducible memory function [90,

93] instead of the second order memory kernel, which has the same mathematical characteristic as the simplified MCT for liquids. The name - irreducible memory kernel - is motivated by the language of diagrammatic quantum field theory, where the first order memory kernel is not one-particle irreducible, whereas the irreducible memory kernel is [90, 94]. Some applications of the irreducible memory kernel can be found in the works of Pitts and Andersen [83, 95] and a diagrammatic derivation in [96]. Now, here we want to motivate the irreducible memory kernel for the Fredrickson-Andersen model.

Since we have two memory kernels the following projection operators will be used [90]

$$\mathcal{P}_{\eta_i} = |\eta_i(0)\rangle \langle \eta_i(0)| \; ,$$
$$\mathcal{P} = \hat{\boldsymbol{U}} |\eta_i(0)\rangle \langle \eta_i(0)|\hat{\boldsymbol{U}}^\dagger \cdot \hat{\boldsymbol{U}}|\eta_i(0)\rangle^{-1} \langle \eta_i(0)| \hat{\boldsymbol{U}}^\dagger \; . \tag{4.3.9}$$

In analogy to chapter 2 the correlation function, $\phi(t)$, will be transformed into the Laplace domain

$$\phi(z) = \langle \eta_i(0)|(z - \hat{H})^{-1}|\eta_i(0)\rangle \; . \tag{4.3.10}$$

With the projection operator, $\mathcal{P}_\eta$,and the appendix A one gets

$$\mathcal{P}_\eta(z - \hat{H})^{-1}\mathcal{P}_\eta = \left[z - \mathcal{P}_\eta \hat{H} \mathcal{P}_\eta - \mathcal{P}_\eta \hat{H}(z - \mathcal{Q}_\eta \hat{H} \mathcal{Q}_\eta)\hat{H}\mathcal{P}_\eta \right]^{-1} \; ,$$
$$= [z - \Omega - M_\eta(z)]^{-1} \; . \tag{4.3.11}$$

The Hamiltonian, H, can be rewritten with the second projection operator, $\mathcal{P}$, to

$$\hat{H} = -\hat{\boldsymbol{U}}^\dagger(\mathcal{P} + \mathcal{Q})\hat{\boldsymbol{U}} = \hat{H}_P + \hat{H}_Q \; ,$$
$$\hat{H}_P = -\hat{\boldsymbol{U}}^\dagger \mathcal{P} \hat{\boldsymbol{U}} = \hat{H} |\eta(0)\rangle \Omega^{-1} \langle \eta(0)| \hat{H} \; ,$$
$$\hat{H}_Q = -\hat{\boldsymbol{U}}^\dagger \mathcal{Q} \hat{\boldsymbol{U}} \; . \tag{4.3.12}$$

To get an irreducible memory kernel the operator identity

$$\frac{1}{z - \mathcal{Q}\hat{H}\mathcal{Q}} = \frac{1}{z - \mathcal{Q}\hat{H}_Q\mathcal{Q}} + \frac{1}{z - \mathcal{Q}\hat{H}\mathcal{Q}} H_P \frac{1}{z - \mathcal{Q}\hat{H}_Q\mathcal{Q}} \; .$$

will be used so that the memory kernel can be written as

$$M_\eta(z) = M_\eta^{\mathrm{irr}}(z) + M_\eta(z)\Omega^{-1}M_\eta^{\mathrm{irr}}(z) \ ,$$

$$\Rightarrow M_\eta(z) = \frac{M_\eta^{\mathrm{irr}}(z)}{1 - \Omega^{-1}M_\eta^{\mathrm{irr}}(z)} \ ,$$

with

$$M_\eta^{\mathrm{irr}}(z) = \langle \eta(0)|\hat{H}\mathcal{Q}_\eta \frac{1}{z - \mathcal{Q}_\eta \hat{H}_Q \mathcal{Q}_\eta} \mathcal{Q}_\eta \hat{H}|\eta(0)\rangle \ .$$

With the irreducible memory kernel the correlation function, $\phi(z)$, is given as

$$\phi(z) = \frac{1}{z - \Omega - \Omega^2 \frac{m_\eta^{\mathrm{irr}}(z)}{1-m_\eta^{\mathrm{irr}}(z)\Omega}} = \frac{1}{z - \frac{\Omega}{1-m_\eta^{\mathrm{irr}}(z)\Omega}}$$

where $m_\eta^{\mathrm{irr}}(z) = M_\eta^{\mathrm{irr}}(z)\Omega^{-2}$ is the dimensionless irreducible memory-kernel.
In the time domain one gets the Brownian of motion:

$$\dot{\phi}(t) + \Omega\phi(t) + \Omega \int_0^t \mathrm{d}\tau m_\eta^{\mathrm{irr}}(t-\tau)\dot{\phi}(\tau) = 0 \ , \qquad (4.3.13)$$

with the frequency (calculation in appendix G)

$$\Omega_{k,f} = \omega_0 p \left(1 - \frac{\sum_{i=0}^{f-1} \binom{k}{i} \mathrm{e}^{-(k-i)\beta}}{(1+\mathrm{e}^{-\beta})^k} \right) \quad \Rightarrow \quad \Omega_{3,2} = \omega_0 p \left(1 - \frac{\mathrm{e}^{-3\beta} + 3\mathrm{e}^{-2\beta}}{(1+\mathrm{e}^{-\beta})^3} \right) \ .$$
$$(4.3.14)$$

The system frequency, ω_0, can be determined for small times,$t \to 0$. The convolution is vanishing for $t \to 0$ and Eq. (4.3.13) becomes the easy solvable homogeneous differential $\dot{\phi}(t) + \Omega\phi(t) = 0$ which is solved with the ansatz $\phi(t) \propto \exp(\Omega t)$. Now, since the frequency, Ω, is propotional to ω_0, one can match ω_0 for a given concentration p. The frequency, Ω, and the initial up-spin concentration, p, have the same behavior. Both are starting at one (here Ω is normalized by ω_0) and they decay exponentially to a finite value.
In this section we defined a correlation function for the up-spins, $\phi(t)$, and introduced
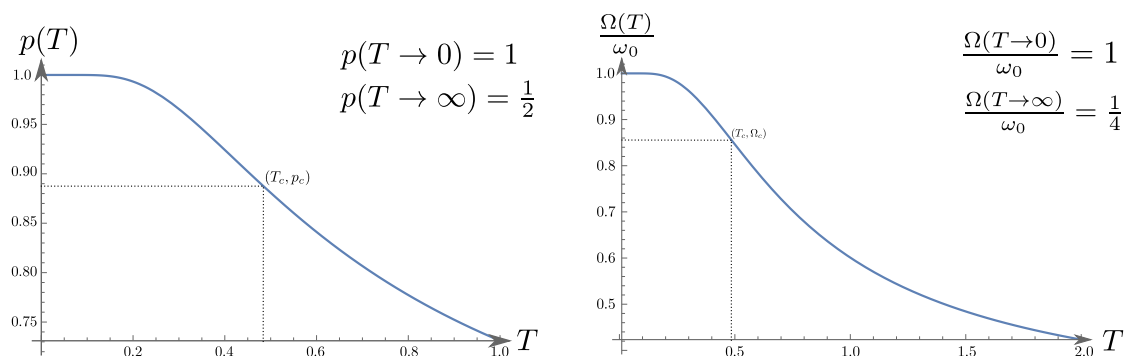
Figure 4.3.1: *Left side*: For $T \to 0$ the up spin concentration is $p(0) = 1$, so the Bethe lattice only has up spins. For larger temperatures $T \to \infty$ the concentration converges to $p(T \to \infty) = 1/2$. One also can see the critical temperature T_c for having up-spin clusters.*Right side*: The frequency Ω, normalized by ω_0, as a function of the temperature (concentration). For decreasing temperature, the frequency goes to the normalized system frequency, ω_0. For increasing temperature the frequency decreases to a quarter of its initial value.

the irreducible memory kernel, motivated from the works of Kawasaki, to get the Brownian of motion for the Fredrickson-Andersen model. We also have an analytical expression for the frequency, Ω. In the next section we try to connect the microscopic dynamics of the correlation function, $\phi(t)$, with the long time limit of the persistence function, $\psi^\infty(t)$.

4.4   Bifurcation Scenario in the Spin Model

In section 4.2 we introduced in Eq. (4.2.1) the probability of up-spins in the ground state, q, which is a function of the initial up-spin concentration, p. We also know that there is a critical concentration $p_c < 1$ where some up-spin clusters will survive in the ground state. Below this concentration the probability of an up-spin is zero, $q = 0$, and at the critical concentration there is an discontinuous jump from $q = 0$ to $q = q_c > 0$. In the work of Sellitto it is shown that above the critical concentration, $p > p_c$, the probability grows with the square root of the distance to the critical point, $q \propto \sqrt{\epsilon}$, where $\epsilon = (p - p_c)/p$ is the separation parameter [77]. Now, this phenomenon should be shown here for the simplest case $(k, f) \to (3, 2)$, where Eq. (4.2.1) becomes

$$q = p(q^3 + 3(1 - q)q^2) \ . \tag{4.4.1}$$

The solutions of this are

$$q = 0 \qquad \text{and} \qquad q_\pm = \frac{3}{4} \pm \frac{3}{4}\sqrt{\frac{p - \frac{8}{9}}{p}} \ . \tag{4.4.2}$$

Since the probability can only be a real number, the radicand can not be negative. So the condition for the critical concentration p_c is a vanishing radicand at $p_c = 8/9$. At p_c the critical probability of an up-spin in the ground state is given by $q_c = 3/4$. So q has the form $q_\pm = q_c\,(1 \pm \sqrt{\epsilon})$. From the two solutions, q_+ and q_-, we need the one which fulfills the condition $q(p = 1) = 1$, which means that an fully occupied lattice with up-spins is not affected from the percolation and so the ground state is occupied with only up-spins, too. We are starting the Fredrickson-Andersen model with the initial concentration, p, then some of the up-spins will be flipped into down-spins, so the next stable state for the up-spins is given by $q = 0$ or q_+. For $p > p_c$ the up-spin concentration only decays to q_+, so the only physical solution here is q_+ and not zero, although $q = 0$ is a mathematical solution of Eq. (4.2.1). So the solution of Eq. (4.2.1) is $q = 0$ for $p \in [0, 8/9)$ and $q = (1 + \sqrt{\epsilon})$ for $p \in [8/9, 1]$.

One can find the same behavior, in the persistence function, too. It is zero till the critical concentration, here the persistence function and the correlation function have the same critical up-spin concentration, and at the critical concentration both are jumping to a finite value, q_c or ψ_c^∞, and behave like $\sqrt{\epsilon}$ above p_c.

In Fig. 4.4.1 one can see this behavior for both functions, this discontinuous change of the function at a critical point is called bifurcation [4].

Now, we want to connect the Fredrickson-Andersen model with the mode coupling theory. In section 4.3 we introduced the spin autocorrelation function in Eq. (4.3.8) and the corresponding Brownian equation of motion in Eq. (4.3.13). In the long time limit, $t \to \infty$ the spin autocorrelation function converges to the up-spin probability in the ground state, $\phi(t \to \infty) = q$. So the long time limit of the equation of motion turns into to the bifurcation equation, which is derived in section 2.6. Here, we have for the long time limit of the correlation function the following expression

$$m(t \to \infty) = \frac{q}{p - q} = \frac{p(q^3 + 3(1 - q)q^2)}{p - q} \ . \tag{4.4.3}$$
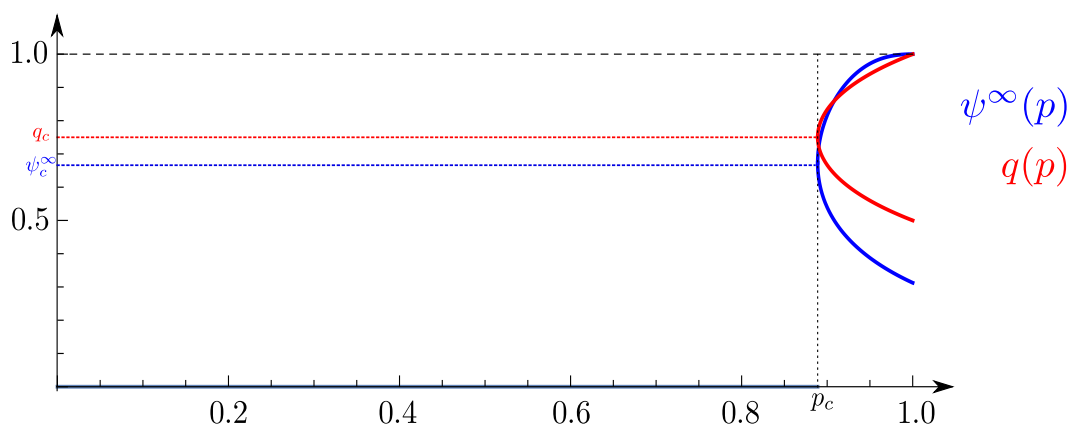
Figure 4.4.1: Bifurcation scenario in FA model for the couple $(f, k) \to (2, 3)$. The red curve is the solution of Eq. 4.4.1. At a value of $(p_c, q_c) = (8/9, 3/4)$ the probability of up spins in the groundstate, $q(p)$, jumps discontinuously from the solution $q = 0$ to the solution $q_\pm = q_c(1 \pm \sqrt{\epsilon})$. The blue curve is the persistence function, $\psi_\pm^\infty(p)$, which is given by Eq. 4.2.3. The discontinuous jump is at point $(p_c, \psi_c^\infty) = (8/9, {}^{2757}/_{4096})$. For both functions a monotonic increasing up spin probability, so $q_+(p)$ and $\psi_+(p)$, is the physical solution.

Here, the peculiarity of Eq.(4.4.3) should be emphasized, we have a memory kernel without any approximations. We know the memory kernel for the long time limit exactly.

Till now we only know the memory kernel for $t \to \infty$ without any approximations and we are interested in the dynamics of the Fredrickson-Andersen model. There are many possibilities to get the limit in Eq. (4.4.3). An intuitive way to do this is to say that the q results from the spin autocorrelation function, $\phi(t)$, and replace all the q's with it, $q \to \phi(t)$. Nevertheless, there are other completely monotonic functions [97, 98] like the compositions, $\phi(f(t))$, where $f(t)$ is also a completely monotonic function, which have the same long time limit as Eq. (4.4.3). Another problem is, that the memory kernel $\tilde{m}(\phi(t))$ could be a product between our known memory kernel and a factor, which goes to one for $t \to \infty$ like $\tilde{m}(\phi(t)) = m(\phi(t)) \cdot \exp(\frac{\tau}{t})$. In this case $\exp(\frac{\tau}{t})$ goes to one for long times and $\tilde{m}(\phi(t \to \infty)) = m(\phi(t \to \infty))$. In this thesis we will conjecture that we can replace the q intuitively with $\phi(t)$ and that the memory function is not a product of more functions.

Why do we need this assumption? We are interested into the dynamics of the FA-model and to describe the dynamics we use the language of the mode coupling theory, which

gives us two exponents, a and b, for the decay of the correlation function. In Eq. (2.6.6) one can see that the exponent parameter λ, which is related to the two exponents, can only be calculated with the knowledge of the Laplace transformation of the master function, $G(t)$. In Eq. (2.6.6) we have $\phi(t) \propto G(t)$, now if we change our correlation function, $\phi(t) \rightarrow \phi(f(t))$, or multiply and additional term to our memory kernel, we need to rewrite the equation and get some prefactors, which are changing the definition of our exponent parameter, λ.

We calculate λ for our assumption, $q \rightarrow \phi(t)$: With Eq. (4.4.3) we have $\Delta\mathcal{F}$ which is defined in section 2.6.1. So we can calculate the different δ_k-terms of Eq. (2.6.6) and get $\delta_0 = 0$ and $\delta_1 = 0$. The first non-vanishing term is δ_2, which occurs at an A_2-singularity, with (see appendix C)

$$\delta_2 = \frac{1}{2!} \left. \frac{\partial^2 \Delta\mathcal{F}[p_c, q]}{\partial q^2} \right|_{q=q_c} \frac{(p_c - q_c)^3}{p_c} = -\frac{25}{864} \ . \tag{4.4.4}$$

Now, the exponent parameter, $\lambda = 1 + \delta_2$, can be calculated exactly to the value $^{839}/_{864}$. With the exponent parameter, we have the two exponents we need to describe the dynamics, $a = 0.121...$ and $b = 0.147...$.

For microscopic times $t \rightarrow 0$ the correlation function goes to $\phi(t \rightarrow 0) \rightarrow p$, as we can see directly in Eq. (4.4.3) the memory kernel diverges, $m(p, \phi(t) \rightarrow p) \propto (p - \phi(t))^{-1}$. To regularize the memory kernel we rewrite the divergent term, $(p - \phi(t))^{-1} = p^{-1} \sum_i^M (\phi(t)/p)^i$, which is exact for $M \rightarrow \infty$ and can be interpreted as a resummation of many-site interactions.

The same calculations can be done for different (f, k)-pairs to get A_2 bifurcations with different critical values, which can be seen in Fig. 4.4.2. In MCT the range of the exponent parameter is $\lambda \in [0.5, 1]$ [9] and we want to find out the upper and lower limit in the FA model on the Bethe lattice. To calculate λ for any (f, k)-pair we need the real roots of Eq. (4.2.1), which is a polynomial of the degree of k. After that we have to find out, which of the real roots is belonging to the bifurcation. Here we use the condition $q(p = 1) = 1$ to find out the critical value for a given (f, k)-couple. For $(3, 2)$ we made the calculations above, here we only have a polynomial of third order. With the knowledge of the $q = 0$ solution, we can factorize q and get a polynomial of second order which can be calculated easily. All of the three solutions are real functions and we can describe the corresponding bifurcation. For a high connectivity, k, it is

even problematic to get the roots with some numerics. I made the calculation for the first 20 couples to get an intuition for the range of λ. In Fig. 4.4.2 one can see that λ is decreasing for $\lim_{k\to\infty}(k-1,k)$. At the moment I don't know the limit. Based on MCT I would speculate $\lambda = 0.5$ as the limit, but there is no reason why it should be. The exponent parameter λ decreases very slowly even for the pair $(99, 100)$ its value is $\lambda = 0.8432...$. An increasing λ can be seen for $\lim_{k\to\infty}(f_{\text{const}}, k)$, where f_{const} is a fixed facilitation parameter. It seems that λ converges here to one, which is an A_3-singularity in Arnold's terminology. Since the decay at an A_3 singularity is a logarithmic one, we expect for $\lambda \to 1$ very slow decays. So to compare our theory with some simulations at least we need 6 orders of magnitude in time to represent the relaxation to the plateau.
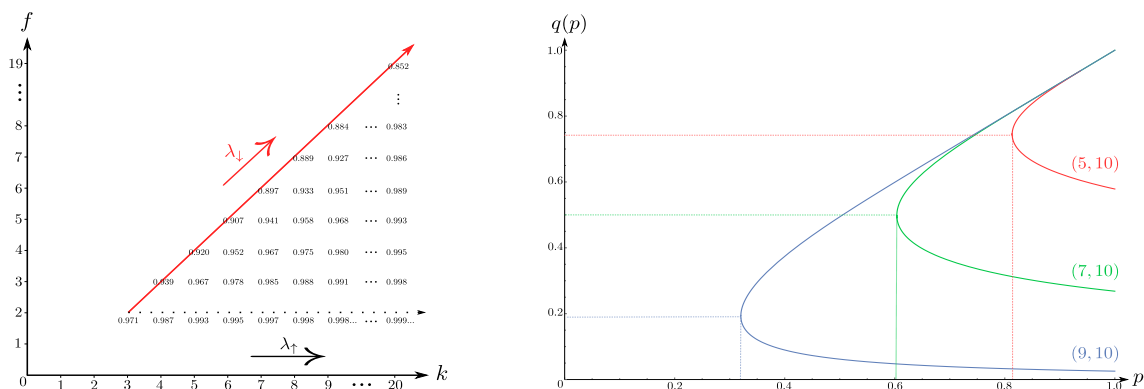
Figure 4.4.2: *Left*: The exponent parameter, λ, for different (f, k)-couple. One can see an increasing exponent parameter, $\lambda \to 1$, for the limit $\lim_{k\to\infty}(f_{\text{const}}, k)$. A decreasing λ is given for the limit $\lim_{k\to\infty}(k-1,k)$. *Right*: Different bifurcation scenarios for different (f, k)-couples. One can see a shrinking curvate from the $(5, 10)$-couple to the $(9, 10)$-couple, which means a decreasing λ

From the geometrical point of view, the exponent parameter is the curvature of the bifurcation. In Fig. 4.4.2 one can see the bifurcation for different (f, k)-pairs. In all of the pairs the connectivity is fixed to $k = 10$. One can see that the critical initial concentration of up-spins is decreasing for increasing facilitation parameter, f. This is intuitive, for $f = 5$ you at least need only 5 down spin neighbors to flip a spin, and for $f = 9$ you need 9 down spin neighbors. So the initial critical up spin concentration, p_c, must be bigger for $f = 5$ than for $f = 9$. The larger the initial up spin concentration the higher the value of the exponent parameter, λ. In Tab. 4.4.1 one can see different critical initial up spin concentrations, p_c, the critical ground state probability, q_c, and

Table 4.4.1: Different (f, k)-couples and the corresponding parameters, p_c, q_c, and λ. For a constant facilitation parameter, f, and a diverging connectivity, $k \to \infty$, the critical values , p_c and q_c, are going to one. A decreasing to zero of the critical values is given for $f = k - 1$ and $k \to \infty$.

(f, k)	p_c	q_c	λ
$(2, 3)$	$8/9$	$3/4$	$839/864$
$(2, 4)$	0.9493	0.8936	0.9868
$(2, 5)$	0.9710	0.9413	0.9925
$(3, 4)$	0.7249	0.5435	0.9395
$(3, 5)$	0.8349	0.7265	0.9668
$(4, 5)$	0.6025	0.4180	0.9203
$(2, 20)$	0.9987	0.9978	0.9987
$(19, 20)$	0.1641	0.0958	0.8583

the different exponent parameter, λ, for different pairs of (f, k).

In Tab. 4.4.1 one can see that the initial up-spin concentration is always higher than the one in the groundstate, $p_c > q_c$. Since the Hamiltonian prefers down spins, the up-spin concentration will never increase.

From the definition above we know that the long time limit of the persistence function, ψ^∞, is connected to the long-time limit of the correlation function, $\phi(t \to \infty)$. Near the plateau, ψ^∞ we can expand the persistence function to

$$\psi(t \sim t_\sigma) \simeq \psi_c^\infty + \frac{\partial \psi^\infty(q)}{\partial q}\bigg|_{q=q_c} [\phi(t) - q_c] \ . \tag{4.4.5}$$

As Eq. (4.4.5) shows, the correlation function, $\phi(t)$, is the only time depending term of the persistence function. Therefore, the bifurcation and especially the exponent parameter, λ, will be inherited. So the calculated exponents, a and b, remains the same. We also know that for $t \to 0$ the convolution vanishes, $\int_0^{t \to 0} m(t - \tau)\dot{\phi}(\tau) \to 0$, so that the EOM is solved by an exponential decay, $\psi(t) \sim e^{-t/\tau_\psi}$, in the microscopic time scale, τ_ψ. The decay from the plateau at a time scale $\tau_\alpha \sim t_{\sigma'} \propto \sigma^{-\gamma}$ is well described by an exponential relaxation, $\psi(t \sim t_{\sigma'}) \simeq e^{-t/\tau_\alpha}$ [99]. So the persistence function is well

known at all times and we can interpolate it to

$$\psi(t) = \mathrm{e}^{-t/\tau_\psi} + \left[\psi_c^\infty + \left. \frac{\partial \psi^\infty(q)}{\partial q} \right|_{q=q_c} [\phi(t) - q_c] \right] (1 - \mathrm{e}^{-t/\tau_\psi}) \mathrm{e}^{-t/\tau_\alpha} \ . \qquad (4.4.6)$$
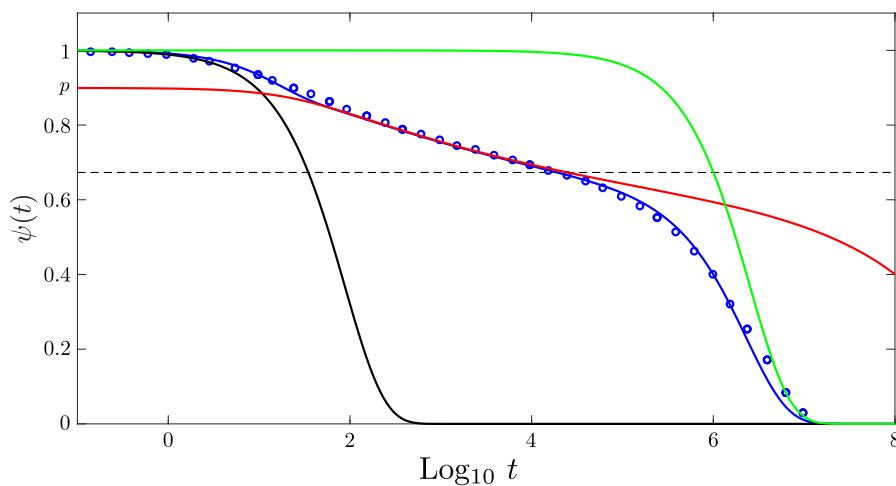
Figure 4.4.3: The persistence function, $\psi^\infty(t)$, for the FA-model on the Bethe lattice for an initial up-spin concentration of $p = 0.885 < 8/9 = p_c$. The dotted points are from the simulations of Sellitto [8], and the straight blue curve is the persistence function, $\psi(t)$, which is defined in Eq. (4.4.6), here we used the regularized memory kernel and cut at $M = 23$. The red curve is the correlation function, $\phi(t)$, one can see here that the correlation function starts at p, $\phi(0) = p$. According to Eq. (4.4.5), the correlation function fits the persistence function very well near the plateau. The black curve is the short time evolution, $\psi(t) \sim \mathrm{e}^{-t/\tau_\psi}$, of the persistence function. Here the microscopic timescale is $\psi_\tau = 88$. The green curve is the $\psi(t \sim t_{\sigma'}) \simeq \mathrm{e}^{-t/\tau_\alpha}$ relaxation, with the relaxation time $\tau_\alpha = 175000$.

In Fig. 4.4.3 we see the simulation of Sellitto [8] and compare it with our theoretical calculations. In chapter 5 we will discuss more results and we will also analyze some problems of the simulations.

Nevertheless, we are using in Fig. 4.4.3 a regularized memory kernel, and we cut the upper limit of the sum, M, at some point to avoid divergences. The summation limit, M, is for a given (f, k)-couple and a given initial concentration p a fit parameter and can not be extracted from the theory.

Conclusion

The main idea of this chapter is to identity Eq. (4.2.1) as a bifurcation equation in the sense of the mode coupling theory. With those bifurcations we derive in MCT the dynamics of the system. Therefore, we only need the exponent parameter, λ. Now, for the calculation of λ we assume that we can replace the ground state probability with the correlation function, $q = \phi(t)$. We have to show that this assumption is the only physically correct one.

When we compare our calculated exponent parameter, $\lambda = 0.971$, with the fitted one from Sellitto, $\lambda_s = 0.815$, we see a large deviation. Notice, in MCT the range of the exponent parameter is given by $\lambda \in [0.5, 1]$. There could be two reasons for that: First, we calculated the exponent parameter at the critical point, whereas the simulation is far away from the critical point and it is only for a finite lattice. So the fitted λ_s does not reflects the FA-model on the Bethe lattice. The second reason could be a wrong assumption $q \to \phi(t)$, so that the dynamics is described with a much more complicated $\mathcal{F}[\phi(f(t))]$.

Nevertheless, in Fig. 4.4.3 we see a good agreement between the simulation and the theoretical calculated persistence function.

Bibliography

[1] U. Bengtzelius, W. Götze and A. Sjölander, J. Phys. C **17**, 5915 (1984).

[2] W. Götze, *Liquids, Freezing and Glass Transition*, pages 287–503. (North-Holland, Amsterdam, 1991).

[3] W. Götze and L. Sjögren, J.Phys.: Condens. Matter **1**, 4183 (1989).

[4] V. I. Arnold, *Dynamical Systems V, Encyclopedia of Mathematical Science.* (Springer-Verlag, 1994).

[5] W. Götze and L. Sjögren, J.Phys. C **17**, 5759 (1984).

[6] M. Mezard, G. Parisi and M. Virasoro, *Spin Glass Theory and Beyond.* (WORLD SCIENTIFIC, 1986).

[7] K. Binder and W. Kob, *Glassy Materials and Disordered Solids.* (WORLD SCIENTIFIC, Revised edition, 2011).

[8] M. Sellito, Phys. Rev. Lett. **115**, 225701 (2015).

[9] W. Götze, *Complex dynamics of glass-forming liquids: A mode-coupling theory.* (Oxford University Press (OUP), Oxford, 2009).

[10] J.-P. Boon and S. Yip, *Molecular Hydrodynamics.* (McGraw-Hill, New York, 1980).

[11] J.-P. Hansen and I. R. McDonald, *Theory of Simple Liquids.* (Academic Press, London, 2nd edition, 1986).

[12] D. Foster, *Hydrodynamic Fluctuations , Broken Symmetry, and Correlation Functions.* (Benjamin, Reading, MA, 1975).

[13] R. Haussmann, Z. Phys. B **79**, 143 (1990).

[14] J. L. Barrat, W. Götze and A. Latz, J. Phys.: Condens. Matter **1**, 7163 (1989).

[15] H. W. Jackson and E. Feenberg, Rev. Mod. Phys. **34**, 686 (1962).

[16] G. Szamel and H. Löwen, Phys. Rev. A **44**, 8215 (1991).

[17] M. Fuchs, Dissertation, TU München, (1993).

[18] P. N. Pusey, *Liquids, Freezing and Glass Transition*, page 763. (North-Holland, Amsterdam, 1991).

[19] V. I. Arnold, Funct. Anal. Appl. **6**, 254-272 (1972).

[20] V. I. Arnold, Russ. Math. Survey **30**, 1-75 (1975).

[21] T. Franosch, M. Fuchs, W. Götze, M. R. Mayr and A. P. Singh, Phys. Rev. E **55**, 6 (1997).

[22] K. Dawson, G. Foffi, M. Fuchs, W. Götze F. Sciortino, M. Sperl P. Tartaglia, T. Voigtmann and E. Zaccarelli, Phys. Rev. E **63**, 011401 (2000).

[23] W. Götze and M. Sperl, J. Phys.: Cond. Matter **15**, 11 (2003).

[24] W. Götze and M. Sperl, J. Phys.: Cond. Matter **16**, 42 (2004).

[25] H. Ikeda, K. Miyazaki and G. Biroli, Europhys. Lett. **116**, 56004 (2016).

[26] M. Sperl, Dissertation, TU München, (2003).

[27] A. Liluashvili, Dissertation, Universität Düsseldorf, (2017).

[28] E. Leutheusser, Phys. Rev. A **29**, 2765 (1984).

[29] W. Götze and M. Sperl, Phys. Rev. Lett. **92**, 105701 (2004).

[30] M. Sperl, Phys. Rev. E **74**, 011503 (2006).

[31] T. R. Kirkpatrick and D. Thirumalai, Phys. Rev. B **37**, 5342 (1988).

[32] W. Götze and M. Sperl, Phys. Rev. E **66**, 011405 (2002).

[33] J. Bosse and U. Krieger, J. Phys. C **19**, L609 (1987).

[34] M. Sperl, AIP Conference Proceedings **708**, 559 (2004).

[35] E. Frey and F. Schwabl, Hyperfine Interact. **50**, 765 (1989).

[36] P. K. Haff, J Fluid Mech. **134**, 401 (1983).

[37] N. V. Brilliantov, F. Spahn, J. M. Hertzsch and T. Pöschel, Phys. Rev. E **53**, 5382 (1996).

[38] L. Laurent, A. D. Rosato and R. N. Dave, Phys. Rev. E, **56**, 5717 (1997).

[39] T. Aspelmeier, F. Gerl and A. Zippelius, *A microscopic modell of energy dissipation in granular collisions*, pages 287–503. (Kluwer Academic, 1998).

[40] I. Goldhirsch, Annu. Rev. Fluid Mech **35**, 267 (2003).

[41] N. Brilliantov and T. Pöschel, *Kinetic Theory of Granular Gases.* (Oxford University Press, 2nd edition, 2004).

[42] T. Pöschel and S. Luding, *Free Cooling of Particle with Rotational Degree of Freedom*, pages 31–58. (Springer-Verlag, Berlin, 2001).

[43] B. L. Holian and D. J. Evans, J. Chem. Phys. **83**, 3560 (1985).

[44] J. B. Javier, D. Cubero, *Hydrodynamic Transport Coefficients of Granular Gases*, pages 59–78. (Springer, 2001).

[45] M. Born and H. S. Green, Proc. R. Soc. A **188**, 1012 (1946).

[46] M. H. Ernst, J. R. Dorfmann, W. R. Hoegy and J. M. J. van Leeuwen, Proc. R. Soc. A **188**, 1012 (1946).

[47] W. T. Kranz, Dissertation, Universität Göttingen, (2011).

[48] A. R. Altenberger, Physica A **80**, 46 (1975).

[49] T. P. C. Noije and M. H. Ernst, Granular Matter **1**, 57 (1998).

[50] G. W. Baxter and J. S. Olafsen, Phys. Rev. Lett. **99**, 028001 (2007).

[51] W. T. Kranz, M. Sperl and A. Zippelius, Phys. Rev. E, **87**, 022207 (2013).

[52] Y. Uehara, Y. T. Lee, T. Ree and F. H. Ree, J. Chem. Phys. **70**, 1884 (1979).

[53] B. Bildstein and G. Kahl, J. Chem. Phys. **100**, 5882 (1994).

[54] J. G. Kirkwood, J. Chem. Phys **3**, 300 (1935).

[55] J. G. Kirkwood and E. M. Boggs, J. Chem. Phys **10**, 394 (1942).

[56] A. F. E. M. Haffmans, I. M. de Schepper, J. P. J. Michels and H. van Beijeren, Phys. Rev. A **37**, 2698 (1988).

[57] A. Singer, J. Chem. Phys **121**, 3657 (2004).

[58] J. K. Percus and G. J. Yevick, Phys. Rev. **110**, 1 (1958).

[59] A. Latz, Dissertation, Technische Universität München, (1991).

[60] T. Voigtmann, Dissertation, Technische Universität München, (2003).

[61] J. G. Kirkwood, J. Chem. Phys **15**, 72 (1947).

[62] J. L. Lebowitz and J. S. Rowlinson, J. Chem. Phys. **41**, 133 (1964).

[63] J. A. Mydosh, *Spin Glasses.* (Taylor&Francis, 1st edition, 1993).

[64] S. F. Edwards and P. W. Anderson, J. Phys. F **5**, 965 (1975).

[65] D. Sherrington and S. Kirkpatrick, Phys. Rev. Lett. **35**, 1792 (1975).

[66] D. Panchenko, J. Stat. Phys. **149**, 362 (2012).

[67] B. Derrida, Phys. Rev. Lett. **45**, 79 (1980).

[68] B. Derrida, Phys. Rev. B **24**, 2613 (1981).

[69] T. Castellani and A. Cavagna, J. Stat. Mech **2005**, P05012 (2005).

[70] D. Gaunt and M. E. Fisher, J. Chem. Phys. **43**, 2840 (1965).

[71] D. Gaunt, J. Chem. Phys. **46**, 3237 (1967).

[72] W. Kob and H. C. Andersen, Phys. Rev. E **48**, 4364 (1993).

[73] M. Sellitto, J Phys: Cond. Matter **14**, 1455 (2002).

[74] G. H. Fredrickson and H. C. Andersen, Phys. Rev. Letter **53**, 1244 (1984).

[75] L. Berthier and G. Biroli, Rev. Mod. Phys. **83**, 587 (2011).

[76] F. Ritort and P. Sollich, Adv. Phys. **52**, 219 (2003).

[77] M. Sellitto, G. Biroli and C. Toninelli, Europhys. Lett. **69**, 496 (2005).

[78] R. Peierls, Mathm. Proc. Cam. Phil. Soc. **32**, 477 (1936).

[79] I. S. Graham, L. Piché and M. Grant, Phys. Rev. E **55**, 2132 (1997).

[80] G. H. Fredrickson and S. A. Brawer, J. Chem. Phys **84**, 3351 (1986).

[81] N. Cancrini, F. Martinelli, C. Robert and C. Toninelli, *Methods of contemporary mathematical statistical physics*, page 307. (Springer, 2009).

[82] A. C. D. van Enter, J.Stat.Phys. **48** 943 (1987).

[83] S. J. Pitts and H. C. Andersen, J. Chem. Phys. **113**, 3945 (2000).

[84] J. Reiter, F. Mauch and J. Jäckle, Physica A **184**, 458 (1992).

[85] M. Mézard and G. Parisi, Euro, Phys. B **20**, 217 (2001).

[86] J. Chalupa, P. L. Leath and G. R. Reich, J. Phys. C **12**, L31 (1979).

[87] J. Adler, Physica A **171**, 453 (1991).

[88] S. N. Dorogovtsev, A. V. Goltsev and J. F. F. Mendes, Rev. Mod. Phys. **80**, 1275 (2008).

[89] H. Risken, *The Fokker-Planck Equation*. (Springer-Verlag, 2nd edition, 1984).

[90] K. Kawasaki, Physica A **215**, 61 (1995).

[91] W. Götze and L. Sjögren, Trans. Theo. Stat. Phys. **24**, 801 (1995).

[92] J. Jäckle and D. Sappelt, Physica A **192**, 691 (1993).

[93] K. Kawasaki, J. Stat. Phys. **87**, 981 (1997).

[94] B. Cichocki and W. Hess, Physica A **141**, 475 (1987).

[95] S. J. Pitts, T. Young and H. C. Andersen, J. Chem. Phys. **113**, 8671 (2000).

[96] S. J. Pitts and H. C. Andersen, J. Chem. Phys. **114**, 1101 (2001).

[97] T. Franosch and T. Voigtmann, J. Stat. Phys. **109**, 237 (2002).

[98] G. Gripenberg, S. O. Londen and O. Staffans: *Volterra Integral and Functional Equations.* Encyclopedia of Mathematics and its Applications, (Cambridge University Press, 1990).

[99] N. Cancrini, F. Martinelli, C. Roberto and C. Toninelli, Probab. Theory Relat. Fields **161**, 247 (2015).

Part II
Application

Asymptotically Exact Solution of the Fredrickson-Andersen Model

K.Önder[1,2], M.Sperl[2,1], and W.T.Kranz[1]

[1] *Institut für Theoretische Physik, Universität zu Köln, 50937 Köln, Germany*

[2] *Institut für Materialphysik im Weltraum, Deutsches Zentrum für Luft- und Raumfahrt (DLR), 51170 Köln, Germany*

Abstract

The Fredrickson-Andersen (FA) model—a kinetically constrained lattice model—displays an ergodic to non-ergodic transition with a slow two-step relaxation of dynamical correlation functions close to the transition point. We derive an asymptotically exact solution for the dynamical occupation correlation function of the FA model on the Bethe lattice by identifying an exact expression for its memory kernel. The exact solution fulfills a scaling relation between critical exponents and allows to calculate the exponents explicitly. In addition, we propose an approximate dynamics that describes numerical data away from the critical point over many decades in time.

Slow relaxation is not restricted to molecular fluids dominated by pairwise interactions. On the contrary, systems abound where the effective dynamics is facilitated by the number of neighbors in a favorable state exceeding a threshold. Dynamic facilitation applies to opinion dynamics [1], voter models [2, 3], and infection spreading [4] but has also been used to understand the low temperature phase of magnetic alloys [5, 6], granular compaction [7], rigidity percolation [8], and the jamming transition [9, 10].

Most prominently it lies at the heart of the dynamic facilitation picture [11–16] of the glass transition [17–20]. The k-core decomposition of graphs [21, 22] yields a statistical description of, *e.g.*, social groups [21] and the brain [23]. K-core decomposition can be framed as a dynamic facilitation problem [24] yielding, *e.g.*, insight into the resilience of social network data sets against de-anonymization [25].

A paradigmatic example of a kinetically constraint model [15, 26] implementing dynamic facilitation is the Fredrickson-Andersen (FA) model which is defined on a lattice with sites $i = 1, \ldots, N$ decorated with occupation numbers $n_i \in \{0, 1\}$. The Hamiltonian $\mathcal{H} = \mu \sum_i n_i$ is trivial and $\mu > 0$ favors the empty lattice. A site i may, however, only change its state if it has at least f empty nearest neighbors [12, 27]. Bootstrap percolation [6, 28–30] is concerned with the ground state of the FA model that is kinetically reachable from an initial condition with an occupation probability p. For $p = 1$, clearly the occupation probability in the ground state $q = 1$, whereas for $p \approx 0$ an empty ground state, $q = 0$, can be reached almost surely. The question arises, if there is a nontrivial concentration, p_c, for the emergence of an infinite occupied cluster in the ground state, $q > 0$. For $f = 1$ and for arbitrary f on hypercubic lattices $\mathbb{Z}^d$ it has been shown that $p_c = 1$ [27, 31]. Bootstrap percolation on the Bethe lattice and on random graphs, however, feature a transition at a finite $p_c < 1$ [6, 32, 33].

At finite temperatures $T > 0$ [1] [34] we equip the FA model with transition rates that satisfy detailed balance. Without constraints, the Hamiltonian $\mathcal{H}$ would entail an equilibrium mean occupation $\langle n_i \rangle = 1/(1 + e^{1/T})$. This still holds under the constrained dynamics as long as $\langle n_i \rangle < p_c$, however, for $\langle n_i \rangle > p_c$, the dynamics is restricted to the sites that are not permanently constrained by the frozen percolating cluster [35]. For $\langle n_i \rangle \nearrow p_c$, numerical simulations of the FA model [36–39] show a two-step relaxation of time-correlation functions, $\phi(t)$, with a fast relaxation to a plateau value, $\phi(t) \simeq q > 0$, followed by a second relaxation, $\phi(t) \to 0$, on a time scale that diverges towards p_c. A two-step relaxation with a divergent relaxation time is one of the experimental fingerprints of the glass transition [17] and motivated the FA model as an effective description of the glass transition. Close to the plateau, $|\phi(t) - q| \ll 1$, the relaxation

---

[1]Temperature is measured in units of $|\mu|/k_B$
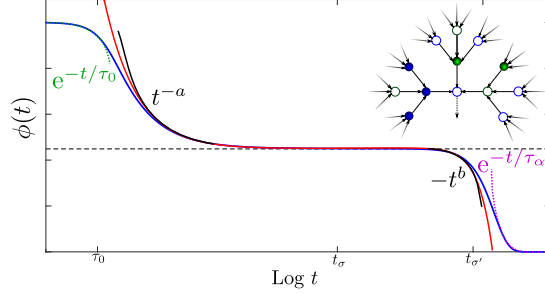
Figure 5.1.1: Generic occupation correlation $\phi(t)$ (blue) of the oriented FA model (OFA) close to the critical point, $\sigma \ll 1$, compared to the asymptotic scaling function $G_\sigma(t) \simeq \phi(t) - q_c$ [Eq. (5.1.8), red] and the critical laws t^{-a} and $-t^b$ [Eq. (5.1.1), black]. The plateau q_c (horizontal dashed line) is crossed, on a divergent timescale $t_\sigma \sim \sigma^{-\delta}$ and $G_\sigma(t)$ provides a faithful description in a divergent time window $\tau_0 \ll t \ll t'_\sigma \sim \sigma^{-\gamma}$ beyond the microscopic relaxation time τ_0, followed by exponential relaxation on a timescale $\tau_\alpha \sim t'_\sigma$. *Inset:* Section of the OFA for coordination $k = 3$, and facilitation $f = 2$. Arrows denote the orientation, filled (open) vertices denote occupied (empty) sites, and blue vertices are frozen while green may change. See Table 7.2.1 for values of the critical exponents.

is generically well described by power laws [40],

$$\phi(t) - q \propto \begin{cases} t^{-a} \text{ for } \phi(t) > q, \\ -t^b \text{ for } \phi(t) < q. \end{cases} \tag{5.1.1}$$

A complementary description of the glass transition, independent of the dynamic facilitation picture, is provided by mode-coupling theory (MCT) [41–43] which starts from the formally exact equation of motion

$$\tau_0 \dot{\phi}(t) + \phi(t) + \int_0^t \mathrm{d}t' m(t - t') \dot{\phi}(t') = 0, \tag{5.1.2}$$

where the dot denotes the time derivative and τ_0^{-1} is the short time relaxation rate. The eponymous mode-coupling approximation (MCA) expresses the unknown memory kernel $m(t)$ by a polynomial in $\phi(t)$. Standard MCT predicts a scaling relation,

$$\frac{\Gamma^2(1-a)}{\Gamma(1-2a)} = \frac{\Gamma^2(1+b)}{\Gamma(1+2b)}, \tag{5.1.3}$$

Table 5.1.1: Critical exponents $a, b, \delta = 1/2a, \gamma = (1/2a) + (1/2b)$ and exponent parameter λ characterizing the slow relaxation of the FA model for coordination $k = 3$ and facilitation $f = 2$ (see Fig. 5.1.1). Comparing the exact results derived here to fits from simulation data.

	Theory	Simulation	
		Sellitto [38]	de Candia *et al.*[39]
λ	$^{839}/_{864}$	0.815	0.79
a	$0.121\ldots$	0.27	0.29
b	$0.147\ldots$	0.45	0.50
δ	$4.13\ldots$	1.85	1.72
γ	$7.53\ldots$	2.96	2.72

between the exponents in Eq. (5.1.1) involving the Euler Gamma-function. MCAs have been attempted for the FA model [44–48] starting with Fredrickson and Andersen [12] but were of limited success. In particular, MCT for the FA model has a tendency to predict spurious transitions [15]. Also other approaches did not capture the slow relaxation [49].

Recent numerical evidence, however has shown that despite these reservations, the scaling relation (5.1.3) seems to be verified in the FA model on the Bethe lattice modeled as a random regular graph (RRG) [36–39, 50]. Proof for this surprising discovery is highly desired [27, 51] but missing so far.

In this letter we derive an asymptotically exact solution of Eq. (5.1.2) for the FA model on the Bethe lattice. We show that Eq. (5.1.1) constitutes the lowest order in a series expansion of this solution and that the scaling relation (5.1.3) holds exactly. Encouraged by these results we propose an approximate, regularized memory kernel valid for all times. Comparing with numerical data far away from the critical point, we are able to describe the two step relaxation of the FA model over many decades in time.

Model.—We consider the oriented FA model (OFA) with facilitation parameter $f \geq 2$ on the Bethe lattice. To be precise, we define the Bethe lattice [52] as the infinite k-ary rooted tree [53], $2 \leq f < k$. In line with Sellitto's numerical work [36–38] we assume Metropolis dynamics with transition rates $w(n_i \to 1 - n_i) = \exp[(n_i - 1)/T]C_f(\mathcal{K}_i)$. Here $\mathcal{K}_i$ denotes the set of children of site i and $C_f : \mathcal{K}_i \mapsto \{0, 1\}$ implements the kinetic

constraint [2] [54] (cf. Fig. 5.1.1).

For simplicity we aim to describe the relaxation to equilibrium from a well defined initial condition. Assume the initial $n_i(0)$ are drawn from a Bernoulli distribution with $p = 1/(1 + e^{-1/T}) > 1/2$ [3] [55]. To assure ergodicity, we limit our discussion to $p < p_c$.

Percolation Transition.—Recall that the probability, q, that a site is occupied in the ground state can be given implicitly as [6]

$$q = pQ(q) := p \sum_{i=0}^{f-1} \binom{k}{i} q^{k-i}(1-q)^i. \qquad (5.1.4)$$

Note that as $p > q$, the largest real solution of Eq. (5.1.4) is physically relevant. Trivially, $q = 0$ is always a solution of Eq. (5.1.4). The critical probability p_c locates a bifurcation to additional solutions. Generically, Eq. (5.1.4) displays a fold bifurcation (Arnold's type A_2 [56]) with a finite $q_c \equiv q(p_c) > 0$ and close to the transition $q(p > p_c) - q_c \sim \sqrt{p - p_c}$.

Equation of Motion.—We wish to describe the single site occupation correlation function

$$\phi(t) = \langle n_s(0)n_s(t) \rangle, \qquad (5.1.5)$$

where n_s denotes the occupation number of an arbitrary but fixed site s and the average $\langle \cdot \rangle$ is taken with respect to the initial distribution. Note that $\phi(t)$ is normalized such that $\phi(0) = p$ and $\phi(t \to \infty) = q$.

For $p < p_c$, the OFA is a Markov process obeying detailed balance. Hence standard techniques allow to give the time evolution of the distribution function in terms of an effective Hamiltonian H [57]. Applying a Mori projector, $n_s \rangle \langle n_s^2 \rangle^{-1} \langle n_s$, and rewriting the memory kernel in terms of its irreducible counterpart, $m(t)$, yields Eq. (5.1.2) [58]. The rate τ_0^{-1} can be calculated explicitly [4] [59]. The memory kernel, however, is only known formally.

Critical Dynamics.—It is instructive to rewrite Eq. (5.1.2) in the Laplace domain,

---

[2]$C_f(\mathcal{K}_i) = \Theta\big(k - f + 1/2 - \sum_{j \in \mathcal{K}_i} n_i\big)$, with the Heaviside step-function $\Theta(x)$.

[3]Think of this distribution as the unconstrained model's equilibrium for $\mu < 0$

[4]$\tau_0^{-1} = p - p(1-p)^k \sum_{i=0}^{f-1} \binom{k}{i}[p/(1-p)]^i$

$\hat{\phi}(z) = \mathsf{LT}[\phi](z)$ [5] [60]. For $z \ll \tau_0^{-1}$ one finds

$$\frac{z\hat{\phi}(z)}{p + z\hat{\phi}(z)} = z\hat{m}(z). \tag{5.1.6}$$

In particular $q/(p - q) = m(t \to \infty)$. Comparing this with Eq. (5.1.4) we arrive at our central result: Asymptotically the memory kernel of the OFA on the Bethe lattice is given exactly as

$$m(t \to \infty) \equiv m(p, q) = pQ(q)/(p - q). \tag{5.1.7}$$

Sufficiently close to the critical point, $\sigma := (p_c - p)/p_c \ll 1$, we expect a growing window in time, centered around a diverging time scale t_σ where $\phi(t) = q_c + G_\sigma(t/t_\sigma)$ such that $G_\sigma(t)$ is small, $|G_\sigma(t/t_\sigma)| \ll 1$, and slowly varying, $|\zeta\hat{G}_\sigma(\zeta)| \ll 1$, where $\zeta := zt_\sigma$. To this end we expand Eq. (5.1.6) around q_c to lowest order in G_σ [42, 61],

$$\lambda\mathsf{LT}[G_\sigma^2](\zeta) + \zeta\hat{G}_\sigma^2(\zeta) = -\sigma/\zeta p_c, \tag{5.1.8}$$

where $\lambda := 1 + (p_c - q_c)^3\partial_q^2\Delta m(p_c, q_c)/2p_c < 1$ [6] [62]. As λ can be calculated exactly for the OFA, the same holds for $G_\sigma(t)$. Eq. (5.1.8) can be solved by standard numerical techniques (cf. Fig. 5.1.1) but more information can be gained analytically.

At the critical point, $\sigma \equiv 0$, Eq. (5.1.8) is solved by $G_0(t) \sim t^x$, provided $\lambda = \Gamma^2(1 + x)/\Gamma(1 + 2x)$ [61]. Asymptotically, $G_0(t \to \infty) \sim t^{-a}$, the smallest negative $x \equiv -a < 0$ will dominate. Away from the critical point, for finite σ, $G_\sigma(t) = \sqrt{\sigma}g(t)$ acquires a square-root dependence on σ. Eq. (5.1.8) still admits power law solutions, $g(t) \sim t^x$, iff the left hand side dominates over the right hand side. For the approach to the plateau, $t \to t_\sigma$, $g(t/t_\sigma) \sim (t/t_\sigma)^{-a}$, as long as $(t/t_\sigma)^{2a} \ll 1$. Matching $G_{\sigma\searrow 0}(t/t_\sigma) = G_0(t)$ for $t \to \infty$, yields, $t_\sigma \sim \sigma^{-\delta}$, where $\delta := 1/2a$ [61]. For $\lambda > 1/2$ and times $t > t_\sigma$, the decay away from the plateau is governed by the smallest positive $x \equiv b$, $g(t/t_\sigma) \sim -(t/t_\sigma)^b$, as soon as $g^2(t/t_\sigma) \gg 1$, i.e., dependent on $b < 1/2$ ($b > 1/2$) for times $(t/t_\sigma)^{2b} \gg 1$ ($t/t_\sigma \gg 1$). For long times the validity of this law is limited by the slowly varying condition, $|\zeta\hat{G}_\sigma(\zeta)| \sim \sqrt{\sigma}\zeta^{-b} \ll 1$, i.e., for times $t \ll t_\sigma' \sim \sigma^{-\gamma}$, where $\gamma := (1/2a) + (1/2b)$ [61].

The above constitutes a precise statement of Eq. (5.1.1) for the OFA and proves that

---

[5]$\mathsf{LT}[\phi](z) := i\int_0^\infty \phi(t)e^{izt}\mathrm{d}t$
[6]$\Delta m(p, q) := m(p, q) - q/(p - q)$

the scaling relation (5.1.3) holds exactly. We summarize the (numerically) exact results we obtain for the simplest model, $k = 3$ and $f = 2$ in Tab. 7.2.1.

Asymptotic Relaxation.— The asymptotic relaxation to zero, $\phi(t \to \infty) \to 0$, on times $t/t'_\sigma \gg 1$ is governed by a scaling function, $\phi(t \to \infty) = \tilde{\phi}(t/t'_\sigma)$ [61]. For the OFA it has been shown that $\phi(t) \propto \exp(-t/\tau_\alpha)$ where $\tau_\alpha \sim \sigma^{-\gamma'}$ and the exponent $\gamma' \geq 2$ could only be bounded from below [63]. In terms of the scaling function we find $\tau_\alpha \sim t'_\sigma$ and in particular the preceding analysis determines the exponent $\gamma' \equiv \gamma$ compatible with the bound.

Persistence Function.—The persistence function $\psi(t)$ yields the fraction of sites that have not changed their state since $t = 0$. Its asymptotic value, $\psi_\infty = \psi(t \to \infty)$, does not only include the persistently occupied sites but also a fraction of the empty sites that are permanently frozen, $\psi_\infty(q) = pQ(p) + (1 - p)Q(p) = q/p$. Close to the plateau, $\psi_\infty^c = q_c/p_c$, we can expand

$$\psi(t \sim t_\sigma) \simeq \psi_\infty^c + \partial_q \psi_\infty(q_c)[\phi(t) - q_c], \tag{5.1.9}$$

i.e., $\psi(t) \simeq \psi_\infty^c + \sqrt{\sigma} g(t)/p_c$. In particular, the persistence function is governed by the same critical exponents and master function $g(t)$ that apply to $\phi(t)$.

The FA Model on Random Regular Graphs.—It is known that bootstrap percolation on the oriented and unoriented Bethe lattice of coordination $k + 1$ [53] as well as on random $(k + 1)$-regular graphs [32] have the same critical concentration p_c. Not much is known regarding the dynamic equivalence. Here we conjecture that due to the bifurcation dominating close to the critical point, the fact that the critical point does not change translates to dynamic equivalence close to q_c. For the unoriented FA model the expression for the persistence function, $\tilde{\psi}_\infty(q)$, is slightly more involved [36]. Nevertheless, $\partial_q \tilde{\psi}_\infty(q_c)$ is finite and therefore Eq. (5.1.9) applies and $\tilde{\psi}(t)$ is still governed by the critical exponents and scaling function of the OFA.

Simulations [36–39, 64] of the FA model are conveniently being performed on RRGS with a finite number of sites N. RRGS do not, however, admit an orientation. The effective system size is given by the size of the largest embedded tree $L = O(\log_k N)$ [65] which grows with N but is still small even for $N \simeq 2^{24}$. Therefore the existing numerical data is relatively far from the critical point. In addition the FA model is known to display strong finite size effects [66] which, so far, have not been analyzed
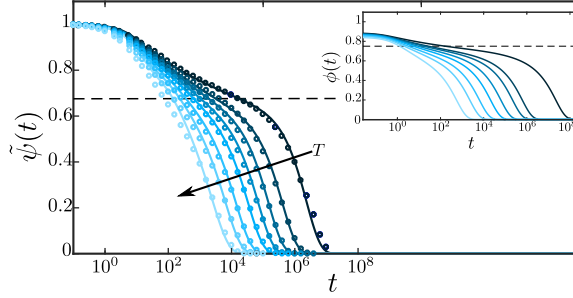
Figure 5.1.2: Persistence function $\tilde{\psi}(t)$ of the unoriented FA model as a function of time for coordination $k = 3$ and facilitation $f = 2$ at a number of temperatures $T = 0.49$, 0.5, 0.51, 0.52, 0.53, 0.55, 0.57, 0.6, above the critical temperature $T_c = 1/\ln 8 = 0.480\ldots$ The dashed line indicates the asymptotic plateau value $\tilde{\psi}_\infty^c = \frac{2757}{4096} = 0.673\ldots$ [36]. Symbols are simulations from Ref. [38] while lines are the theoretical prediction, Eq. (5.1.11). *Inset:* Corresponding theoretical occupation correlation functions $\phi(t)$, Eqs. (5.1.2, 5.1.10). The dashed line indicates the plateau value $q_c = 3/4$.

in detail for RRGs. As a consequence, the empirical critical exponents (Table 7.2.1) are effective exponents and deviate from the analytical predictions. In the following we propose a memory kernel that allows us to solve Eq. (5.1.2) for all times and for appreciable distances σ from the critical point relevant to the numerical data.

Approximate Memory Kernel.—To close Eq. (5.1.2) we propose to approximate the memory kernel by Eq. (5.1.7) for all times as $m(t) \approx \tilde{m}[\phi(t)] \equiv m(p, \phi(t))$. Unfortunately this is not viable as $\tilde{m}[\phi(t) \to p] \sim [p - \phi(t)]^{-1}$ diverges for small times, $\phi(t \to 0) \to p$. In order to regularize the memory kernel we assume the divergent term, $[p - \phi(t)]^{-1} = p^{-1} \sum_i^M [\phi(t)/p]^i, M \to \infty$, to be a resummation of many-site interactions. On a finite lattice, the order of interactions should be finite, $M < \infty$. Therefore we propose a regularized approximate memory kernel whose time-dependence is completely determined by $\phi(t)$,

$$m(t) \approx m[\phi(t)] = Q(\phi(t)) \sum_{i=0}^{M} [\phi(t)/p]^i. \tag{5.1.10}$$

With this Eq. (5.1.2) can be numerically solved for $\phi(t)$ by standard techniques [67]. *Discussion.*—Considering the occupation correlation function $\phi(t)$, Eq. (5.1.5), of the OFA on the Bethe lattice, we have identified an explicit expression, Eq. (5.1.7), for the

long time limit of its memory kernel. Expanding around the bifurcation at p_c that signals the ergodic to non-ergodic transition of the OFA, we find that close to the transition, $\sigma \to 0$, the time evolution of $\phi(t)$ around its plateau value q_c is asymptotically exactly given, $\phi(t) = q_c + \sqrt{\sigma} g(t)$, in terms of a one-parameter scaling function $g(t) \equiv g_\lambda(t)$, Eq. (5.1.8). The exponent parameter $\lambda \equiv \lambda(k, f)$ is known explicitly in terms of the lattice coordination k and the facilitation parameter f. The properties of Eq. (5.1.8), finally, imply Eq. (5.1.1) together with the scaling relation (5.1.3), for $\lambda > 1/2$, times $\tau_0 \ll t \ll t'_\sigma \sim \sigma^{-\gamma}$, and not too close to the plateau, $|\phi(t) - q| \gg \sigma$.

The scaling function $G_\sigma(t)$, however, goes beyond Eq. (5.1.1) as it provides a faithful description of $\phi(t)$ for $\tau_0 \ll t \ll t'_\sigma$, $\lambda > 0$, bounded only by the requirements $|G_\sigma(t)|, |\zeta \hat{G}_\sigma(\zeta)| \ll 1$ (cf. Fig. 5.1.1). On the fast end this could be complemented by ever more sophisticated short-time expansions. On the long-time end, $\phi(t \to \infty) \sim e^{-t/\tau_\alpha}$, with a relaxation time $\tau_\alpha \sim \sigma^{-\gamma}$.

Considering the asymptotic dynamics only, we did not gain information about processes on intermediate time scales. Could we have missed an additional process that will always mask the bifurcation scenario? The answer is no: Any unidentified process must occur on a time scale, τ_u, that remains finite as $\sigma \to 0$. Otherwise it would contribute to Eq. (5.1.4). Therefore we can always find a $\sigma_0 > 0$ such that for $\sigma < \sigma_0$, $t_\sigma \sim \sigma^{-\delta} \gg \tau_u$ and we have a time window which is dominated by the bifurcation.

Given that close to the critical point the persistence function, $\psi(t)$, is governed by the same scaling function $G_\sigma(t)$, Eq. (5.1.9) provides an asymptotically exact description of the persistence function in a divergent time window before the asymptotic exponential relaxation. The form of Eq. (5.1.1) and the scaling relation (5.1.3) equally apply to $\psi(t)$ with the qualifications given above. Thereby we confirm the empirical observation of Sellitto [38] and de Candia *et al.* [39].

To close Eq. (5.1.2), we proposed a memory functional, Eq. (5.1.10), regularized by a finite length scale M we conjecture to be related to the system size. Formally, Eq. (5.1.10) looks like a MCA but let us stress that it was not derived by considering a (physically motivated) coupling of modes, but ultimately from the bifurcation equation (5.1.4) of the underlying bootstrap percolation.

To determine the persistence function of the unoriented FA model for all times, we use

the knowledge gained so far and interpolate

$$\tilde{\psi}(t) = e^{-t/\tau_\psi} + \left\{ \tilde{\psi}^c_\infty + \partial_q \tilde{\psi}_\infty(q_c)[\phi(t) - q_c] \right\} \times \left(1 - e^{-t/\tau_\psi}\right) e^{-t/\tau_\alpha}, \qquad (5.1.11)$$

where τ_ψ^{-1} is the short time relaxation rate of $\tilde{\psi}(t)$. We determine $\phi(t)$ by solving Eq. (5.1.2) with the regularized memory kernel [Eq. (5.1.10)] and treat M as a fit parameter [7] [68]. Fig. 5.1.2 shows excellent agreement between Eq. (5.1.11) and the numerical data for all temperatures and over many decades in time.

The success of this approach, derived for the OFA on the Bethe lattice, in describing simulations of the unoriented FA model on RRGS provides reasons to assume that the similarity between the oriented and unoriented FA model extends beyond a common critical point p_c to a universal dynamics close to p_c. It is, however, obvious, that simulations much closer to the critical point are needed to challenge the conjectures put forward here and to confirm the critical exponents.

While for sake of brevity we have only presented explicit results for the simplest case, $k = 3, f = 2$, our approach holds for more general coordinations $k > 3$, and facilitation parameters $f \geq 2$ provided $k > f$. The consequences of a tunable $\lambda(k, f)$ will be discussed elsewhere, but let us note that for some combinations (k, f), $\lambda < \lambda(3, 2)$. As a result the exponents a, b increase which may be favorable for simulations.

The signature of a fold bifurcation, $q - q_c \sim \sqrt{|\sigma|}$, with a finite critical $q_c > 0$ is observed as a hybrid phase transition in a variety of models [69–71]. A similar analysis to the one introduced here could lead to new insights in those systems as well. Reconciling MCT and replica methods led to many new insights provided by the random first order theory (RFOT) [72]. A deeper analysis of the overlap between MCT and dynamic facilitation theory that has been started here and RFOT and dynamic facilitation [73] is likely to provide additional understanding of the glass transition.

In summary we have provided an asymptotically exact description of the slow relaxation of the oriented Fredrickson-Andersen model on the Bethe lattice close to its critical point, valid over a divergent window in time. We believe our method can be applied to other time correlation functions of the FA and related kinetically constraint models and can provide new insights into the phenomena which can be mapped onto these models.

---

[7]Fitted $M = 6$–23 increase with $\sigma \to 0$ as expected.

Bibliography

[1] M. Ramos, J. Shao, S. D. S. Reis, C. Anteneodo, J. S. Andrade, S. Havlin, and H. A. Makse, Sci. Rep. **5**, 10032 (2015).

[2] C. Castellano, M. A. Muñoz, and R. Pastor-Satorras, Phys. Rev. E **80**, 041129 (2009).

[3] A. Jędrzejewski, Phys. Rev. E **95**, 012307 (2017).

[4] H. Chae, S.-H. Yook, and Y. Kim, New J. Phys. **17**, 023039 (2015).

[5] M. Pollak and I. Riess, phys. stat. sol. (b) **69**, K15 (1975).

[6] J. Chalupa, P. L. Leath, and G. R. Reich, J. Phys. C **12**, L31 (1979).

[7] J. J. Brey, A. Prados, and B. Sánchez-Rey, Phys. Rev. E **60**, 5685 (1999).

[8] C. Moukarzel, P. M. Duxbury, and P. L. Leath, Phys. Rev. E **55**, 5800 (1997).

[9] C. Toninelli, G. Biroli, and D. S. Fisher, Phys. Rev. Lett. **96**, 035702 (2006).

[10] J. M. Schwarz, A. J. Liu, and L. Q. Chayes, Europhys. Lett. **73**, 560 (2006).

[11] S. H. Glarum, J. Chem. Phys. **33**, 639 (1960).

[12] G. H. Fredrickson and H. C. Andersen, Phys. Rev. Lett. **53**, 1244 (1984).

[13] J. P. Garrahan and D. Chandler, Phys. Rev. Lett. **89**, 035704 (2002).

[14] M. R. Evans, J. Phys. Condens. Matter **14**, 1397 (2002).

[15] F. Ritort and P. Sollich, Adv. Phys. **52**, 219 (2003).

[16] D. Chandler and J. P. Garrahan, Annu. Rev. Phys. Chem. **61**, 191 (2010).

[17] C. A. Angell, K. L. Ngai, G. B. McKenna, P. F. McMillan, and S. W. Martin, J. Appl. Phys. **88**, 3113 (2000).

[18] L. Berthier and G. Biroli, Rev. Mod. Phys. **83**, 587 (2011).

[19] G. L. Hunter and E. R. Weeks, Rep. Prog. Phys. **75**, 066501 (2012).

[20] G. Biroli and J. P. Garrahan, J. Chem. Phys. **138**, 12A301 (2013).

[21] S. B. Seidman, Social Networks **5**, 269 (1983).

[22] S. N. Dorogovtsev, A. V. Goltsev, and J. F. F. Mendes, Phys. Rev. Lett. **96**, 040601 (2006).

[23] T. S. Turova, Brain Res. **1434**, 277 (2012).

[24] G. J. Baxter, S. N. Dorogovtsev, K.-E. Lee, J. F. F. Mendes, and A. V. Goltsev, Phys. Rev. X **5**, 031017 (2015).

[25] L. Yartseva and M. Grossglauser, in *Proceedings of the First ACM Conference on Online Social Networks*, COSN '13 (ACM, New York, NY, USA, 2013) p. 119.

[26] J. P. Garrahan, P. Sollich, and C. Toninelli, in *Dynamical Heterogeneities in Glasses, Colloids, and Granular Media*, International Series of Monographs on Physics, Vol. 150, edited by L. Berthier, G. Biroli, J.-P. Bouchaud, L. Cipelletti, and W. van Saarloos (Oxford University Press, Oxford, 2011) Chap. 10, p. 341.

[27] N. Cancrini, F. Martinelli, C. Robert, and C. Toninelli, in *Methods of contemporary mathematical statistical physics*, Lecture Notes in Mathematics, Vol. 1970, edited by R. Kotecký (Springer, Berlin, 2009) p. 307.

[28] J. Adler, Physica A **171**, 453 (1991).

[29] S. N. Dorogovtsev, A. V. Goltsev, and J. F. F. Mendes, Rev. Mod. Phys. **80**, 1275 (2008).

[30] A. A. Saberi, Phys. Rep. **578**, 1 (2015).

[31] A. C. D. van Enter, J. Stat. Phys. **48**, 943 (1987).

[32] J. Balogh and B. G. Pittel, Random Struct. Alg. **30**, 257 (2007).

[33] S. Janson, T. Łuczak, T. Turova, and T. Vallier, Ann. Appl. Probab. **22**, 1989 (2012).

[34] Temperature is measured in units of $|\mu|/k_B$.

[35] N. Cancrini, F. Martinelli, C. Roberto, and C. Toninelli, Probab. Theory Relat. Fields **140**, 459 (2008).

[36] M. Sellitto, G. Biroli, and C. Toninelli, Europhys. Lett. **69**, 496 (2005).

[37] J. J. Arenzon and M. Sellitto, J. Chem. Phys. **137**, 084501 (2012).

[38] M. Sellitto, Phys. Rev. Lett. **115**, 225701 (2015).

[39] A. de Candia, A. Fierro, and A. Coniglio, Sci. Rep. **6**, 26481 (2016).

[40] W. Götze and L. Sjögren, Rep. Prog. Phys. **55**, 241 (1992).

[41] H. Z. Cummins, J. Phys. Condensed Matt. **11**, A95 (1999).

[42] W. Götze, *Complex dynamics of glass-forming liquids: A mode-coupling theory* (OUP, Oxford, 2009).

[43] L. M. C. Janssen, Front. Phys. **6**, 97 (2018).

[44] S. Eisinger and J. Jäckle, J. Stat. Phys. **73**, 643 (1993).

[45] S. J. Pitts, T. Young, and H. C. Andersen, J. Chem. Phys. **113**, 8671 (2000).

[46] S. J. Pitts and H. C. Andersen, J. Chem. Phys. **114**, 1101 (2001).

[47] M. Einax and M. Schulz, J. Chem. Phys. **115**, 2282 (2001).

[48] M. Schulz and S. Trimper, J. Phys. Condens. Matter **14**, 1437 (2002).

[49] P. G. Fennell, J. P. Gleeson, and D. Cellai, Phys. Rev. E **90**, 032824 (2014).

[50] M. Sellitto, D. De Martino, F. Caccioli, and J. J. Arenzon, Phys. Rev. Lett. **105**, 265704 (2010).

[51] T. Rizzo, "The fate of the bootstrap percolation hybrid critical point in finite dimension," (2018), arxiv:1807.08066 .

[52] M. Mézard and G. Parisi, Europhys. J. B **20**, 217 (2001).

[53] F. Martinelli and C. Toninelli, Ann. Appl. Prob. **23**, 1967 (2013).

[54] $C_f(\mathcal{K}_i) = \Theta\big(k - f + 1/2 - \sum_{j \in \mathcal{K}_i} n_i\big)$, with the Heaviside step-function $\Theta(x)$.

[55] Think of this distribution as the unconstrained model's equilibrium for $\mu < 0$.

[56] V. I. Arnol'd, *Catastrophe Theory*, 3rd ed. (Springer, Berlin, 1992).

[57] H. Risken, *The Fokker-Planck Equation: Methods Of Solution And Applications*, 2nd ed. (Springer, Berlin, 1996).

[58] K. Kawasaki, Physica A **215**, 61 (1995).

[59] $\tau_0^{-1} = p - p(1-p)^k \sum_{i=0}^{f-1} \binom{k}{i} [p/(1-p)]^i$.

[60] $\mathsf{LT}[\phi](z) := i \int_0^\infty \phi(t) e^{izt} \mathrm{d}t$.

[61] W. Götze, Z. Phys. B **56**, 139 (1984).

[62] $\Delta m(p,q) := m(p,q) - q/(p-q)$.

[63] N. Cancrini, F. Martinelli, C. Roberto, and C. Toninelli, Probab. Theory Relat. Fields **161**, 247 (2015).

[64] M. Sellitto, J. Chem. Phys. **138**, 224507 (2013).

[65] E. Makover and J. McGowan, "Regular trees in random regular graphs," (2006), arXiv:math/0610858 .

[66] M. Aizenman and J. L. Lebowitz, J. Phys. A **21**, 3801 (1988).

[67] M. Fuchs, W. Götze, I. Hofacker, and A. Latz, J. Phys. Condensed Matt. **3**, 5047 (1991).

[68] Fitted $M = 6$–23 increase with $\sigma \to 0$ as expected.

[69] L. E. Silbert, A. J. Liu, and S. R. Nagel, Phys. Rev. Lett. **95**, 098301 (2005).

[70] W. Cai, L. Chen, F. Ghanbarnejad, and P. Grassberger, Nat. Phys. **11**, 936 (2015).

[71] Y. S. Cho, J. S. Lee, H. J. Herrmann, and B. Kahng, Phys. Rev. Lett. **116**, 025701 (2016).

[72] P. G. Wolynes and V. Lubchenko, *Structural glasses and supercooled liquids: Theory, experiment, and applications* (John Wiley & Sons, New York, 2012).

[73] L. Foini, F. Krzakala, and F. Zamponi, J. Stat. Mech. **2012**, P06013 (2012).

Fitting the Hard-Sphere System
with the schematic Model

The following chapter discusses the application of the schematic models to the Hard Sphere Systems. It is composed in a self-contained way to also in part facilitate the submission of that chapter as a research paper. We intend to submit the manuscript to the Physical Review Series of the American Physical Society.

Abstract

The microscopic mode coupling equations of motion depend on an infinite number of coupling constants, indexed by the wave number, q. Here we explore how well the slow decay of the dynamical scattering function in a hard-sphere fluid near the glass transition can be captured by established schematic models that only depend on a small number of coupling constants. To this end we study the F_{12}-model and the Bosse-Krieger model, with and without coupling to a Sjögren correlator

6.1   Introduction

In the field of glassy dynamics, large and complex data sets became available in the last two decades due to progress both in experimental and computer simulation techniques. Beyond seminal qualitative features such stretching, divergent time scales, or time-temperature superposition, it was also possible to perform detailed quantitative comparisons with theory. Especially for mode-coupling theory (MCT) [1] many data fits are available in the literature [2–4]. This comparison to theory can typically be done in three different ways:

(1) MCT is solved for a microscopic model and from the interaction potential the glassy dynamics is derived [5]. This comparison on the microscopic level is the most demanding and accurate test of the theory since all relevant parameters are fixed. Such tests are done for data from computer simulation [6] or from colloidal suspensions [7–9] and are mostly quite successful. However, such detailed comparison is not feasible if the microscopic interactions are either not known or too complex to be calculated in detail.

This is often the case for molecular glass formers. In this case, one can use asymptotic expansions.

(2) Asymptotic expansions of MCT are derived close to the transition singularity and for long times. Asymptotic expansions yield results like power laws for the divergence of different time scales, power laws in the relaxation master functions, and scaling properties of the correlation functions [10]. These asymptotic laws can then be applied directly to study experimental data involving several fit parameters [11]. It is, however, also known that deviations from the asymptotic results occur when the data are farther from the transition point. In such a case pre-asymptotic corrections can be included which increases the number of parameters [10].

(3) If not enough microscopic information is available for the system under investigation and pre-asymptotic corrections are assumed to be large, another way to describe the data is by means of schematic models. These models capture the essential mathematical structures of MCT, provide the correct asymptotic limits and scaling laws, and in addition incorporate pre-asymptotic corrections in a natural way without introducing additional fit parameters. Such models have been applied to the description of data frequently [12–15]. By their very nature, schematic models have a smaller complexity than microscopic models and it is hence surprising that data fits by schematic models often work well. However, a successful data fit by a schematic model alone might occasionally imply a misrepresentation of the data: The fitted values of the parameters may have unphysical or implausible values. On the other hand, the failure of a specific schematic models to describe a set of data cannot by itself rule out the possibility of a successful description by MCT: The microscopic model might just be incompatible with that specific schematic model.

It is the goal of the present paper to resolve some of the ambiguities in working with schematic models. We shall apply the schematic models to the popular hard sphere system (HSS) and determine where the schematic model describes the HSS well and poorly. The failure of the schematic model to describe specific data from the HSS or a specific other microscopic model should caution the use of the schematic model in similar situations. In situations where the schematic model describes the microscopic data well, a schematic fit will carry more weight. All information available from the microscopic calculations shall be used for the fit to reduce the freedom in the fitting procedure as much as possible. Also, the influence of hopping effects is typically unknown in

comparisons to data, and therefore deviations might be hopping effects.

6.2   Basic Equations and Asymptotic Expansions

In MCT one describes the structural dynamics of a system with N structureless particles with the density autocorrelation function, $\phi_q(t) = \langle \rho_{\vec{q}}(t)\rho_{\vec{q}}(0)\rangle$, where the wave number depending density is given as $\rho_{\vec{q}}(t) = 1/\sqrt{N}\sum_{j=1}^{N}\exp(i\vec{q}\cdot\vec{r}_j(t))$. The equations of motion for the density autocorrelation function, derived within the Mori-Zwanzig formalism [16] is given by

$$\ddot{\phi}_q(t) + \tau_q\dot{\phi}_q(t) + \phi_q(t) + \int_0^t \mathrm{d}t'\, m_q(t-t')\dot{\phi}_q(t') = 0 \ , \qquad (6.2.1a)$$

with the microscopic timescale τ_q and the initial conditions $\phi_q(0) = 1$ and $\partial_t\phi_q(0) = 0$. The relaxation kernel $m_q(t)$ is expressed as a bilinear functional of the density correlators [17]

$$m_q(t) = \mathcal{F}_q[\mathbf{V}, \phi_k(t)] \ , \qquad (6.2.1b)$$

with the functional

$$\mathcal{F}_q[\mathbf{V}, \phi(t)_k] = \frac{1}{2}\int \frac{d^3k}{(2\pi)^3}\mathbf{V}_{\vec{q},\vec{k}}\,\phi(t)_k\phi(t)_{|\vec{q}-\vec{k}|} \ , \qquad (6.2.1c)$$

where the microscopic vertex $\mathbf{V} = \frac{mn}{k_{\mathrm{B}}T}((\hat{q}\cdot\vec{k})c(k) + (\hat{q}\cdot|\vec{q}-\vec{k}|)c(|\vec{q}-\vec{k}|))S(|\vec{q}-\vec{k}|)$, with the Boltzmann constant k_{B}, the structure factor $S(|\vec{q}-\vec{k}|)$, and the direct correlation function $c(k)$, is determined by the interaction potential [46]. To discriminate between the liquid phase and glassy state MCT uses the long-time limit of the density autocorrelation function, $\phi_q(t \to \infty) = f_q$. A vanishing non-ergodicity parameter, $f_q = 0$, means that the correlations of density fluctuations disappear for long times and the system is in a liquid state. For $0 < f_q < 1$ the system is in the ideal glass state, which is also shown by Edwards and Anderson in an other context [18].

For schematic models, the dependence on the wave vector q is replaced by artificial but simpler memory kernels that nevertheless capture the essential mathematical structure of the theory. The full equations for both microscopic and schematic versions of the theory can be solved numerically by established procedures [10, 19].

The long-time limit of Eq. (6.2.1a) and (6.2.1b) leads to the bifurcation equation

$$\frac{f_q}{1 - f_q} = \mathcal{F}_q[\mathbf{V}, f_k(t)] \; . \tag{6.2.2}$$

With Eq. (6.2.1c) one can calculate a matrix C_{qk} with

$$C_{qk} = \frac{\partial \mathcal{F}_q[\mathbf{V}, f]}{\partial f_k}(1 - f_k)^2. \tag{6.2.3}$$

The elements of the matrix C_{qk} are non-negative and from the Frobenius-Perron Theorem[20] we know, that the matrix has a nondegenerated maximum eigenvalue E. If the eigenvalue is $E < 1$ the matrix can be inverted and the nonergodicity parameter f varies with the control parameter. Therefore the glass-transition is characterized by the condition

$$E^c = 1 \; . \tag{6.2.4}$$

The right and left eigenvectors of C_{qk}^c, here the c denotes $\mathbf{V} = \mathbf{V}^c$ which are the parameters at the critical point, shall be denoted by e and $\hat{e}$ with

$$\sum_k C_{qk}^c e_k = e_q \, , \quad \sum_q \hat{e}_q C_{qk}^c = \hat{e}_k \; . \tag{6.2.5}$$

We chose the convention $\sum_q \hat{e}_q e_q = 1$ and $\sum_k \hat{e}_k(1 - f_q^c)e_k^2 = 1$ to fix the vectors. With the eigenvectors one can calculate the critical amplitude

$$h_q = (1 - f_q^c)^2 e_q \; , \tag{6.2.6}$$

and the exponent parameter λ [21]

$$\lambda = \sum_{qkp} \hat{e}_q C_{qkp}^c e_k e_p \tag{6.2.7}$$

with $0.5 \leq \lambda \leq 1$. Note that $\mathbf{V}^c$ is a bifurcation point of Eq. (6.2.2). The f_q are singular functions of the distance parameter going to zero $\epsilon \to 0$, with $\epsilon = (\varphi - \varphi_c)/\varphi_c$. So in MCT cusp bifurcations $A_l, l = 2, 3, ...$ in Arnold's terminology [22] occur. The A_2, also

called Whitney fold bifurcation, occurs for an exponent parameter $\lambda < 1$, obtained by varying a single control paramter [24].

6.2.1　Leading Order and Next-To-Leading Order Asymptotic Expansion

Here, the separation parameter, σ, shall be introduced as a gauged distance to the critical point. It is related to the distance parameter, ϵ via $\sigma = C\epsilon$, with a system depending constant C. For HSS the parameter equals to $C = 1.54$ [10].

For $\lambda < 1$, there is a square root singularity in σ close to the glass transition point. Therefore, the asympotitc expansion of the correlation function starts with a $\sqrt{\sigma}$ in lowest order

$$\phi_q(\hat{t}) = f_q^c + h_q \left[\sqrt{|\sigma|}g^{(1)}(\hat{t}) + |\sigma|g^{(2)}(\hat{t}) + \mathcal{O}(|\sigma|^{3/2}) \right] \ . \tag{6.2.8}$$

Here, the rescaled time is given by $\hat{t} = t/t_\sigma$ and $t_\sigma \propto |\sigma|^\delta$ with $\delta = 1/(2a)$, is the plateau crossing time. Note, for the critical decay, which means a vanishing separation, $\sigma \to 0$, the plateau crossing time diverges so that the timescale becomes $\sqrt{|\sigma|}/t_\sigma = t_0$, where t_0 is a microscopic time scale.

In leading order the master function $g^{(1)}(\hat{t}) = g(\hat{t})$ obeys the β scaling equation [10]

$$-\lambda g^2(\hat{t}) + \frac{\mathrm{d}}{\mathrm{d}t} \int_0^{\hat{t}} g(\hat{t} - \tau)g(\tau)\mathrm{d}\tau = \mathrm{sgn}\,\sigma \ . \tag{6.2.9}$$

The correlator $\phi_q(t)$ exhibits a power-law decay, which is determined by the exponent paramter λ and the two scalars f_q^c and h_q which depends on the wave vector

$$\phi_q(t) = f_q^c + h_q G_\sigma(\hat{t}) \ . \tag{6.2.10}$$

Here, $G_\sigma(\hat{t}) = \sqrt{\sigma}g(\hat{t})$ is the β-correlator. Note, the β-correlator is depending on the master function $g_+(\hat{t})$, in the glassy state ($\sigma > 0$), a master function for the liquid case ($\sigma < 0$), $g_-(\hat{t})$, and at the critical point on $g_{\sigma=0}(\hat{t})$. For all of the three cases the solution in leading order and for $t_0 \ll t \ll t_\sigma$ is given by $g(\hat{t}) \propto \hat{t}^{-a}$. The anomalous exponent a can be calculated from the exponent parameter λ with $\lambda = \Gamma^2(1 - a)/\Gamma(1 - 2a)$. For

long times, $t > t_\sigma$, one finds for a liquid the von Schweidler law

$$\phi_q(t) = f_q^c - h_q \left(\frac{t}{t'_\sigma}\right)^b , \qquad (6.2.11)$$

with the von Schweidler exponent b and the second critical time scale $t'_\sigma \propto |\sigma|^{-\gamma}$, with $\gamma = (1/2a) + (1/2b)$. Both exponents a and b are connected by the exponent parameter λ via

$$\lambda = \frac{\Gamma^2(1-a)}{\Gamma(1-2a)} = \frac{\Gamma^2(1+b)}{\Gamma(1+2b)} , \qquad (6.2.12)$$

here Γ denotes the Gamma function. For the HSS one gets $a = 0.312$ and $b = 0.583$ [10].

The leading order correction for the critical correlator is given by $g^{(2)}\hat{t}) = [\kappa(x) + K_q]g^2(\hat{t}) + \sigma\hat{K}$. The last term, $\sigma\hat{K}$, vanishes at the critical point so that the corrections at the critical point are given by [10]

$$\phi_q(t) = f_q^c + h_q(t/t_0)^{-a} + [K_q + \kappa(a)](t/t_0)^{-2a} , \qquad (6.2.13)$$

$$\text{and}$$

$$\phi_q(t) = f_q^c - h_q(t/t'_\sigma)^b + [K_q + \kappa(-b)](t/t'_\sigma)^{2b} , \qquad (6.2.14)$$

with

$$K_q = \sum_p R_{qp} \left[\sum_{kl} C_{pkl}^c e_k e_l - \lambda(1 - f_p^c)e_p^2 \right] e_q^{-1} ,$$

$$\kappa(x) = \frac{\xi\Gamma(1-3x) - \zeta\Gamma^3(1-x)}{\Gamma(1-x)\Gamma(1-2x) - \lambda\Gamma(1-3x)} . \qquad (6.2.15)$$

The calculation for R_{qk}, ξ and ζ as well as the values for K_q, $\kappa(a) = -0.00165$ and $\kappa(-b) = 0.569$ for the HSS are found in earlier works [10].

6.3 F_{12} Model for HSS

We follow the strategy to match microscopic and schematic models in the asymptotic regime. First, the exponent parameter λ shall be matched which for the HSS is

$\lambda = 0.735$. We introduce the F_{12} model where λ varies between 0.5 and 1 with two control parameters v_1 and v_2 [23]:

$$m(t) = v_1\phi(t) + v_2\phi^2(t) \tag{6.3.1a}$$

In the F_{12} model an A_2-bifurcation occurs and one can calculate the corresponding λ via Eq. (6.2.7). The choice of a particular value for λ fixes all other parameters [17]:

$$f^c = 1 - \lambda,\, h = \lambda, \tag{6.3.1b}$$

$$v_1^c = (2\lambda - 1)/\lambda^2,\, v_2^c = 1/\lambda^2 \,. \tag{6.3.1c}$$

In particular, amplitude and plateau value are related and fixed by $h = 1 - f = \lambda$. Hence, $h(f)$ is represented by a single point in Fig. 6.3.1 where several such points are shown for different values of λ as open circles. Possible relations between f and h only match the values for the HSS for $q \approx 1$ and $q \approx 10$ and the wrong value $\lambda \approx 0.6$. In order to vary f independently, a second correlator is introduced

$$m_A(t) = v_A\phi(t)\phi_A(t) \tag{6.3.2a}$$

and the plateau and amplitude for the second correlator are

$$f_A^c = 1 - 1/(v_A f^c), \qquad \text{and} \qquad h_A = \lambda/(v_A f^{c\,2}) = \frac{\lambda}{v_A(1-\lambda)^2} \tag{6.3.2b}$$

and therefore $h_A(f_A)$ is represented by a line in Fig. 6.3.1,

$$h_A(f_A^c) = \frac{\lambda}{1-\lambda}(1 - f_A^c)\,. \tag{6.3.2c}$$

Lines for different λ all go through $(f_q, h_q) = (1, 0)$ with a slope varying with λ. For setting $\lambda = 0.735$ we get $h_A^{\mathrm{HSS}}(f_A^c) = 2.77(1 - f_A^c)$

Varying $v_A = 5, 15, 40$, various values of f_q can be matched, and the related h_A is found on that line given by cross, star, and plus symbol in Fig. 6.3.1. One can also see that $\lambda = 0.735$, which belongs to the HSS, only occurs as a point in the F_{12}-model and is not in agreement with the HSS data. The wrong $\lambda = 0.6$ is on the data points of the HSS, but it does not describes the dynamics well. Here one can also see, that for the

HSS λ the schematic model only describes the HSS in the $f_q \to 1$ limit. The better match for $\lambda = 2/3$ explains why smaller exponent parameters gave better fits in an earlier work on HSS with the F_{12}-model [15].

Treating HSS in Gaussian approximation,

$$f_q^{s,c} = \mathrm{e}^{-q^2 r_c^2} \ , \ h_q^s = h_{\mathrm{MSD}} q^2 \mathrm{e}^{-q^2 r_c^2} \ , \tag{6.3.3a}$$

where, $f_q^{s,c}$ is the critical glass form factor of the incoherent correlators, one can derive an analytical relation between h_q^s and f_q^s:

$$h_q^s(f_q^s) = -\frac{h_{\mathrm{MSD}}}{r_c^2} f_q^s \ln f_q^s \ , \tag{6.3.3b}$$

which is for the HSS (Fig. 6.3.1 right panel)

$$h_q(f_q) = -2.083 f_q^s \ln f_q^s \ ; \tag{6.3.3c}$$

The expression of the correction amplitude K for an one component model is given by $K = \kappa(x)$ [24] with

$$\kappa(x) = \frac{\frac{1}{2}\Gamma(1 - x^3)}{\lambda \Gamma(1 - 3x) - \Gamma(1 - x)\Gamma(1 - 2x)} \ . \tag{6.3.4}$$

For the second correlator which also has an analog expression for $\phi_a(t)$ one get for the correction amplitude

$$K_A^{crit}(f_A) = K_A(f_A) + \kappa(a) \ , \tag{6.3.5a}$$

$$K_A^{vS}(f_A) = K_A(f_A) + \kappa(-b) \ , \tag{6.3.5b}$$

with

$$K_A(f_A) = [(1 - f_A + \lambda)(1 - \lambda) - \lambda]/[f_A(1 - \lambda)] \ . \tag{6.3.5c}$$

Here, we also use the Gaussian approximation to get the correction amplitude

$$K_q^s = K_{\mathrm{MSD}} - \frac{h_{\mathrm{MSD}}}{2r_c^2} \ln f_q^s = -1.23 - 1.04 \ln f_q^s \ . \tag{6.3.6}$$

In Fig. 6.3.2 one can see that the correction term K_q^s of the HSS has a inverse trend than the correction term K_A from the F_{12} model. One can see that the correction amplitudes of both models has a opposite trend: The correction amplitude of the HSS is decreasing for increasing f, whereas, the correction amplitude of the schematic model increases. The correction amplitude without the second correlator is for all exponent parameters nearly zero and therefore not ploted.

In Fig. 6.3.3 the correlation function $\phi(t)$ is shown for a HSS with a wave number $qd = 4.2$ and the corresponding F_{12}-model, with the exponent parameter $\lambda = 0.735$ and $\lambda = 0.635$. One can see, that the variation of only one parameter is not enough to describe the HSS with a schematic model. The F_{12} model works best for large plateau values f which in turn allows for the possibility of the beta-peak phenomenon [17]. Large plateau values have also been observed for the reorientational dynamics of a linear molecule [25, 26], a single dumbbell [27, 28], and a liquid of dumbbells [29, 30].
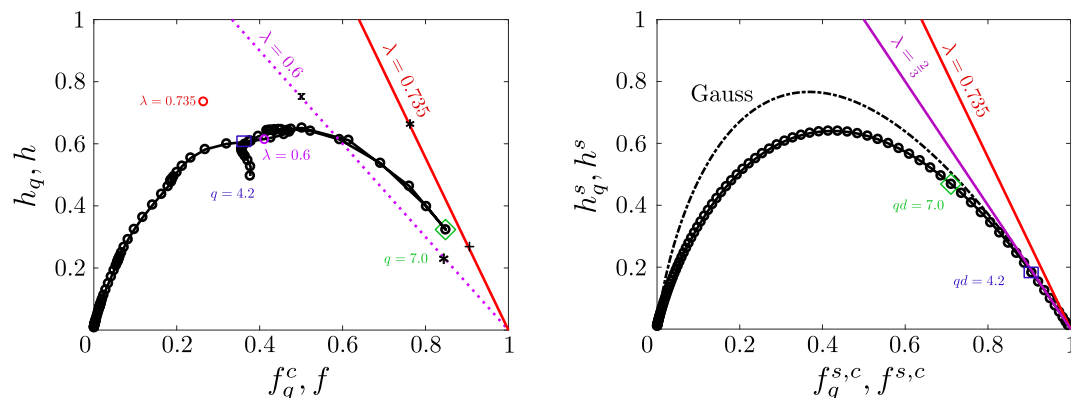
Figure 6.3.1: *Left*: The critical amplitude h_q as a function of the glass form factor f_q. The open circles show the exponent parameter of the F_{12} model, λ. The lines are the results of the second correlator, $m_A(t)$, which has a second variable, v_A. Some different values of v_A are shown as a cross (5), star (15), and plus (40) symbol.
Right: The same physics but for the incoherent correlators of the HSS and its Gaussian approximation which is given by Eq. (6.3.3c). The d is the diameter of the particles
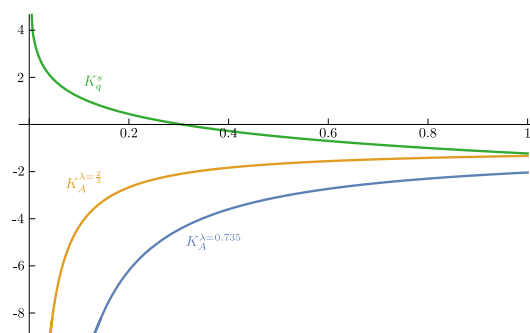
Figure 6.3.2: The correction amplitudes of the HSS, K^s and the F_{12}-model with the second correlator, K_A.
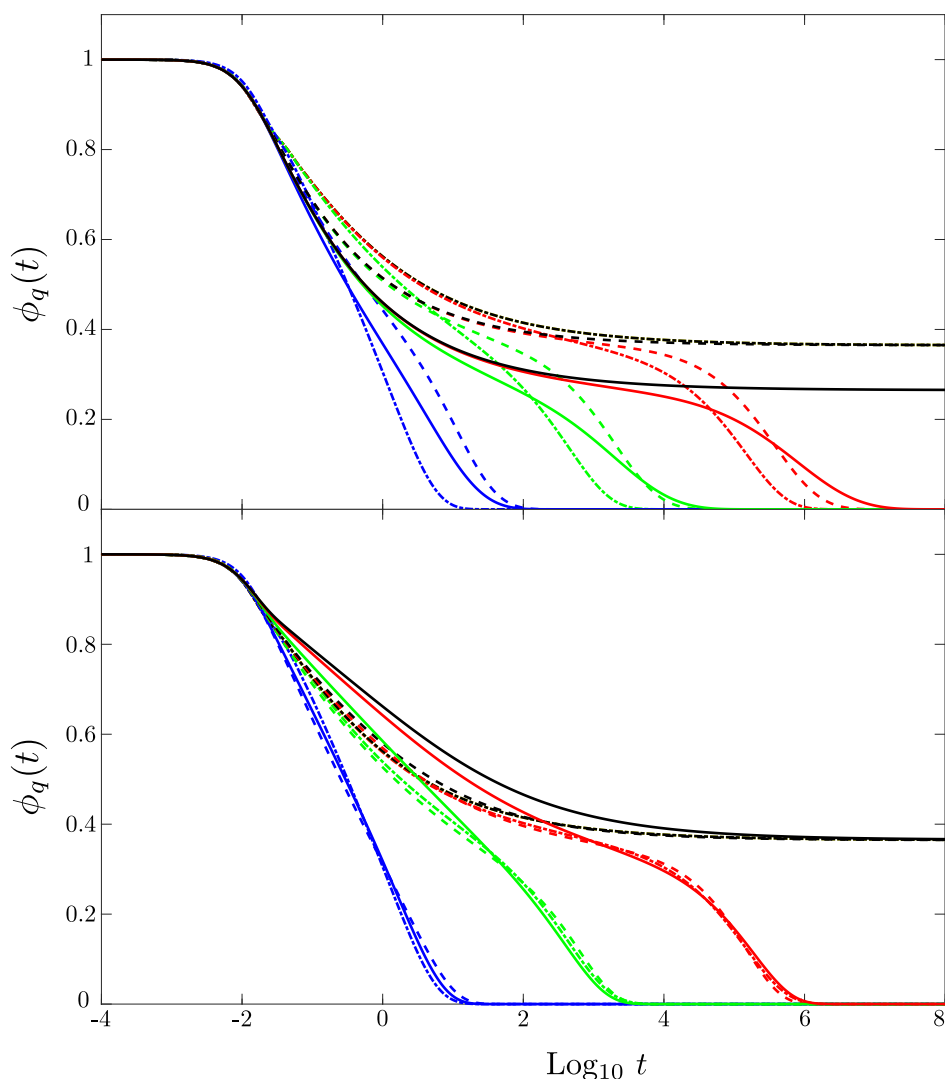
Figure 6.3.3: *Upper panel*: The dot-dashed curves are the correlation function, $\phi_q(t)$, of the HSS for the wave number $q = 4.2$ and the other two curves are the correlation functions for the F_{12}-model. The solid curves are for an exponent parameter of $\lambda = 0.735$, which is the value for the HSS, and the dashed lines are for $\lambda = 0.635$, yielding the correct long time limit, $f^c = 1 - \lambda = 0.365$, at the expense of an altered exponent parameter.. Different colors are for different separation, σ. The black curve is for the critical value ($\epsilon = 0$), the red curve is at $\epsilon = -0.001$, the green curve is for a separation of $\epsilon = -0.01$ and the blue curve for $\epsilon = -0.1$. The system constant is $C = 0.4$. *Lower panel:* The same curve as above, here we use the second correlator, too. The coupling parameter, v_a, is decreasing for increasing separation, ϵ.

6.4   Bosse-Krieger Model for HSS

In this section the Bosse-Krieger model will be used as a two component model. This is the simplest example for a generic swallowtail bifurcation [31] and is given by the functionals [32]

$$m_1 = v_1 \phi_1^2(t) + v_2 \phi_2^2(t) \,, \tag{6.4.1}$$

$$m_2 = v_3 \phi_1(t)\phi_2(t) \,, \tag{6.4.2}$$

with the control-parameter vector, $\mathbf{V} = (v_1, v_2, v_3)$, which has three components, $v_n \geq 0$. For the long-time limit, $\phi(t \to \infty)$, one can rewrite the functionals, m_i, with the Eq. (6.2.1b) and (6.2.2) to

$$\frac{f_1}{1 - f_1} = v_1 f_1^2 + v_2 f_2^2 \,, \tag{6.4.3}$$

$$\frac{f_2}{1 - f_2} = v_3 f_1 f_2 \,. \tag{6.4.4}$$

So, the nonergodicity parameter of the second correlator, f_2, can be written as $f_2 = 1 - 1/(v_3 f_1)$. With the condition in Eq. (6.2.4) one can eliminate one more parameter and express v_1^c and v_2^c as a function of v_3 and f_1. To simplify the notation, variables x and y will be introduced as

$$v_3^c = x, \qquad f_1^c = y \,, \tag{6.4.5}$$

and

$$v_1^c = \frac{3 - (2 + x)y}{2(1 - y)^2(2 - xy)} \,, \tag{6.4.6}$$

$$v_2^c = \frac{x^2 y(y^2 - 2y^3)}{2(1 - y)^2(x^2 y^2 - 3xy + 2)} \,. \tag{6.4.7}$$

The critical parameters, v_1^c and v_2^c, define the surface of bifurcation singularities of Eq. (6.2.2) in the parameter space.

The amplitudes, which can be calculate with Eq. (6.2.6), are

$$h_1 = \frac{(1-y)(2 + x^2 y^2 - 2xy(1+y))}{2 + x - 6xy + 2xy^2 + x^2 y^2} \ , \tag{6.4.8}$$

$$h_2 = \frac{(1-y)(2 + x^2 y^2 - 2xy(1+y))}{xy^2(2 + x - 6xy + 2xy^2 + x^2 y^2)} \ . \tag{6.4.9}$$

From [33] we know the exponent parameter, $\lambda = 1 - \mu_2$:

$$\lambda = 1 - \frac{(3x^2 + 6x)y^3 - (x^2 + 18x + 9)y^2 + (6x + 18)y - 6}{(2x^2 + 4x)y^3 - 12xy^2 + (2x + 4)y} \ . \tag{6.4.10}$$

So, for $h_i(x, f_i)$ there is only one free parameter, x, which can be fixed for a given exponent parameter, λ. In Fig. (6.4.1) one can see $h(x, y)$ for different fit parameter. Since the nonergodicity parameter is quadratic in the leading order, the curves look like parabola. The green crosses represent the value of $\lambda = 0.735$ and the orange plus the value $\lambda = 2/3$, here v_3 is fixed. Non of the exponent parameters are in agreement with the HSS data. At least, in comparison with the one component mode, which gives only one point in the (h, f)-plane, the two component model covers a small region. Nevertheless, the Bosse-Krieger model alone describes the HSS not well enough.
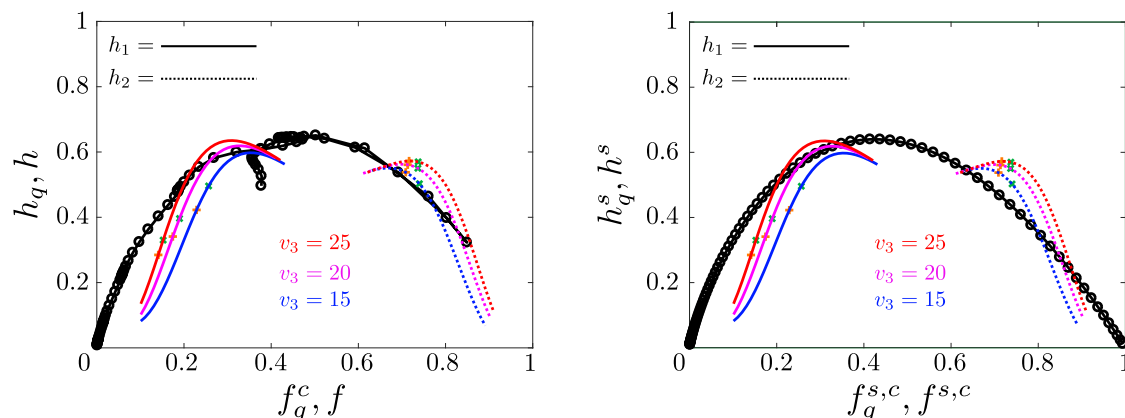
Figure 6.4.1: Results for the Bosse-Krieger model compared to the coherent and incoherent functions of the HSS. One can see that for different control parameter v_3 we match a small region of q-vectors. The HSS $\lambda = 0.735$, here shown as green crosses, as well as $\lambda = \frac{2}{3}$, the orange crosses, are not in an agreement with the HSS data.

Therefore, to get more free parameter we define a Sjögren correlator for the BK model

with:

$$m_A(t) = v_A[\eta\phi_1(t) + (1 - \eta)\phi_2(t)]\phi_A(t) \ . \tag{6.4.11a}$$

Here, v_A is the coupling parameter, and $\eta \in [0, 1]$ is a kind of concentration of the correlation functions. For $\eta = 1$, the Sjögren correlator is a coupling between the first correlation function, $\phi_1(t)$, and ϕ_A. For the opposite case, $\eta = 0$, the correlation function $\phi_1(t)$ gets irrelevant and $\phi_A(t)$ couples only to $\phi_2(t)$.

Here, the long-time limit of Eq. (6.4.11a) also generates a bifurcation with $\phi_A(t \to \infty) = f_A$, and this nonergodicity parameter can be expressed with x and y via

$$f_A = 1 - \frac{1}{v_A \left[\eta y + (1 - \eta)\left(1 - \frac{1}{xy}\right) \right]} \ . \tag{6.4.11b}$$

In analogy to the F_{12}-model we derive an amplitude, h_A, for the Sjögren correlator with

$$h_A(x, y, v_A, \eta) = \tag{6.4.11c}$$
$$\frac{x(1 - y)(2 + x^2y^2 - 2xy(1 + y))(1 + (xy^2 - 1)\eta)}{v_a(2 + x - 6xy + 2xy^2 + x^2y^2)(-1 + \eta + xy(1 + (y - 1)\eta))^2} \ .$$

In Fig. 6.4.2 the results of the coherent and incoherent HSS will be compared with the amplitude $h_A(x, f_A, v_a, \eta)$.
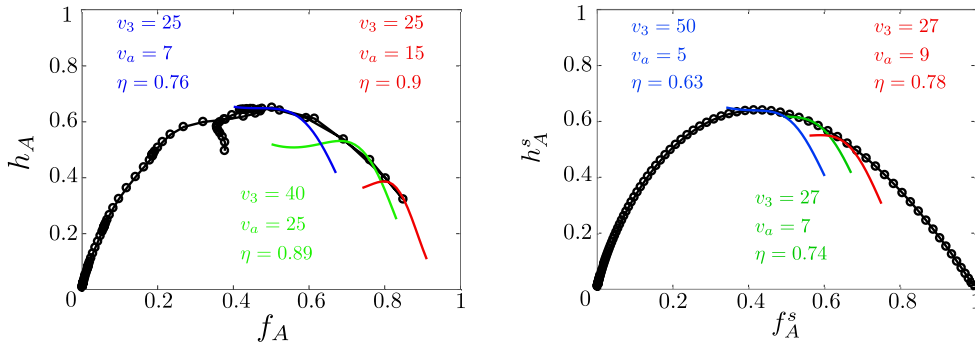
Figure 6.4.2: *Right:* The coherent function of HSS and some chosen values of the Bosse-Krieger model with the Sjögren correlator. One can see that the curves behave parabolic, so one can cover with suitable parameters, v_3, v_a, and η some regions of the HSS data. *Left:* Here, we compare the Bosse-Krieger model with the Sjögren correlator with the incoherent functions of the HSS.

As well for the coherent as for the incoherent functions the with the Sjögren correlator the data points of the HSS can be covered with suitable variables v_3, v_A, and η, fully. The correction amplitudes of the BK model, K_1 and K_2, can be calculated with Eq.(6.2.15). In Fig. 6.4.3 we compare the correction amplitudes from the BK model with the amplitudes of the HSS. One can see that K_1 and K_2 differ from the corrections of the HSS. Even the limits $K_1(f_q \rightarrow 0) = K_2(f_q \rightarrow 0) = \infty$ and $K_1(f_q \rightarrow \infty) = K_2(f_q \rightarrow \infty) = 0$ are incorrect.
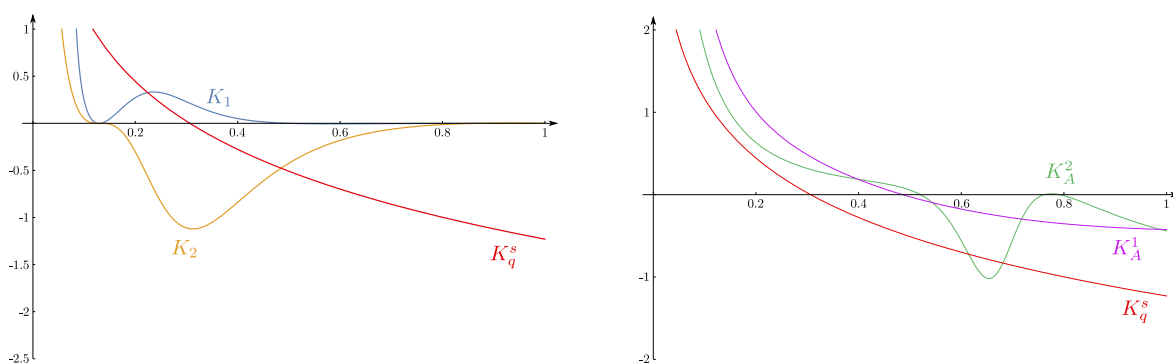
Figure 6.4.3: *Left:* The correction amplitudes K_1 and K_2 for a fixed control parameter $v_3 = 15$. One can see that the HSS results and the amplitudes from the BK model are not in agreement. The correction amplitudes are going to zero for $f \rightarrow 1$. *Right:* The correction amplitudes with the Sjögren correlator. For low f_q the trend of the curves are in good agreement. The values for the purple curve, K_A^1 are: $v_3 = 11$, $\eta = 0.7$, and $v_a = 2$ and the values of the green curve, K_A^2, are: $v_3 = 15$, $\eta = 0.4$, and $v_a = 5$.

The correction amplitude of the Sjögren correlator K_A is also displayed in Fig. 6.4.3 (right side). The correction amplitudes have the same trend, for small f_q and small v_3 the curves are quite parallel. With increasing v_a the correction amplitude starts to oscillate.

To compare the dynamics of the HSS with the Bosse-Krieger model, we took two different correlation functions, $\phi_{q=4.2}(t)$ and $\phi_{q=7.0}(t)$. The dynamics is shown in Fig. 6.4.4. In both plots we fixed the nonergodicity parameter of the second correlator, f_2, to the long time value of the hard sphere data. In the upper panel the value of x and y are fixed by the condition that the exponent parameters of both systems should be equal, $\lambda = 0.735$. Therefore, the nonergodicity parameter of the first correlator, f_1, deviates from the hard sphere data. In the lower panel I fixed the two parameters so

that the nonergodicity parameter for both correlators are given by their value for the HSS, $y = f_2$. Here the exponent parameter is given by $\lambda = 0.763$.

One can see that the description of microscopic time is not in a good agreement for both correlators.
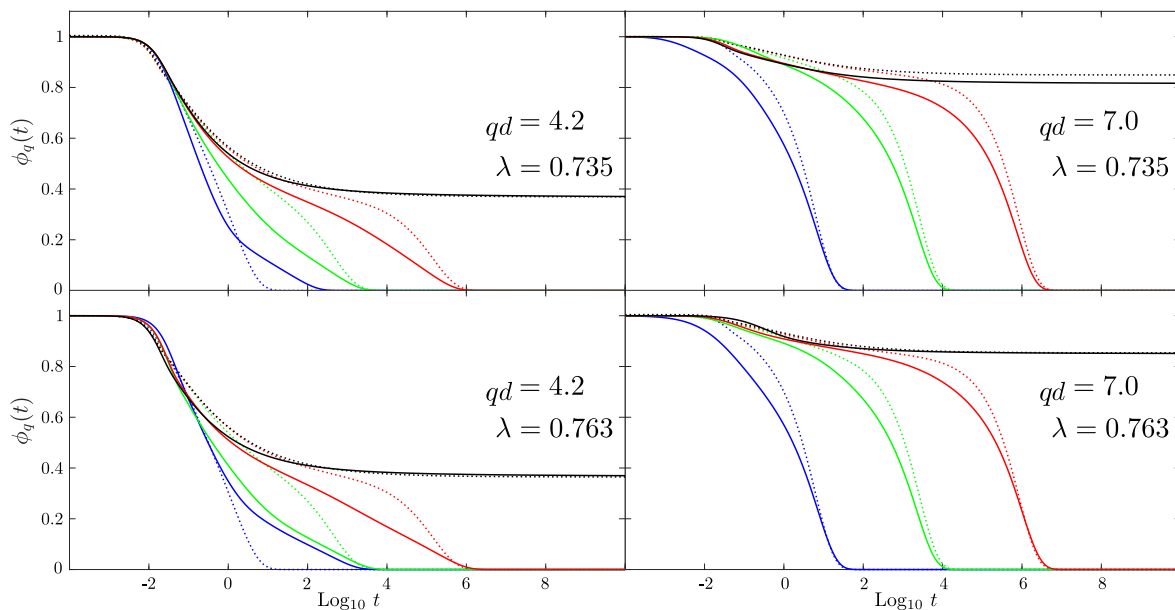
Figure 6.4.4: The correlation functions of the HSS, $\phi_{q=4.2}(t)$ and $\phi_{q=7.0}(t)$, and for the Bosse-Krieger model, $\phi_1(t)$ and $\phi_2(t)$. The solid lines are from the schematic model and the dotted lines from the simulation of the HSS. *Upper panels*: Here the exponent parameter of the Bosse-Krieger model is fixed to the HSS, $\lambda = 0.735$, which is given for $v_3 = 14.7$. Therefore, for $q = 7.0$ the nonergodicity parameter deviates from the HSS result.

Lower panels: The parameter of the system, $v_3 = 18.18$, is fixed to the nonergodicity parameter of the HSS. Here the exponent parameter of the BK model is $\lambda = 0.763$.

6.5 Conclusion

In summary, we explored descriptions of the HSS with a schematic model of MCT. With the one component F_{12}-model we were able to fix one point on the (f_q, h_q)-plane for a given λ. Since we want to cover more than one point we introduced the Sjögren correlator which is comparable with the incoherent function, ϕ^s. With one more parameter we obtained a line instead of a fixed point, Eq. (6.3.2c). But even with a line the agreement

of the HSS results and the schematic models are only acceptable for $f_q \rightarrow 1$, which is the trivial case, but at least helpful in light-scattering experiments.

With the Bosse-Krieger model, we tried to fit the HSS with a two component model. As we have a $h(f) \propto f^2$ relation for some chosen control parameter, we have a small regime which can be matched with the BK model. After introducing the Sjögren correlator for mixtures, Eq (6.4.11a), we get more parameters and can cover with these bigger parts of the (f_q, h_q)-plane. The correction amplitudes of both schematic models fail to describes the HSS and both models also have difficulties to characterize the dynamics of the HSS on short time scales. The correlation functions of both models are not describing the correlations of the HSS satisfactorily, even the Bosse-Krieger model has not enough free parameter to fit the HSS faithfully. As we discussed in the beginning, microscopic models—like the HSS—have an infinite number of parameters indexed by the wave number q. The schematic models we used here do not have a sufficient number of coupling parameters to describe such microscopic models. The next step is to use the Sjögren correlator for the Bosse-Krieger model and compare the correlation functions. With the Sjögren we could introduce two more parameters, η and v_a.

Nevertheless, one may use the schematic models to describe for a single wave numbers, q, some of the behavior of the HSS like the critical decay or the von Schweidler decay. The fits presented here, show that the conventional schematic models we tested are not complex enough to capture the complete dynamics of a microscopic model like the HSS.

6.6   Acknowledgment

I specifically thank M. Sperl and T. Kranz for the discussion about section 6.3 and 6.4, respectively, and I look forward to elaborate the chapter in a joint publication.

Bibliography

[1] W. Götze, *Complex dynamics of glass-forming liquids: A mode-coupling theory* (OUP, Oxford, 2009).

[2] W. Götze, J. Phys. Condens. Matter **11**, A1 (1999).

[3] A. Tölle, Rep. Prog. Phys. **64**, 1473 (2001).

[4] S. Adichtchev, T. Blochowicz, C. Tschirwitz, V. N. Novikov, and E. A. Rössler, Phys. Rev. E **68**, 011504 (2003).

[5] U. Bengtzelius, W. Götze, and A. Sjolander, Phys. Rev. E **17**, 5915 (1984).

[6] T. Voigtmann, A. M. Puertas, and M. Fuchs, Phys. Rev. E **70**, 061506 (2004).

[7] T. Voigtmann, Phys. Rev. E **68**, 051401 (2003).

[8] K. N. Pham, S. U. Egelhaaf, P. N. Pusey, and W. C. K. Poon, Phys. Rev. E **69**, 011503 (2004).

[9] M. Sperl, Phys. Rev. E **71**, 060401 (2005).

[10] T. Franosch, M. Fuchs, W. Götze, M. R. Mayr, and A. Singh, Phys. Rev. E **55**, 7153 (1997).

[11] W. Götze and L. Sjögren, Rep. Prog. Phys **55**, 241 (1992).

[12] V. Krakoviack, C. Alba-Simionesco, and M. Krauzman, J. Chem. Phys **107**, 3417 (1997).

[13] V. Krakoviack and C. Alba-Simionesco, J. Chem. Phys **117**, 2161 (2002).

[14] W. Götze and M. Sperl, Phys. Rev. Lett. **92**, 105701 (2004).

[15] M. Sperl, Phys. Rev. E **74**, 011503 (2006).

[16] J. P. Hansen and I. R. McDonald, *Theory of Simple Liquids* (Academic, London, 1986).

[17] U. Bengtzelius, W. Götze, and A. Sjolander, J. Phys. C **17**, 5915 (1984).

[18] S. F. Edwards and P. W. Anderson, J. Phys. F **5**, 965 (1975).

[19] M. Fuchs, I. Hofacker, and A. Latz, Phys. Rev. A **45**, 898 (1992).

[20] F. R. Gantmacher, *The Theory of Matrices Vol. II.* (American Mathematical Society, New York, 1960).

[21] W. Götze, Z. Phys. B **60**, 195 (1985).

[22] V. I. Arnol'd, *Catastrophe Theory, 3rd ed.* (Springer-Verlag, Berlin, 1992).

[23] W. Götze, Z. Phys. B **56**, 139 (1984).

[24] W. Götze and L. Sjögren, J. Phys.: Condens. Matter **1**, 4183 (1989).

[25] T. Franosch and A. P. Singh, J. Non-Cryst. Solids **235**, 150 (1998).

[26] W. Götze, A. P. Singh, and T. Voigtmann, Phys. Rev. E **61**, 6934 (2000).

[27] S.-H. Chong, W. Götze, and A. P. Singh, Phys. Rev. E **63**, 011206 (2000).

[28] S.-H. Chong, W. Götze, and M. R. Mayr, Phys. Rev. E **64**, 011503 (2001).

[29] S.-H. Chong and W. Götze, Phys. Rev. E **65**, 041503 (2002).

[30] S.-H. Chong and W. Götze, Phys. Rev. E **65**, 051201 (2002).

[31] M. Sperl, AIP Conference Proceedings **708**, 559 (2004).

[32] J. Bosse and U. Krieger, J. Phys. C **19**, L609 (1987).

[33] W. Götze and M. Sperl, Phys. Rev. E **66**, 011405 (2002).

Schematic Mode Coupling Theory and the Fredrickson-Andersen Model

The following chapter discusses the application of the schematic models to the Fredrickson-Andersen model. It is composed in a self-contained way to also in part facilitate the submission of that chapter as a research paper. We intend to submit the manuscript to the Physical Review Series of the American Physical Society.

Abstract

Kinetically constrained lattice models (KCM) will be used to describe glassy behavior in a compact way. Many effects like stretched exponential relaxation, self-diffusion, and dynamical heterogeneity can be shown in such models. The Fredrickson-Anderson (FA) model, a KCM with facilitated dynamics, displays a dynamical transition on the Bethe lattice, which is close to the predicted ones by the mode coupling theory (MCT). The strategy of this present work is to use the schematic MCT to characterize such transitions and find the similarities of both theories, the FA model and the MCT.

7.1   Introduction

While cooling or pressing glass-forming liquids a two step relaxation occurs [1]. Depending on the temperature or pressure a stretching of the decay function over several orders of magnitude in time t or frequence ω is to observed. The phenomenon of stretching in time was firstly observed by Kohlrausch in dielectric relaxation [2]. Von Schweidler finds, that the parts which are shifted over two or three decades in the dielectric loss spectra in ω obey the power law $\chi''(\omega) \propto (\omega\tau)^{-b}$ with $b < 1$ [3]. Mode-coupling theory, which is based on regular equations of motion for a set of autocorrelation functions, describes the structural relaxation and the stretching of glass-forming liquid very well and is consistent with the experimental measurements. So MCT predicts a critical spectrum $\chi''(\omega) \propto \omega^a$, with $0 < a < 0.5$ which is confirmed in molten salt $Ca(NO_3)_2KNO_3$ (CKN) [4–6] or in associated liquid glycerol [7–9].

In MCT the dynamics of a glass forming liquid will be described by a correlation

function of the density fluctuations, $\rho_{\vec{q}}$, which in general depends on the wave vector, $\vec{q}$. The correlation function is given by $\phi_q(t) = \langle \rho_{\vec{q}}^*(t)\rho_{\vec{q}} \rangle / \langle \rho_{\vec{q}}^*\rho_{\vec{q}} \rangle$, where the denominator is the static structure factor, $S_q = \langle \rho_{\vec{q}}^*\rho_{\vec{q}} \rangle$. With the Mori-Zwanzig formalism [10–13] and considering colloidal particles, a Brownian equation of motion (EOM) can be derived. The exact memory function, $m_q(t)$, which comes from the Mori-Zwanzig method, is given by the fluctuating forces and can not be calculated exactly for a general potential. To understand the concept of MCT, the memory function will be approximated by a functional, $\mathcal{F}_q[\mathbf{V}, \phi]$, which is called schematic model. Although schematic models have less complexity than the microscopic theory, they describe some phenomena surprisingly well [14–17]. Furthermore, with the long time limit of the correlation function, $\phi_q(t \to \infty)$, MCT describes the bifurcative behavior during the glass-transition in Arnold's terminology [18]. So depending on the control parameter of the system, which in microscopic models is typically the temperature , T, or the packing fraction, φ, the correlation function, $\phi(t)$, goes in a glassy state to a finite value, $\phi(t \to \infty) \to f$, where f is the so-called non-ergodicity parameter, or to zero in the liquid state. With those bifurcation equations, which occur for the long time limit of the correlation function, MCT derives a power law, t^{-a}, here a is the critical exponent, for the critical decay to the plateau ,f, and obtains also the von Schweidler law, $-t^b$, from the plateau to zero for a liquid. So for a given memory kernel MCT predicts the dynamics for the system and the glass transition.

Efficient models for analyzing glassy behavior are kinetically constrained models [19, 20], especially the Fredrickson-Andersen model (FA) [21] with dynamic facilitation. In that model the lattice with sites $i = 1, ..., N$ is decorated with up- and down-spins and the the Hamiltonian describes uncoupled Ising spins, $\sigma_i \in \{-1, 1\}$, in an external magnetic field, $\mathcal{H} = \mu \sum_i \sigma_i$, which prefers down spins, $\mu > 0$ [22, 23]. A spin on site i only flips if it has at least f_a down-spin neighbors [21, 24]. Here f_a is the facilitation parameter and is a number between zero and the lattice connectivity, k. The kinetic constraint can be interpreted as the cage effect in glass forming liquids. A particle is arrested in a cage formed by its surrounding neighbors and motion can only happen cooperatively. The Fredrickson-Andersen model on the Bethe lattice is a candidate where a dynamical transition, similar to the MCT, occurs [25–28]. Several phenomena which are predicted by the MCT like the two step relaxation or a stretched exponential relaxation can be observed on the Bethe lattice [29]. Since a fold bifurcation, an A_2-singularity in

Arnold's terminology, occurs we want to describe the dynamics with MCT. The goal of the paper is to find a schematic model which fits the simulation done by Sellitto [29].

7.2　Fredrickson-Andersen Model on the Bethe lattice

The Bethe lattice [30] is a regular graph with a fixed connectivity, k [31]. Now, consider N Ising spins , $\sigma_i \in \{-1, 1\}$, on the sites i of the Bethe lattice. The spins don't have any coupling effect, $J = 0$, where J is the coupling constant, and therefore the Hamiltonian is given by $\mathcal{H} = -\frac{1}{2} \sum_i^N \sigma_i$. The constrained dynamics, which is a Markov-process of Glauber type, depends on two variables, the facilitation parameter f_a, and the connectivity k. Each time step a random spin will be chosen and iff this spin has f_a or more down-spin neighbors it will be flipped with a rate, $\omega = \min\{1, \mathrm{e}^{\beta\sigma_i}\}$, where β is the inverse temperature.

We now introduce the Bootstrap percolation (BP) [32–35] which is concerned with the ground state of the FA model. Here the temperature is $T = 0$, which means that only up-spins can be flipped with a rate of $\omega = 1$ to down-spins iff they fulfill the condition. So starting with an initial up-spin concentration, p, we want to know if all the up-spins will be flipped into down-spins or if some up-spin clusters will- because of the constrainment- remain.

In different publications [24, 36] it is shown that independent of the facilitation parameter, f_a, in hypercubic lattices $\mathbb{Z}^d$ the up-spins can only survive for $p = 1$. On the Bethe lattice or other random graphs a transition occurs for $1 < f_a < k$ [26, 27] and a finite critical concentration $p_c < 1$ [32, 37, 38]. The probability of an up-spin in the ground state, q, is known exactly for the BP [28, 32] and is given as

$$q = pQ(q) := p \sum_{i=0}^{f-1} \binom{k}{i} q^{k-i}(1-q)^i. \tag{7.2.1}$$

Notice, the inital concentration, p, is always larger than the up-spin probability, q, except for $p \in \{0, 1\}$ where both are equal. The physically relevant solution of Eq. (7.2.1) is the largest real one. A fold bifurcation, a type A_2 in Arnold's terminology, occurs at the critical concentration $q_c \equiv q(p_c) > 0$.

7.2.1 Bifurcation Scenario in the FA Model

The easiest case, where a transition takes place, is given by the couple $(f_a, k) = (2, 3)$ and Eq. (7.2.1) simplifies to

$$q = p \left(3(1-q)q^2 + q^3 \right) \ , \tag{7.2.2}$$

with the roots

$$q = 0$$
$$q_\pm = \frac{3}{4} \pm \frac{3}{4}\sqrt{\epsilon} \ . \tag{7.2.3}$$

Here, $\epsilon = \frac{p-p_c}{p_c}$ is the separation parameter, which gives the distance to the critical point. The critical point is at $p_c = 8/9$ and the critical probability, $\epsilon = 0$, is at $q_c = 3/4$. One also can see the square root singularity, $q(p) - q_c \sim \sqrt{p - p_c}$. Since we know, that the groundstate probability of up-spins, q, is for $p = 1$ also one, the physically relevant solution is $q_+ = q_c + 3/4\sqrt{\epsilon}$. For initial concentrations below the critical one, $p < p_c$ the solution is $q = 0$.

In Fig. 7.2.1 one can see the probability q depending on the concentration p of the up spins for the easiest case. At the critical concentration, p_c, there is a discontinuous jump from $p = 0$ to $p = 8/9$.

Of special interest is the persistence function $\psi(t)$, which gives the fraction of the spins that have not changed their orientation since $t = 0$ [19, 28]. The long time limit, which the persistence function reaches asymptotically, gives the fraction of the so called frozen spins, which are never flipped. In analogy to the glass-theory, here we also have two possibilities: (1) the initial concentration of up-spins is below the critical one, $p < p_c$, then the persistence function will have relaxation to zero, like the auto-correlation function, $\phi(t)$, in MCT, or the concentration is high enough, $p > p_c$, and some up-spin clusters will remain and the persistence function will go to a finite value, f.

The decay from the plateau to zero is an exponential one, $\psi(t) \sim \exp(-t/\tau_\alpha)$, where $\tau_\alpha \sim \epsilon^{-\gamma'}$, with the exponent $\gamma' \geq 2$, is the timescale of the α-relaxation time [39]. The
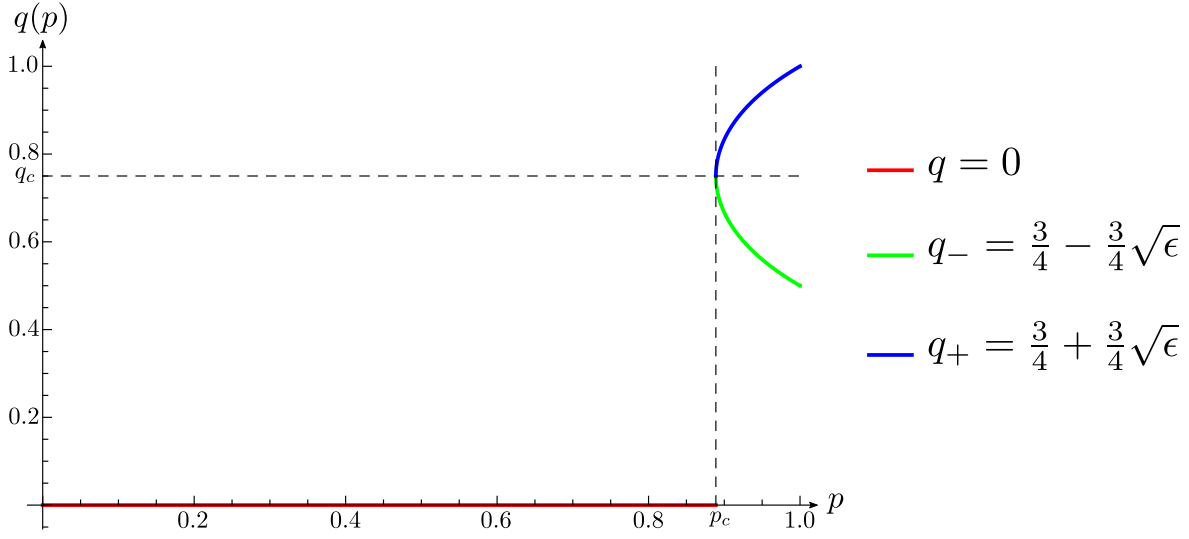
Figure 7.2.1:   The up-spin concentration of the ground state, $q(p)$, as a function of the initial up-spin concentration, p. Here the facilitation parameter is $f_a = 2$ and the connectivity $k = 3$. One can see a discontinuous jump at the critical point $(p_c, q_c) = (8/9, 3/4)$. For $p > p_c$ there is a square root singularity, $q(p > p_c) \sim \sqrt{\epsilon}$.

long time limit of the critcal persistence function, $\psi^c(t \to \infty) = \psi_\infty^c$, is given as [28]

$$\psi_\infty^c(p_c, q_c) = p_c \sum_{i=0}^{f-1} \binom{k+1}{i} q_c^{k+1-i}(1-q_c)^i$$

$$+ (1 - p_c) \sum_{i=0}^{f-1} \binom{k+1}{i} (p_c C_{k,f})^{k+1-i}(1 - p_c C_{k,f})^i. \qquad (7.2.4)$$

which $C_{k,f} = \sum_{i=0}^{f-2} \binom{k}{i} q_c^{k-i}(1-q_c)^i$. For the standard case of $f = 2$ and $k = 3$ the asymptotic plateau value is $\psi_\infty^c = \frac{2757}{4096} \approx 0.673096\dots$.

In Tab. (7.2.1) one can see some configurations of the Bethe lattice and all the corresponding critical values. Here one should know that for getting the critical value of a couple (f, k) one has to calculate the roots of a polynomial of order k and find the right root which belongs to the condition $q(p = 1) = 1$, which make the calculations for high polynomials difficult.

As well the bifurcation scenario as the two-step behavior of the persistence function motivates us to compare the Fredrickson-Andersen model with the mode-coupling theory.

Table 7.2.1: Here the critical parameter for different topological configuration of the Bethe lattice are given. One can see, that for a fixed facilitation, f_a, and increasing connectivity, $k \to \infty$, the concentrations, p_c and q_c and therefore the critical plateau value, ψ_∞^c are increasing to one. The temperatures, however, decreases. The opposite happens for the case $\lim_{k \to \infty}(k-1, k)$, where the critical concentrations are decreasing and the temperature increases.

(f_a, k)	p_c	q_c	ψ_∞^c
$(2, 3)$	$8/9$	$3/4$	$2757/4096$
$(2, 4)$	$0.949\ldots$	$0.894\ldots$	$0.925\ldots$
$(2, 5)$	$0.971\ldots$	$0.941\ldots$	$0.977\ldots$
$(3, 4)$	$0.725\ldots$	$0.544\ldots$	$0.277\ldots$
$(3, 5)$	$0.835\ldots$	$0.727\ldots$	$0.599\ldots$
$(4, 5)$	$0.603\ldots$	$0.418\ldots$	$0.121\ldots$
$(2, 20)$	$0.999\ldots$	$0.998\ldots$	$0.999\ldots$
$(19, 20)$	$0.164\ldots$	$0.096\ldots$	$0.001\ldots$

7.3   Mode Coupling Theory

In the mode coupling theory the microscopic dynamics of N interacting particles will be described by autocorrelation functions of the density fluctuations, $\rho_{\vec{q}} = \frac{1}{\sqrt{N}} \sum_j^N e^{i\vec{q}\vec{r}_j}$, which are given by

$$\phi_q(t) \frac{\langle \rho_{\vec{q}}(t) | \rho_{\vec{q}} \rangle}{\langle |\rho_{\vec{q}}|^2 \rangle} \ . \tag{7.3.1}$$

The brackets, $\langle A|B \rangle = \langle \delta A^* \delta B \rangle$ and $\delta A = A - \langle A \rangle$, denotes canonical averages. The time dependency of the density fluctuations, $\rho_{\vec{q}}(t)$, is given by the Lioville equation

$$\dot{\rho}_{\vec{q}}(t) = i\mathcal{L}\rho_{\vec{q}} \ , \tag{7.3.2}$$

as $\rho_{\vec{q}}(t) = \rho_{\vec{q}} e^{i\mathcal{L}t}$. Now, applying the Mori-Zwanzig formalism [10–13] for colloidal particles the Brownian equation of motion is derived

$$\tau_q \dot{\phi}_q(t) + \phi_q(t) + \int_0^t \mathrm{d}\tau m_q(t - t')\dot{\phi}_q(t') = 0 \tag{7.3.3}$$

where τ_q is the microscopic time scale and $m_q(t)$ the memory kernel. With the initial conditions, $\phi_q(0) = 1$ and $\dot{\phi}_q(0) = 0$, the equation of motion has only one analytical solution [40].

Now we use the Laplace transformation - with the convention $\mathrm{LT}[\phi](z) = \mathrm{i} \int_0^\infty \mathrm{d}t \, \mathrm{e}^{\mathrm{i}zt} \phi(t)$ - to bring the EOM in a compact form

$$\phi_q(z) = \frac{1}{z + \frac{1}{\tau + m_q(z)}} \ . \tag{7.3.4}$$

7.3.1   Dynamics in the β-Regime

While in the liquid state the correlations vanishes for long times, $\phi_q^{\mathrm{l}}(t \to \infty) = 0$, for glassy systems it converges to a finite value, $\phi_q^{\mathrm{g}}(t \to \infty) = f_q$, the non-ergodicity parameter. To have an analogy to a thermodynamical phase transition, the non-ergodicity parameter can be seen as an order parameter. So to make any predictions about the glass transition, we are interested in the long time limit. The microscopic time scale is negligible for long times and Eq. (7.3.4) will be

$$\frac{\phi(z)}{1 + z\phi(z)} = m_q(z) \ . \tag{7.3.5}$$

Now, we assume that the memory function can be written as a polynomial of the correlation function, $m_q(t) = \mathcal{F}_q[\mathbf{V}, \phi_k(t)]$, where $\mathbf{V}$ is a control parameter vector. Then for glassy systems both the correlation function and the memory kernel exhibit a non ergodicity pole for z going to zero, $\lim_{z \to 0} z\phi_q(z) \to -f_q$ respectively $zm_q(z) \to \mathcal{F}_q[\mathbf{V}, f_k]$. So Eq. (7.3.4) is a bifurcation equation

$$\frac{f_q}{1 - f_q} = F_q[\mathbf{V}, f_k] \ . \tag{7.3.6}$$

For a given functional, $F_q[f_k]$, Eq. (7.3.6) can have more than one analytical solution, say $\tilde{f}_q$, but with the maximum theorem [41, 42], the glass form factor, f_q, is distinguished by: $\tilde{f}_q \leq f_q, \forall q$.

To eliminate the non ergodicity pole the correlation function, $\phi(t)$, will be expressed

with a master function, $G_\sigma(t)$, the glass form factor, f_c, and an amplitude $h = (1 - f_c)$

$$\phi(t) = f_c + hG_\sigma(t) \text{ and } z\phi(z) = -f_c + zhG_\sigma(t) \ . \qquad (7.3.7)$$

The master function can be factorized to $G_\sigma(t) = \sqrt{\sigma}g(t)$, where $\sigma = C\epsilon$ is the separation multiplied by a system depending constant C and $g(t)$, which is the solution of the EOM.

With the transformation in Eq. (7.3.7) the non-ergodicity pole vanishes and $|zG(z)|$ gets small for small frequencies, so $|{}^{zG(z)}\!/_{(1-f)}|$ is an useful small parameter to extend. The master function $G^{n+1}(t)$ decreases faster than $G^n(t)$ to zero so that the ratio ${}^{G^{n+1}(t)}\!/_{G^n(t)}$ gets smaller for $t \to \infty$.

With both assumptions Eq. (7.3.5) can be expanded in terms of $G(t)$ [43]:

$$
\begin{aligned}
&-\frac{\delta_0}{z} + \delta_1 hG(z) \\
&+ (1 + \delta_2)h^2\mathrm{LT}[G(t)^2] + zh^2G(z)^2 \\
&+ (\gamma_3 + \delta_3)h^3\mathrm{LT}[G(t)^3] - \gamma_3 z^2 h^3 G(z)^3 \\
&+ (\gamma_4 + \delta_4)h^4\mathrm{LT}[G(t)^4] + \gamma_4 z^3 h^4 G(z)^4 \\
&+ \ .... = 0
\end{aligned}
\qquad (7.3.8)
$$

with the coefficients

$$
\begin{aligned}
\gamma_k &= \frac{1}{(1 - f)^{k-2}} \ , \\
\delta_k &= \frac{\partial^k \Delta\mathcal{F}(\mathbf{V}, f)}{\partial f^k}\frac{(1 - f)^3}{k!} \ , \\
\Delta\mathcal{F}(\mathbf{V}, f) &= \mathcal{F}(\mathbf{V}, f) - \frac{f}{1 - f} \ .
\end{aligned}
\qquad (7.3.9)
$$

The order of $G(t)$ is related to the typ of bifurcation of a given system. With the derivatives of $\Delta\mathcal{F}(\mathbf{V}, f)$ one can calculate the generic singularities of type A_l with

$$
A_l : \quad
\begin{aligned}
\frac{\partial^k \Delta\mathcal{F}(\mathbf{V}, f)}{\partial f^k} &= 0, \qquad \text{for } k < l, \\
\frac{\partial^k \Delta\mathcal{F}(\mathbf{V}, f)}{\partial f^k} &\neq 0, \qquad \text{for } k = l.
\end{aligned}
\qquad (7.3.10)
$$

In Fig. (7.2.1) one can deduce a square root singularity, which is an type A_2 singularity in Arnold's definition, so that in our case the dynamics obeys in leading order to

$$\lambda h^2 \mathrm{LT}[G(t)^2] + z h^2 G(z)^2 = \frac{\sigma}{z} \ . \tag{7.3.11}$$

Where $\lambda \coloneqq 1 + (1 - f_q^c)^3 \partial_{f_q^2} \Delta \mathcal{F}_q[\mathbf{V}^c, f^c]/2$ is called the exponent parameter. Here f_q^c is the value at the critical point, $\mathbf{V}^c$. The Eq. (7.3.11) can be solved numerically which will be done later for some given memory kernels.

More interesting is the analytical solution, which can be done easily for the critical value, $\sigma = 0$. Here, it can be solved by $G_0(t) \sim t^x$, which fixes the exponent parameter, $\lambda = {}^{\Gamma^2(1+x)}/_{\Gamma(1+2x)}$ [44]. The critical decay, which is the decay to the plateau, the master function obeys the power law $G_0(t) \sim t^{-a}$, where the critical exponent a is defined as the smallest negative $x \equiv -a < 0$. For finite σ, the right-hand side of Eq. (7.3.11) does not vanishes and the master function has a square root dependency on σ, $G_\sigma(\hat{t}) = \sqrt{\sigma} g(\hat{t})$, where $\hat{t} = t/t_\sigma$ with $t_\sigma \propto |\sigma|^\delta$ is a rescaled time. t_σ itself is the plateau crossing time, and $\delta = 1/(2a)$ a scaling exponent [44]. In the liquid state there is a second decay after crossing the plateau, $t > t_\sigma$, which can be described with the von Schweidler law. Here, the solution of Eq. (7.3.11) is $g({}^t/_{t_{\sigma'}}) \sim -({}^t/_{t_{\sigma'}})^b$, where $t_{\sigma'} \sim \sigma^{-\gamma}$ with $\gamma = {}^1/_{2a} + {}^1/_{2b}$ is the time scale for the decay away from the plateau. The von Schweidler exponent, b, is the smallest positive x.

7.3.2   Schematic Models for the FA-Model

The Eq. (7.3.3) is exact but useless since nothing is known about the memory kernel, $m_q(t)$. Nevertheless, with some approximations one can show the main idea of the MCT. Therefore the memory kernel will now approximated as

$$m[\phi] = \mathcal{F}[\phi] \approx \sum_{i=1}^{N} v_n \phi^n(t) \ . \tag{7.3.12}$$

The simplest form, $\mathcal{F}_1[\phi(t)] = v_1 \phi(t)$, is a mathematically trivial form. The $\mathcal{F}_2[\phi(t)] = v_2 \phi^2(t)$ model generates a bifurcation, but there is no stretching in the α-relaxation [45, 46]. With the F_{12}-model, $\mathcal{F}_{12} = v_1 \phi(t) + v_2 \phi^2(t)$, we have the simplest form of a polynomial to generate an A_2 bifurcation with an α-relaxation [17]. Now, one can use

the bifurcation equation, $f^c/(1 - f^c) = v_1 f^c + v_2 f^{2c}$, and its derivative with respect to f, $1/(1 - f^c)^2 = v_1 + 2v_2 f$, to write the critical control parameters as a function of f^c: $v_1^c = (1 - 2f^c)/(1 - f^c)^2$ and $v_2^c = 1/(1 - f^c)^2$.

The exponent parameter, λ, is easy to calculate with the definition above and is given by $\lambda = 1 - f^c$. So all the critical parameters of this F_{12}-model are fixed by only one parameter:

$$v_1^c = \frac{2\lambda - 1}{\lambda^2} \quad \text{and} \quad v_2^c = \frac{1}{\lambda^2} \ . \tag{7.3.13}$$

To compare any experimental results or simulation data with the F_{12}-model, one has to find the exponent parameter, $0.5 < \lambda < 1$. Since $\lambda > 0.5$ the critical plateau value, $f^c = 1 - \lambda$, is always below $\frac{1}{2}$. This makes describing some systems unphysical, like the hard sphere system, where $\lambda = 0.735$ [9] but the critical plateau is not fixed to $f^c = 0.265$. Therefore, we introduce a second correlator, the so-called Sjögren correlator, with the memory function

$$m_A = v_a \phi(t) \phi_A(t) \ . \tag{7.3.14}$$

This can be seen as a single particle, $\phi_A(t)$, which couples to the density fluctuations, $\phi(t)$. The coupling constant, v_A, gives the system one more degree of freedom. Here, we also can use the bifurcation equation for f_A^c, and get $f_A^c = 1 - 1/(v_A^c f^c)$. Since the Fredrickson-Andersen model generates an A_2 bifurcation and is an one component model, without any wave-vector dependency, the description of the F_{12}-model could help to understand the microscopics of the FA model.

7.4   Microscopic Dynamics of the FA-model

Here, the microscopic dynamics of one up-spin will be used to derive a correlation function, $\phi(t)$, for up-spins. As microscopic variable we introduce $\eta_{\sigma_i}(t) = \delta_{1,\sigma_i}(t)$, which is one when the spin on site i is an up-spin or zero for a down-spin. Now, we define the correlation function as

$$\phi(t) = \langle \eta_{\sigma_i}(0) | \eta_{\sigma_i}(t) \rangle \ , \tag{7.4.1}$$

with the long-time limit $\phi(t \to \infty) = q$. The normalization to q as the long time limit is important, here q is in analogy to the non-ergodicity parameter f. Since the correlation function is normalized to its long time value, $t \to \infty$, the value at $t = 0$ is not normalized to one anymore, but to the inital up-spin concentration, $\phi(t = 0) = p$.

With the Fokker-Planck equation [47]

$$\dot{P}(\{\sigma\}_\alpha, t) = \underline{\Omega} P(\{\sigma\}_\alpha, t) \ , \tag{7.4.2}$$

where P is the probability distribution function and $\underline{\Omega}$ a stochastic operator, one can derive an Hamiltonian for the time evolution of the microscopic variable, $\eta_{\sigma_i}(t)$. The stochastic operator for the spin system is given by [48]

$$\underline{\Omega} = \sum_\alpha \left(\hat{S}_\alpha - 1 \right) \omega_\alpha(\{\sigma\}_\alpha) \ , \tag{7.4.3}$$

with the spin-operator, $\hat{S}_\alpha$, which flips a spin and the transition probability of the spin α, $\omega_\alpha(\{\sigma\}_\alpha)$. The Hamiltonian is given by

$$\mathcal{H} = P_{\text{eq}}^{-1/2}(\{\sigma\}_\alpha) \underline{\Omega} P_{\text{eq}}^{1/2}(\{\sigma\}_\alpha) \tag{7.4.4}$$

where the index eq denotes the equilibrium state. With this Hamiltonian we define projection operators and use the Mori-Zwanzig formalism to get the EOM like Eq. (7.3.3) for a spin autocorrelation function, $\phi(t)$ [27, 49]. The microscopic time-scale, τ can be calculate exactly for this model and is given by

$$\tau = \omega_0 p \left(1 - \frac{\sum_{i=0}^{f-1} \binom{k}{i} \mathrm{e}^{-(k-i)\beta}}{(1 + \mathrm{e}^{-\beta})^k} \right)^{-1} . \tag{7.4.5}$$

Since we fixed the long-time limit of our autocorrelation function to the probability of up-spins in the ground state, $\phi(t \to \infty) = q$, equation of motion becomes a bifurcation equation with the inital value $\phi(0) = p$

$$\frac{q}{p-q} = p \sum_{i=0}^{f-1} \binom{k}{i} q^{k-i}(1-q)^i. \tag{7.4.6}$$

Here, we assume that Eq. (7.4.6) is the long-time limit of the EOM, which is based on the correlation function, $\phi(t)$. Notice, there are more completely monotonous functions with the same long time limit, like $\phi(\log(t))$ which also converges to q for $t \to \infty$. With the conjecture that $\phi(t)$ generates the EOM we can derive the exponent parameter, λ,

for the FA model with

$$\lambda = 1 + \frac{(p_c - q_c)^3}{2p_c} \left. \frac{\partial \Delta \mathcal{F}[p, q]}{\partial q} \right|_{p=p_c, q=q_c} . \qquad (7.4.7)$$

Notice, because of the normalization, $\phi(0) = p$, the prefactor here is $(p_c - q_c)^3/p_c$ instead of $(1 - f^c)^3$ which is derived in section 7.3.1. For the standard case of $(f, k) \rightarrow (2, 3)$ the exponent parameter is $\lambda = {}^{839}\!/_{864} \approx 0.971$.

7.5   The F_{12} Model and the FA Model

In this section we will fit the Fredrickson-Andersen model with the F_{12} model. Since the exponent parameter, λ, fixes the control parameter we will also use the Sjögren correlator and fit at least one parameter. We want to use two different exponent parameters, $\lambda_S = 0.815$ from fitting Sellittos numerical data [29] and $\lambda_K = {}^{839}\!/_{864}$ from the calculation above.

The separation, σ, can be written explicitly for the F_{12}-model as [17]

$$\sigma = [\hat{v}_1 + \hat{v}_2(1 - \lambda)] \lambda(1 - \lambda), \quad \hat{v}_i = v_i^c - v_i . \qquad (7.5.1)$$

Since we know all the initial concentrations of the simulation data and the critical concentration, $p_c = 8/9$, the distance parameter, ϵ, can be calculated and we only have to fit the system variable C to have the right separation, σ. With the separation parameter and Eq. (7.5.1) we can get different paths in the (v_1, v_2)-plane, some of them can be seen in Fig. (7.5.1).

Now, for the path $v_1 = \text{const}$, we will fit the simulation data. In this case v_2 is a function of the separation and we only have to fit C:

$$v_2 = v_2^c - \frac{C\epsilon}{\lambda(1 - \lambda)^2} . \qquad (7.5.2)$$

In Fig (7.5.2) and (7.5.3) one can see the simulation data and the results of the schematic model (the other paths are in appendix H). For the fitted exponent parameter, λ_S, the curves are in a better agreement than for the calculated one. Since the calculated exponent parameter is close to $\lambda = 1$, which describes a higher order singularity, it
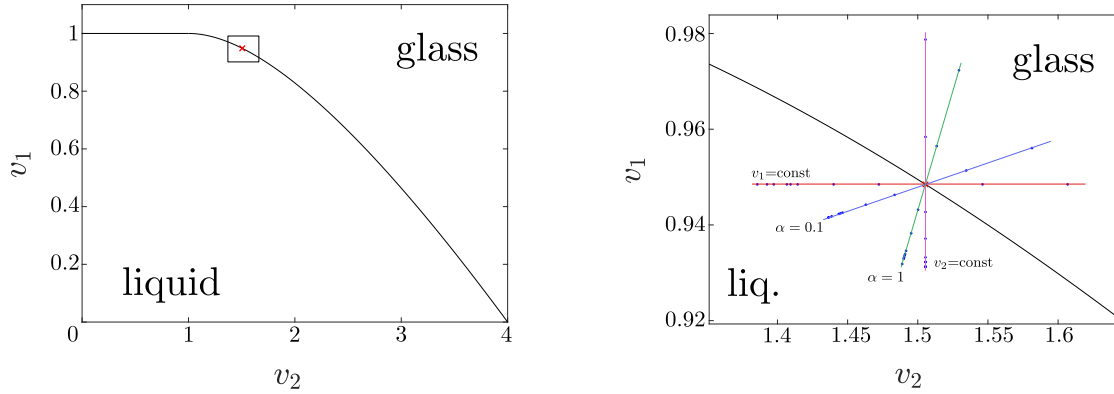
Figure 7.5.1: *Left:* The (v_1, v_2)-plane of the F_{12}-model, with the liquid-glass transition line. Above the black straight line the system is in the glass state and below the line in the liquid state. The red cross marks $\lambda_S = 0.815$. *Right:* Here one can see four different paths for the fixed exponent parameter, λ_S. The horizontal path is at $v_1 = v_1^c = $ const and a varying v_2, whereas the perpendicular path is at the opposite point, $v_2 = v_2^c = $ const and a varying v_1. The other two paths are given by the straight line $v_1 = \alpha v_2$, where α is the slope. Here we use $\alpha = 0.1$ and $\alpha = 1$.
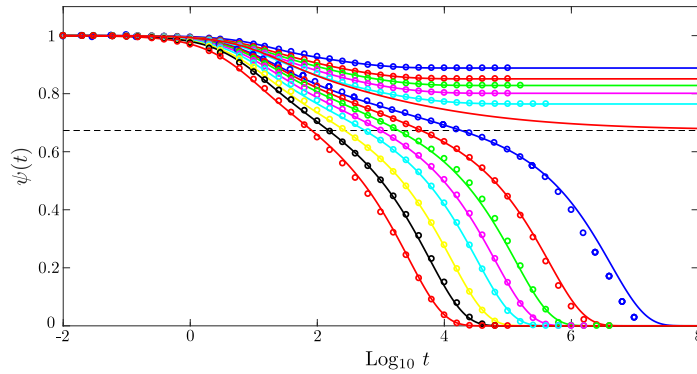
Figure 7.5.2: The simulation data [29] and the results of the F_{12}-model with a fitted exponent parameter, λ_S=0.815, for a fixed $v_1 = v_1^c$ and variable v_2. In the glass state, below the critical temperature, $T = 1/\log(8)$, the temperatures are $T = 0.42, 0.44, 0.45$. 0.46, and 0.47. In the liquids states Sellitto simulated the temperatures $T = 0.49$, $0.5, 0.51, 0.52, 0.53, 0.55, 0.57$, and 0.6 The black dashed line is the critical plateau, $\psi_\infty^c = \frac{2757}{4096}$ and the dashed red line the decay at the critical point, $\sigma = 0$. Here, the value of the coupling constant is fixed for all curves, $v_A(f_A^c, \lambda) = v_A(\frac{2757}{4096}, 0.815) = 16.54...$ and the frequencies are fixed to one $\Omega = \Omega_A = 1$.
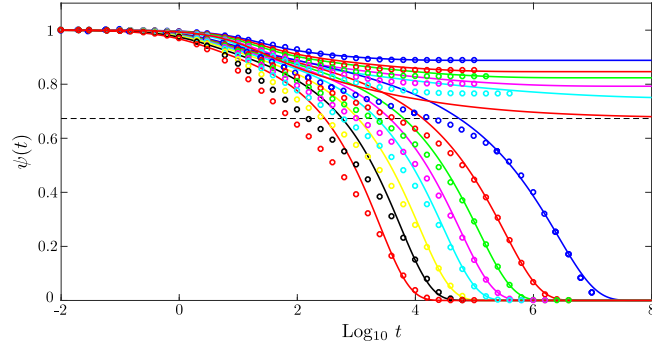
Figure 7.5.3: Here we see the simulation data [29] and the results of the F_{12}-model for the calculated exponent parameter, $\lambda_K = \frac{839}{864}$, and for a fixed $v_2 = v_2^c$ and variable v_1. The temperatures are the same as Fig. (7.5.2). The value of the coupling constant is fixed for all curves, $v_A(f_A^c, \lambda) = v_A(\frac{2757}{4096}, \frac{839}{864}) = 105.719...$ and the frequencies are fixed to one $\Omega = \Omega_A = 1$.

was expected that the F_{12} will have some difficulties for such an λ. Therefore, in the next section the Bosse-Krieger model will be used to fit the simulation data with the calculated λ_K.

The evolution of the microscopic parameters are in Fig (7.5.4). Those microscopic parameter are for the fitted exponent parameter λ_S, the trend for the calculated one, λ_K is the same.
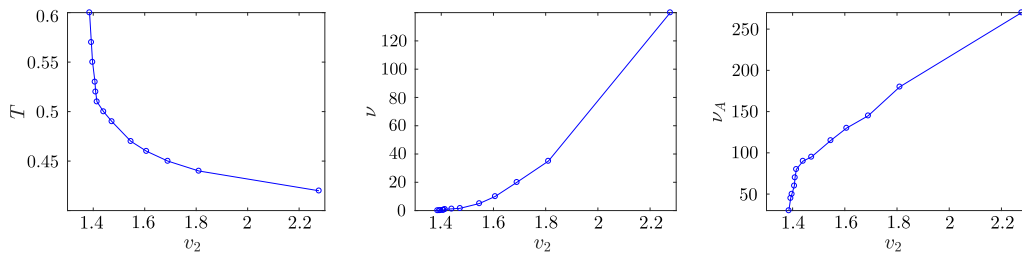
Figure 7.5.4: Different microscopic parameters as a function of v_2 at a fixed $v_1 = v_1^c$ and λ_S. The critical value, where the transition from glass to liquid happens is at $v_2^c = 1/\lambda^2 = 1.50551$. The microscopic time scale is defined as $\tau = \nu/\Omega^2$, where Ω and ν are frequencies. The frequency Ω and Ω_A are fixed to one. One can see that all three parameters are monotonic.

7.6   Bosse-Krieger Model for the FA Model

The theoretically calculated exponent parameter, λ_K is close to one, which makes the fitting with the F_{12}-model difficult. In Fig (7.5.1) one can see the phase diagram of the F_{12}-model, at the horizontal line $(v_2 = 0, v_1 = 1) \rightarrow (v_2 = 1, v_1 = 1)$, which is called type-$A$ line, the exponent parameter is $\lambda = 1$. So for large λ all the paths like in Fig (7.5.1) are close to the A-line and therefore close to the A_3-singularity. This higher order singularity, which is described by a logarithmic decay [52], can affect our chosen path. To avoid this effect we want to use the Bosse-Krieger model, where we have a type-B line, which can be shifted by f_1^c.

The Bosse-Krieger (BK) model is a two-component model which was introduced to describe symmetric molten salt [50, 51]. The two kernels of the model are given by

$$m_1 = v_1 \phi_1(t)^2 + v_2 \phi_2(t)^2$$
$$m_2 = v_3 \phi_1(t) \phi_2(t) \tag{7.6.1}$$

where $v_i \geq 0$ are the control parameters. With the two conditions from the long-time limit, $f_1^c/(1 - f_1^c) = v_1 f_1^{c2} + v_2 f_2^{c2}$ and $f_2^c/(1 - f_2^c) = v_3 f_1^c f_2^c$, one gets the critical control parameter as a function of $v_3 = x$ and $f_1^c = y$ [52]

$$v_1^c = \frac{3 - (2 + x)y}{2(1 - y)^2(2 - xy)} \; ,$$
$$v_2^c = \frac{x^2 y(y^2 - 2y^3)}{2(1 - y)^2(x^2 y^2 - 3xy + 2)} \; . \tag{7.6.2}$$

The exponent parameter is also a function of the two variables and is defined for $x > 4$ and $\frac{3}{2+x} \leq y \leq \frac{1}{2}$ as [52]

$$\lambda = 1 - \frac{(3x^2 + 6x)y^3 - (x^2 + 18x + 9)y^2 + (6x + 18)y - 6}{(2x^2 + 4x)y^3 - 12xy^2 + (2x + 4)y} \; . \tag{7.6.3}$$

In this section we want to compare the simulation data with the Bosse-Krieger model and we want a fixed exponent parameter, $\lambda_K = \frac{839}{864}$. In Fig. 7.6.1 one can see that for a choosen value of v_3, that the exponent parameter of Eq. (7.6.3) can reach the value of λ_K two times, one time or never. For large v_3 a higher order singularity occurs which can be seen in Fig 7.6.1 as an open circle. To compare the simulation data with the
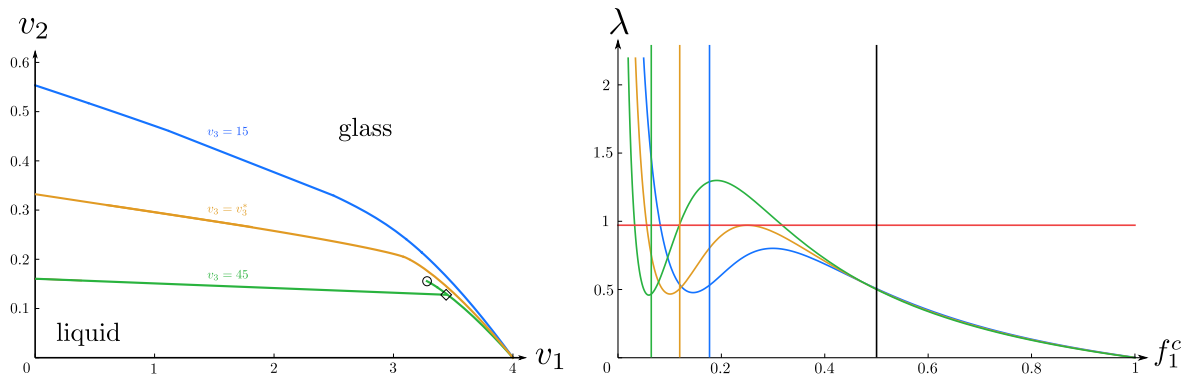
Figure 7.6.1: *Left:* The (v_1, v_2)-phase diagram of the Bosse-Krieger model. The lines are cuts through the bifurcation surface for some choosen control parameter v_3. For large control parameter, here shown by $v_3 = 45$, an A_3-singularity occurs, which is marked by a circle. One also can see a crossing point for this transition line, here marked by a diamond. At the value $v_3^* = 23.2433..$ the exponent parameter, λ, touches the calculated λ_K once. *Right:* The exponent parameter λ as a function of the non-ergodicity parameter f_1^c for some fixed control parameter $v_3 = 15$ (blue), 23.2433... (orange), 45 (green). The straight red line is the value of the theoretical calculated exponent parameter $\lambda_K = \frac{839}{864}$. The perpendicular lines are giving the range of f_1^c with $^3/_{2+v_3} < f_1^c < ^1/_2$. One can see that for a choosen v_3 both functions crosses two times (green curve), one time (orange curve) or never (blue curve).

Bosse-Krieger model, we fix the control parameter to $v_3 = 25$. So it is far enough from the A_3-singularity which could affect our calculations, and it higher than $v_3 = 24.7...$ where an A_4 singularity [52] occurs which also could influence our results.

For $v_3 = 25$, the exponent parameter crosses the λ_K-line twice, and since we are generically interested in small control parameters v_1, the lower f_1^c is relevant.
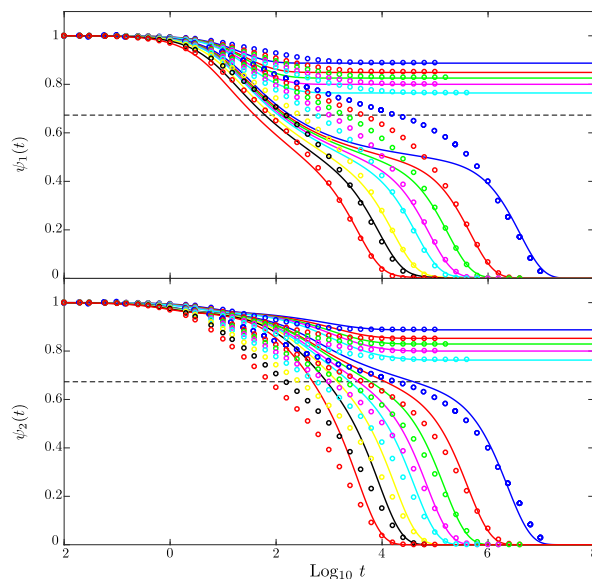
Figure 7.6.2: The simulation data from Sellitto [29] and the Bosse-Krieger model for a fixed exponent parameter $\lambda_K = \frac{839}{864}$. Here, ψ_1 is the first and ψ_2 the second correlator. One can see that the second decay- von Schweidler law- is described with the Bosse-Krieger model very well, but for the critical decay the deviations are large.

7.7   Conclusion

For the F_{12}-model the best agreement between the simulation data and the schematic model is given with the fitted exponent parameter $\lambda_S = 0.815$. The calculated exponent parameter, $\lambda_K = {}^{839}/_{864}$, is close to one, which makes the applications of the F_{12}-model difficult. For high λ the F_{12}-model has a A-line which generates a higher order singularity, and could affect the calculations with λ_K.

The Bosse-Krieger model itself can handle higher order singularities. There is a Type-B line which can be shift with f_1^c. So with a suitable control parameter v_3 one should avoid the effects of higher order singularities. But even here, the deviations between

the simulation data and the Bosse-Krieger model is large. The Bosse-Krieger model describes the von Schweidler law very well but it fails for the microscopic time scales. One interpretation is that the simulation data are far away from the critical value, so the simulations are not representing the real dynamics of the Fredrickson-Andersen model on the Bethe lattice. Our calculations are at the critical point and we assume an infinitely large lattice. The simulation data, on the other hand, are for finite lattice where finite size effect could occur. Therefore, the fitted exponent parameter, λ_S, exactly reproduces the dynamics of the simulation data, but this does not necessarily have to be from the Fredrickson-Andersen model.

7.8   Acknowledgment

I specifically thank M. Sperl and T. Kranz for the discussion about section 7.5 and 7.6, respectively, and I look forward to elaborate the chapter in a joint publication.

Bibliography

[1] J. Wong and C. A. Angell, *Glass: Structure by Spectroscopy* (Dekker, New York, 1976).

[2] R. Kohlrausch, Pogg. Ann. Phys. **4**, 56 (1854).

[3] E. R. v. Schweidler, Ann. Phys. **329**, 711 (1907).

[4] W. Knaak, F. Mezei, and B. Farago, Europhys. Lett.) **7**, 529 (1988).

[5] N. J. Tao, G. Li, and H. Z. Cummins, Phys. Rev. Lett. **66**, 1334 (1991).

[6] G. Li, W. M. Du, X. K. Chen, H. Z. Cummins, and N. J. Tao, Phys. Rev. A **45**, 3867 (1992).

[7] J. Wuttke, J. Hernandez, G. Li, G. Coddens, H. Z. Cummins, F. Fujara, W. Petry, and H. Sillescu, Phys. Rev. Lett. **72**, 3052 (1994).

[8] J. Wuttke, W. Petry, G. Coddens, and F. Fujara, Phys. Rev. E **52**, 4026 (1995).

[9] T. Franosch, W. Götze, M. R. Mayr, and A. P. Singh, Phys. Rev. E **55**, 3183 (1997).

[10] H. Mori, Prog. Theo. Phys. **33**, 423 (1965).

[11] H. Mori, Prog. Theo. Phys. **34**, 399 (1965).

[12] R. Zwanzig, J. Chem. Phys. **33**, 1338 (1960).

[13] R. Zwanzig, Phys. Rev. **124**, 983 (1961).

[14] V. Krakoviack, C. Alba-Simionesco, and M. Krauzman, J. Chem. Phys **107**, 3417 (1997).

[15] V. Krakoviack and C. Alba-Simionesco, J. Chem. Phys **117**, 2161 (2002).

[16] W. Götze and M. Sperl, Phys. Rev. Lett. **92**, 105701 (2004).

[17] M. Sperl, Phys. Rev. E **74**, 011503 (2006).

[18] V. I. Arnol'd, *Catastrophe Theory* (Springer-Verlag, Berlin, 1992).

[19] F. Ritort and P. Sollich, Adv. Phys. **52**, 219 (2003).

[20] J. P. Garrahan, P. Sollich, and C. Toninelli, in *Dynamical Heterogeneities in Glasses, Colloids, and Granular Media*, International Series of Monographs on Physics, Vol. 150, edited by L. Berthier, G. Biroli, J.-P. Bouchaud, L. Cipelletti, and W. van Saarloos (Oxford University Press, Oxford, 2011) Chap. 10, p. 341.

[21] G. H. Fredrickson and H. C. Andersen, Phys. Rev. Lett. **53**, 1244 (1984).

[22] G. H. Fredrickson and S. A. Brawer, J. Chem. Phys. **84**, 3351 (1986).

[23] I. S. Graham, L. Piché, and M. Grant, Phys. Rev. E **55**, 2132 (1997).

[24] N. Cancrini, F. Martinelli, C. Robert, and C. Toninelli, in *Methods of contemporary mathematical statistical physics*, Lecture Notes in Mathematics, Vol. 1970, edited by R. Kotecký (Springer, Berlin, 2009) p. 307.

[25] C. Toninelli, G. Biroli, and D. S. Fisher, Phys. Rev. Lett. **92**, 185504 (2004).

[26] J. Reiter, F. Mauch, and J. Jäckle, Physica A **184**, 458 (1992).

[27] S. J. Pitts, T. Young, and H. C. Andersen, J. Chem. Phys.**113**, 8671 (2000).

[28] M. Sellitto, G. Biroli, and C. Toninelli, Europhys Lett. **69**, 496 (2005).

[29] M. Sellitto, Phys. Rev. Lett. **115**, 225701 (2015).

[30] M. Mézard and G. Parisi, Europhys. J. B **20**, 217 (2001).

[31] F. Martinelli and C. Toninelli, Ann. Appl. Prob. **23**, 1967 (2013).

[32] J. Chalupa, P. L. Leath, and G. R. Reich, J. Phys. C **12**, L31 (1979).

[33] J. Adler, Physica A **171**, 453 (1991).

[34] S. N. Dorogovtsev, A. V. Goltsev, and J. F. F. Mendes, Rev. Mod. Phys. **80**, 1275 (2008).

[35] A. A. Saberi, Phys. Rep. **578**, 1 (2015).

[36] A. C. D. van Enter, J. Stat. Phys. **48**, 943 (1987).

[37] J. Balogh and B. G. Pittel, Random Struct. Alg. **30**, 257 (2007).

[38] S. Janson, T. Łuczak, T. Turova, and T. Vallier, Ann. Appl. Probab. **22**, 1989 (2012).

[39] N. Cancrini, F. Martinelli, C. Roberto, and C. Toninelli, Probab. Theory Relat. Fields **161**, 247 (2015).

[40] R. Haussmann, Z. Phys. B **79**, 143 (1990).

[41] D. E. Evans and R. Høegh-Krohn, J. Lon. Math. Soc. **s2-17**, 345.

[42] W. Götze, in *Liquids, Freezing and Glass Transition*, Proceedings of the Les Houches Summer School of Theoretical Physics, Session LI,1989, edited by J. R. Hanssen, D. Levesque, and J. Zinn-Justin (North-Holland, Amsterdam, 1991) pp. 287–503.

[43] W. Götze and L. Sjögren, J. Phys. Condensed Matt. **1**, 4183 (1989).

[44] W. Götze, Z. Phys. B **56**, 139 (1984).

[45] E. Leutheusser, Phys. Rev. A **29**, 2765 (1984).

[46] U. Bengtzelius, W. Gotze, and A. Sjolander, J. Phys. C **17**, 5915 (1984).

[47] H. Risken, in *The Fokker-Planck Equation: Methods of Solution and Applications* (Springer Berlin Heidelberg, Berlin, Heidelberg, 1996) pp. 63–95.

[48] K. Kawasaki, Physica A **215**, 61 (1995).

[49] S. J. Pitts and H. C. Andersen, J. Chem. Phys **114**, 1101 (2001).

[50] J. Bosse and U. Krieger, J. Phys. C **19**, L609 (1986).

[51] U. Krieger and J. Bosse, Phys. Rev. Lett. **59**, 1601 (1987).

[52] W. Götze and M. Sperl, Phys. Rev. E **66**, 011405 (2002).

Appendix

A Projection-Operator

$$(z - \mathcal{L})(z - \mathcal{L})^{-1} = 1 \quad |\text{Add a } (\mathcal{P} + \mathcal{Q}) = 1$$
$$(z - \mathcal{L})\mathcal{P}(z - \mathcal{L})^{-1} + (z - \mathcal{L})\mathcal{Q}(z - \mathcal{L})^{-1} = 1 \quad |\mathcal{P}\cdot \text{ or } \mathcal{Q}\cdot \text{ from left} \qquad \text{(A.1.1)}$$

So we have the two following equations:

$$(\mathcal{P}z\mathcal{P} - \mathcal{P}\mathcal{L}\mathcal{P})(z - \mathcal{L})^{-1} + \mathcal{P}\mathcal{L}\mathcal{Q}(z - \mathcal{L})^{-1} = \mathcal{P}, \quad \text{(I)}$$
$$(\mathcal{Q}z\mathcal{Q} - \mathcal{Q}\mathcal{L}\mathcal{Q})(z - \mathcal{L})^{-1} + \mathcal{Q}\mathcal{L}\mathcal{P}(z - \mathcal{L})^{-1} = \mathcal{Q}. \quad \text{(II)} \qquad \text{(A.1.2)}$$

Multiply (I) and (II) with $\mathcal{P}$ from right:

$$(z - \mathcal{P}\mathcal{L})\mathcal{P}(z - \mathcal{L})^{-1}\mathcal{P} + \mathcal{P}\mathcal{L}\mathcal{Q}(z - \mathcal{L})^{-1}\mathcal{P} = \mathcal{P}, \quad \text{(III)}$$
$$(z - \mathcal{Q}\mathcal{L}\mathcal{Q})\mathcal{Q}(z - \mathcal{L})^{-1}\mathcal{P} + \mathcal{Q}\mathcal{L}\mathcal{P}(z - \mathcal{L})^{-1}\mathcal{P} = 0. \quad \text{(IV)} \qquad \text{(A.1.3)}$$

Insert equation (III) in (IV):

$$(z - \mathcal{Q}\mathcal{L}\mathcal{Q})\mathcal{Q}(z - \mathcal{L})^{-1}\mathcal{P} = -\mathcal{Q}\mathcal{L}\mathcal{P}(z - \mathcal{L})^{-1}\mathcal{P} \quad |(z - \mathcal{Q}\mathcal{L})^{-1}$$
$$\Rightarrow \mathcal{Q}(z - \mathcal{L})^{-1}\mathcal{P} = -(z - \mathcal{Q}\mathcal{L}\mathcal{Q})^{-1}\mathcal{Q}\mathcal{L}\mathcal{P}(z - \mathcal{L})^{-1}\mathcal{P} \qquad \text{(A.1.4)}$$

$$(z - \mathcal{P}\mathcal{L})\mathcal{P}(z - \mathcal{L})^{-1}\mathcal{P} + \mathcal{P}\mathcal{L}\mathcal{Q}\mathcal{Q}(z - \mathcal{L})^{-1}\mathcal{P} = \mathcal{P}$$
$$(z - \mathcal{P}\mathcal{L})\mathcal{P}(z - \mathcal{L})^{-1}\mathcal{P} - \mathcal{P}\mathcal{L}\mathcal{Q}(z - \mathcal{Q}\mathcal{L}\mathcal{Q})^{-1}\mathcal{Q}\mathcal{L}\mathcal{P}(z - \mathcal{L})^{-1}\mathcal{P} = \mathcal{P}$$
$$\Rightarrow ((z - \mathcal{P}\mathcal{L})\mathcal{P} - \mathcal{P}\mathcal{L}\mathcal{Q}(z - \mathcal{Q}\mathcal{L}\mathcal{Q})^{-1}\mathcal{Q}\mathcal{L}\mathcal{P})(z - \mathcal{L})^{-1}\mathcal{P} = \mathcal{P} \qquad \text{(A.1.5)}$$

So we get for $\mathcal{P}(z - \mathcal{L})^{-1}\mathcal{P}$:

$$\mathcal{P}(z - \mathcal{L})^{-1}\mathcal{P} = \left[z - \mathcal{P}\mathcal{L}\mathcal{P} - \mathcal{P}\mathcal{L}\mathcal{Q}(z - \mathcal{Q}\mathcal{L}\mathcal{Q})^{-1}\mathcal{Q}\mathcal{L}\mathcal{P}\right]^{-1}$$
$$= [z - \Omega - M(z)]^{-1} \qquad \text{(A.1.6)}$$

B   MCT for Binary Mixture

Define the state vector $|a(\vec{q})\rangle$ with

$$\langle a(\vec{q})| = S_{\alpha\beta}^{-1/2} \langle \rho_\alpha(\vec{q})| + J_{\alpha\beta}^{-1/2} \langle j_\alpha^{\mathrm{L}}(\vec{q})| \ ,$$
$$|a(\vec{q})\rangle = S_{\alpha\beta}^{-1/2} |\rho_\beta(\vec{q})\rangle + J_{\alpha\beta}^{-1/2} |j_\beta^{\mathrm{L}}(\vec{q})\rangle \ . \tag{B.1.1}$$

In the Laplace-domain the correlation matrix is given as

$$\Phi_{\alpha\beta}(q) = \langle a(\vec{q})| \frac{1}{z - \mathcal{L}} |a(\vec{q})\rangle \tag{B.1.2}$$

We introduce within the Mori-Zwanzig formalism the projector $\mathcal{P}$

$$\mathcal{P} = \sum_{\alpha\beta} |\rho_\alpha(\vec{q})\rangle S_{\alpha\beta}^{-1} \langle \rho_\beta(\vec{q})| + \sum_{\alpha\beta} |j_\alpha^{\mathrm{L}}(\vec{q})\rangle J_{\alpha\beta}^{-1} \langle j_\beta^{\mathrm{L}}(\vec{q})| \ . \tag{B.1.3}$$

From Appendix A we know

$$\mathcal{P} \frac{1}{z - \mathcal{L}} \mathcal{P} = \left[z - \mathcal{PLP} - \mathcal{PLQ}(z - \mathcal{QLQ})^{-1} \mathcal{QLP} \right]^{-1} \ .$$

For the inverse correlation matrix one has

$$\Phi_{\alpha\beta}^{-1}(q) = \langle a(\vec{q})| z - \mathcal{PLP} - \mathcal{PLQ}(z - \mathcal{QLQ})^{-1} \mathcal{QLP} |a(\vec{q})\rangle \ . \tag{B.1.4}$$

Now we calculate all the matrix elements

- The frist term of B.1.4 (z-term):

$$\langle a(\vec{q})| z |a(\vec{q})\rangle = (S_{\alpha\beta}^{-1/2} \langle \rho_\alpha(\vec{q})| + J_{\alpha\beta}^{-1/2} \langle j_\alpha^{\mathrm{L}}(\vec{q})|) z (S_{\alpha\beta}^{-1/2} |\rho_\beta(\vec{q})\rangle + J_{\alpha\beta}^{-1/2} |j_\beta^{\mathrm{L}}(\vec{q})\rangle)$$
$$= z(S_{\alpha\beta}^{-1} \langle \rho_\alpha(\vec{q})|\rho_\beta(\vec{q})\rangle + J_{\alpha\beta}^{-1} \langle j_\alpha^{\mathrm{L}}(\vec{q})|j_\beta^{\mathrm{L}}(\vec{q})\rangle$$
$$+ S_{\alpha\beta}^{-1/2} J_{\alpha\beta}^{-1/2} (\langle \rho_\alpha(\vec{q})|j_\beta^{\mathrm{L}}(\vec{q})\rangle + \langle j_\alpha^{\mathrm{L}}(\vec{q})|\rho_\beta(\vec{q})\rangle)) \ . \tag{B.1.5}$$

- The $\mathcal{PLP}$-term:

$$\langle a|\mathcal{PLP}|a\rangle =$$
$$\sum_{\alpha\beta} \langle a|(|\rho_\alpha(\vec{q})\rangle S_{\alpha\beta}^{-1} \langle\rho_\beta(\vec{q})| + |j_\alpha^{\mathrm{L}}(\vec{q})\rangle J_{\alpha\beta}^{-1} \langle j_\beta^{\mathrm{L}}(\vec{q})|)\mathcal{L}(|\rho_\alpha(\vec{q})\rangle S_{\alpha\beta}^{-1} \langle\rho_\beta(\vec{q})| + |j_\alpha^{\mathrm{L}}(\vec{q})\rangle J_{\alpha\beta}^{-1} \langle j_\beta^{\mathrm{L}}(\vec{q})|)|a\rangle ,$$

(B.1.6)

here we get the frequencies

$$\Omega_{\rho\rho}(q) = S_{\alpha\beta}^{-1}(q) \langle\rho_\beta(\vec{q})|\mathcal{L}|\rho_\alpha(\vec{q})\rangle = 0 ,$$
$$\Omega_{j\rho}(q) = S_{\alpha\beta}^{-1/2}(q)J_{\alpha\beta}^{-1/2} \langle j_\beta^{\mathrm{L}}(\vec{q})|\mathcal{L}|\rho_\alpha(\vec{q})\rangle ,$$
$$\Omega_{\rho j}(q) = S_{\alpha\beta}^{-1/2}(q)J_{\alpha\beta}^{-1/2} \langle\rho_\beta(\vec{q})|\mathcal{L}|j_\alpha^{\mathrm{L}}(\vec{q})\rangle ,$$
$$\Omega_{jj}(q) = J_{\alpha\beta}^{-1} \langle j_\beta^{\mathrm{L}}(\vec{q})|\mathcal{L}|j_\alpha^{\mathrm{L}}(\vec{q})\rangle .$$

(B.1.7)

- and the $\mathcal{PLQ}(z - \mathcal{QLQ})^{-1}\mathcal{QLP}$-term:
  because of the relation $\mathcal{QLP}|\rho(\vec{q})\rangle = 0$ we only get two matrix elements

$$K_{\alpha\beta}(q) = S_{\alpha\beta}^{-1/2}(q)J_{\alpha\beta}^{-1/2} \langle\rho_\beta(\vec{q})|\mathcal{LQ}(z - \mathcal{QLQ})^{-1}\mathcal{QL}|j_\alpha^{\mathrm{L}}(\vec{q})\rangle ,$$
$$M_{\alpha\beta}(q) = J_{\alpha\beta}^{-1} \langle j_\beta^{\mathrm{L}}(\vec{q})|\mathcal{LQ}(z - \mathcal{QLQ})^{-1}\mathcal{QL}|j_\alpha^{\mathrm{L}}(\vec{q})\rangle .$$

(B.1.8)

with the definiton

$$L_{\alpha\beta}(q) = \frac{K_{\alpha\beta}(q)}{\Omega_{\rho j}(q)} = \frac{\langle\rho_\beta(\vec{q})|\mathcal{LQ}(z - \mathcal{QLQ})^{-1}\mathcal{QL}|j_\alpha^{\mathrm{L}}(\vec{q})\rangle}{\langle\rho_\beta(\vec{q})|\mathcal{L}|j_\alpha^{\mathrm{L}}(\vec{q})\rangle} ,$$
$$\Omega(q)^2 = \Omega_{\rho j}(q)\Omega_{j\rho}(q)$$

(B.1.9)

we get

$$\underline{\underline{\Phi}}_{\alpha\beta}(q) = \frac{1}{z(z-\Omega_{jj}(q)-M_{\alpha\beta}(q))-\Omega^2(q)[1+L_{\alpha\beta}(q)]} \begin{pmatrix} z - \Omega_{jj}(q) - M_{\alpha\beta}(q) & \Omega_{\rho j}(q)[1 + L_{\alpha\beta}(q)] \\ \Omega_{j\rho}(q) & z \end{pmatrix}$$

The density density autocorrelation function is given as

$$\phi_{\alpha\beta}(q) = \frac{1}{z - \frac{\Omega^2(q)[1+L_{\alpha\beta}(q)]}{z-\Omega_{jj}(q)-M_{\alpha\beta}(q)}}$$

(B.1.10)

Mode Coupling Approximation:

Introduce the second projector $\mathcal{P}^{\mathrm{MCT}}$ with

$$\mathcal{P}^{\mathrm{MCT}} = \sum_{\substack{\alpha\beta\alpha'\beta' \\ \vec{k}>\vec{p},\vec{k}'>\vec{p}'}} |\rho_\alpha(\vec{k})\vec{\rho}_\beta(\vec{p})\rangle\, g_{\alpha\beta}^{\alpha'\beta'}(\vec{k}\,\vec{p},\vec{k}'\vec{p}')\, \langle\rho_{\alpha'}(\vec{k}')\vec{\rho}_{\beta'}(\vec{p}')| \tag{B.1.11}$$

use the MCA for the resolvent $\mathcal{R}(z) = \frac{1}{z-\mathcal{QLQ}}$ as $\mathcal{R}(z) \approx \mathcal{P}^{\mathrm{MCT}}\mathcal{R}(z)\mathcal{P}^{\mathrm{MCT}}$.
The memory kernel $L_{\alpha\beta}(q)$ vanishes

$$L_{\alpha\beta}(q) \approx \frac{\langle\rho_\beta(\vec{q})|\mathcal{LQP}^{\mathrm{MCT}}\mathcal{RP}^{\mathrm{MCT}}\mathcal{QL}|j_\alpha^{\mathrm{L}}(\vec{q})\rangle}{\langle\rho_\beta(\vec{q})|\mathcal{L}|j_\alpha^{\mathrm{L}}(\vec{q})\rangle}$$

$$= \sum_{\substack{\alpha\gamma\alpha'\gamma' \\ \vec{k}>\vec{p},\vec{k}'>\vec{p}'}} \sum_{\substack{\gamma\beta\alpha'\gamma' \\ \vec{k}>\vec{p},\vec{k}'>\vec{p}'}}$$

$$\frac{\langle\rho_\beta(\vec{q})|\mathcal{LQ}\rho_\alpha(\vec{k})\vec{\rho}_\gamma(\vec{p})\rangle\, g_{\alpha\gamma}^{\alpha'\gamma'}\, \langle\rho_{\alpha'}(\vec{k}')\vec{\rho}_{\gamma'}(\vec{p}')\mathcal{R}\rho_\gamma(\vec{k})\vec{\rho}_\beta(\vec{p})\rangle\, g_{\beta\gamma}^{\beta'\gamma'}\, \langle\rho_{\gamma'}(\vec{k}')\vec{\rho}_{\beta'}(\vec{p}')\mathcal{QL}|j_\alpha^{\mathrm{L}}(\vec{q})\rangle}{\langle\rho_\beta(\vec{q})|\mathcal{L}|j_\alpha^{\mathrm{L}}(\vec{q})\rangle}$$

$$= 0$$

because $\langle\rho_\beta(\vec{q})|\mathcal{LQ}\rho_\alpha(\vec{k})\vec{\rho}_\gamma(\vec{p})\rangle = 0$
For $M_{\alpha\beta}(q)$ we have

$$M_{\alpha\beta}(\vec{q}) \approx J_{\alpha\beta}^{-1}\, \langle j_\beta^{\mathrm{L}}(\vec{q})|\mathcal{LQP}^{\mathrm{MCT}}\mathcal{RP}^{\mathrm{MCT}}\mathcal{QL}|j_\alpha^{\mathrm{L}}(\vec{q})\rangle$$

$$= J_{\alpha\beta}^{-1} \sum_{\substack{\gamma'\delta'\epsilon\psi, \\ \vec{k}>\vec{p},\vec{k}'>\vec{p}'}} \mathcal{V}_{\beta\gamma\delta}(\vec{q}\vec{k}\vec{p})\mathcal{Z}_{\epsilon\psi}^{\gamma'\delta'}(\vec{k}'\vec{p}',\vec{k}\,\vec{p})\mathcal{W}_{\epsilon'\psi'\alpha}(\vec{k}'\vec{p}'\vec{q}) \tag{B.1.12}$$

with

$$\mathcal{V}_{\beta\gamma\delta}(\vec{q}\vec{k}\vec{p}) = \sum_{\substack{\gamma''\delta'' \\ \vec{k}''\vec{p}''}} \langle j_\beta^{\mathrm{L}}(\vec{q})|\mathcal{LQ}\rho_{\gamma''}(\vec{k}'')\rho_{\delta''}(\vec{p}'')\rangle\, g_{\gamma\delta}^{\gamma''\delta''}(\vec{k}''\vec{p}'',\vec{k}\,\vec{p}) \tag{B.1.13}$$

$$\mathcal{W}_{\epsilon'\psi'\alpha}(\vec{k}'\vec{p}'\vec{q}) = \sum_{\substack{\epsilon''\psi'' \\ \vec{k}''\vec{p}''}} \langle\rho_{\epsilon''}(\vec{k}'')\rho_{\psi''}(\vec{p}'')\mathcal{LQ}|j_\alpha^{\mathrm{L}}(\vec{q})\rangle)\, g_{\epsilon'\psi'}^{\epsilon''\psi''}(\vec{k}''\vec{p}'',\vec{k}'\,\vec{p}') \tag{B.1.14}$$

$$\mathcal{Z}_{\epsilon\psi}^{\gamma'\delta'}(\vec{k}'\vec{p}',\vec{k}\,\vec{p}) = \langle\rho_{\gamma'}(\vec{k}')\rho_{\delta'}(\vec{p}')|\mathcal{R}|\rho_\epsilon(\vec{k})\rho_\psi(\vec{p})\rangle$$

$$\approx \langle\rho_{\gamma'}(\vec{k}')|\mathcal{R}|\rho_\epsilon(\vec{k})\rangle\, \langle\rho_{\delta'}(\vec{p}')|\mathcal{R}|\rho_\psi(\vec{p})\rangle$$

$$= \Phi_{\gamma'\epsilon}(k,t)\Phi_{\delta'\psi}(p,t)\delta_{\vec{k}\vec{k}'}\delta_{\vec{p}\vec{p}'} \tag{B.1.15}$$

C   Asymptotic Expansion

In this appendix I will derive the asymptotic expansion for $\phi(0) = p$, which is relevant for the calculation of the exponent parameter, λ, in the Fredrickson-Andersen model. When we assume that the initial value of the correlation function $\phi(0) = \phi_0$, with $\phi_0 \leq 1$ the equation of motion (EOM) in the Laplace domain for $t \to \infty$ will be

$$\frac{\phi(z)}{\phi_0 + z\phi(z)} = \text{LT}\left[\mathcal{F}(\phi(t))\right](z) \ . \tag{C.1.1}$$

We introduce some not yet specified real parameters f and function $G(t)$ to rewrite

$$\phi(t) = f + G(t) \qquad z\phi(z) = -f + zG(z) \ , \tag{C.1.2}$$

and use the following two assumptions

$$\left|\frac{zG(z)}{\phi_0 - f}\right| \ll 1 \ ,$$
$$\left|\frac{\text{LT}[G(t)^{n+1}](z)}{\text{LT}[G(t)^n](z)}\right| \ll 1 \ . \tag{C.1.3}$$

So we now expand the EOM in terms of $G(t)$

$$\frac{-\frac{f}{z} + G(z)}{\phi_0 - f + zG(z)} = \text{LT}[\mathcal{F}(f + G(t))](z) \ . \tag{C.1.4}$$

For the lhs we get

$$\frac{-\frac{f}{z} + G(z)}{\phi_0 - f + zG(z)} = \frac{1}{z}\frac{-f}{\phi_0 - f}\frac{1}{1 + \frac{zG(z)}{\phi_0 - f}} + \frac{1}{z}\frac{\frac{zG(z)}{\phi_0 - f}}{1 + \frac{zG(z)}{\phi_0 - f}} \ . \tag{C.1.5}$$

Now we can use the first assumption with

$$\frac{1}{1 - x} \approx 1 - x + x^2 - x^3 + \mathcal{O}(x^4) \tag{C.1.6}$$
$$\frac{x}{1 - x} \approx x - x^2 + x^3 - x^4 + \mathcal{O}(x^5) \tag{C.1.7}$$

and get

$$
\frac{1}{z}\frac{-f}{\phi_0 - f}\frac{1}{1 + \frac{zG(z)}{\phi_0 - f}} + \frac{1}{z}\frac{\frac{zG(z)}{\phi_0 - f}}{1 + \frac{zG(z)}{\phi_0 - f}} =
$$

$$
\frac{1}{z}\frac{-f}{\phi_0 - f}\left(1 - \frac{zG(z)}{\phi_0 - f} + \frac{z^2 G^2(z)}{(\phi_0 - f)^2} + \mathcal{O}(G^3(z))\right) + \frac{1}{z}\left(\frac{zG(z)}{\phi_0 - f} - \frac{z^2 G^2(z)}{(\phi_0 - f)^2} + \mathcal{O}(G^3(z))\right) =
$$

$$
\frac{1}{z}\frac{-f}{\phi_0 - f} + G(z)\left(\frac{f}{(\phi_0 - f)^2} + \frac{1}{\phi_0 - f}\right) - zG^2(z)\left(\frac{f}{(\phi_0 - f)^3} + \frac{1}{(\phi_0 - f)^2}\right) + \mathcal{O}(G^3(z)) =
$$

$$
\frac{1}{z}\frac{-f}{\phi_0 - f} + G(z)\frac{\phi_0}{(\phi_0 - f)^2} - zG^2(z)\frac{\phi_0}{(\phi_0 - f)^2} + \mathcal{O}(G^3(z)) \qquad | \cdot (\phi_0 - f)^3 =
$$

$$
-\frac{f(\phi_0 - f)^2}{z} + G(z)(\phi_0(\phi_0 - f)) - zG^2(z)\phi_0 + \mathcal{O}(G^3(t)) \tag{C.1.8}
$$

If we introduce $\hat{\gamma}_k = \frac{\phi_0}{(\phi_0 - f)^{k-2}}$, we can rewrite the lhs as

$$
\frac{1}{z}\frac{-f}{\phi_0 - f}\frac{1}{1 + \frac{zG(z)}{\phi_0 - f}} + \frac{1}{z}\frac{\frac{zG(z)}{\phi_0 - f}}{1 + \frac{zG(z)}{\phi_0 - f}} =
$$

$$
-\frac{f(\phi_0 - f)^2}{z} + G(z)\hat{\gamma}_1 - zG^2(z)\hat{\gamma}_2 + \mathcal{O}(G^3(z)) \ . \tag{C.1.9}
$$

Now we consider the rhs of the equation

$$
(\phi_0 - f)^3 \mathrm{LT}[\mathcal{F}(f + G(t))](z) = (\phi_0 - f)^3 \mathrm{LT}\left[\mathcal{F}\left(\underbrace{f - \frac{f}{\phi_0 - f}}_{\Delta\mathcal{F}} + \frac{f}{\phi_0 - f} + G(t)\right)\right](z) \ , \tag{C.1.10}
$$

and expand in $G(t)$

$$
(\phi_0 - f)^3 \mathrm{LT}\left[\mathcal{F}\left(\Delta\mathcal{F} + \frac{f}{\phi_0 - f} + G(t)\right)\right](z) =
$$

$$
(\phi_0 - f)^3 \left[\left(\frac{1}{0!}\frac{\partial^0 \Delta\mathcal{F}}{\partial f^0} + \frac{1}{0!}\frac{\partial^0 \frac{f}{\phi_0 - f}}{\partial f^0}\right)\underbrace{\mathrm{LT}[G^0(t)](z)}_{-\frac{1}{z}} + \left(\frac{1}{1!}\frac{\partial^1 \Delta\mathcal{F}}{\partial f^1} + \frac{1}{1!}\frac{\partial^1 \frac{f}{\phi_0 - f}}{\partial f^1}\right)G(z) + \mathcal{O}(G^2(t))\right] \tag{C.1.11}
$$

We also can introduce (for $k \geq 1$)

$$\hat{\delta}_k = \frac{(\phi_0 - f)^3}{k!} \frac{\partial^k \Delta \mathcal{F}}{\partial f^k} \qquad \hat{\gamma}_k = \frac{(\phi_0 - f)^3}{k!} \frac{\partial^k \frac{f}{\phi_0 - f}}{\partial f^k} = \frac{\phi_0}{(\phi_0 - f)^{k-2}} \ , \qquad \text{(C.1.12)}$$

so we have

$$
\begin{aligned}
& -\frac{\hat{\delta}_0}{z} + \hat{\delta}_1 \\
& + (\hat{\gamma}_2 + \hat{\delta}_2)\mathrm{LT}[G^2(t)](z) + \hat{\gamma}_2 z G^2(z) \\
& + (\hat{\gamma}_3 + \hat{\delta}_3)\mathrm{LT}[G^3(t)](z) + \hat{\gamma}_3 z G^3(z) \\
& + (\hat{\gamma}_4 + \hat{\delta}_4)\mathrm{LT}[G^4(t)](z) + \hat{\gamma}_4 z G^4(z) + \ldots = 0 \ . \qquad \text{(C.1.13)}
\end{aligned}
$$

For the special case of an A_2-bifurcation we have

$$\hat{\lambda}\mathrm{LT}[G^2(t)](z) + z G^2(z) = 0 \ , \qquad \text{(C.1.14)}$$

with $\hat{\lambda} = 1 + \delta_2^c / \gamma_2^c$.

D   Vertex Calculation for Binary Mixture

Calculation of the left vertex $\mathcal{V}_{\beta\gamma\delta}$:

$$
\mathcal{V}_{\beta\gamma\delta}(\vec{q}\vec{k}\vec{p}) = \sum_{\substack{\gamma''\delta'' \\ \vec{k}''\vec{p}''}} \langle j_\beta^{\mathrm{L}}(\vec{q})|\mathcal{L}\mathcal{Q}\rho_{\gamma''}(\vec{k}'')\rho_{\delta''}(\vec{p}'')\rangle\, g_{\gamma\delta}^{\gamma''\delta''}(\vec{k}''\vec{p}'',\vec{k}\,\vec{p})\ ,
$$

$$
= \sum_{\substack{\gamma''\delta'' \\ \vec{k}''\vec{p}''}} \Big[\langle j_\beta^{\mathrm{L}}(\vec{q})|\mathcal{L}\rho_{\gamma''}(\vec{k}'')\rho_{\delta''}(\vec{p}'')\rangle - \langle j_\beta^{\mathrm{L}}(\vec{q})|\mathcal{L}\mathcal{P}\rho_{\gamma''}(\vec{k}'')\rho_{\delta''}(\vec{p}'')\rangle\Big]\, g_{\gamma\delta}^{\gamma''\delta''}(\vec{k}''\vec{p}'',\vec{k}\,\vec{p})\ ,
$$

$$
= \sum_{\substack{\gamma''\delta'' \\ \vec{k}''\vec{p}''}} \Big[(\hat{q}\cdot\vec{k}'')\,\langle j_\beta^{\mathrm{L}}(\vec{q})|j_{\gamma''}^{\mathrm{L}}(\vec{k}'')\rho_{\delta''}(\vec{p}'')\rangle + (\hat{q}\cdot\vec{p}'')\,\langle j_\beta^{\mathrm{L}}(\vec{q})|\rho_{\gamma''}(\vec{k}'')j_{\delta''}^{\mathrm{L}}(\vec{p}'')\rangle
$$

$$
- \sum_{\phi\psi} \langle j_\beta^{\mathrm{L}}(\vec{q})|\mathcal{L}\rho_\phi(\vec{q})\rangle\, S_{\phi\psi}^{-1}(\vec{q})\,\langle \rho_\psi(\vec{q})|\rho_{\gamma''}(\vec{k}'')\rho_{\delta''}(\vec{p}'')\rangle\Big]\, g_{\gamma\delta}^{\gamma''\delta''}(\vec{k}''\vec{p}'',\vec{k}\,\vec{p})\ ,
$$

$$
= \sum_{\substack{\gamma''\delta'' \\ \vec{k}''\vec{p}''}} \frac{\delta(\vec{k}''+p'',\vec{q})}{V}\Bigg[\frac{k_{\mathrm{B}}T_\beta}{m_\beta}\Big((\hat{q}\cdot\vec{k}'')\delta_{\beta\gamma''}S_{\beta\delta''}(p'') + (\hat{q}\cdot\vec{p}'')\delta_{\beta\delta''}S_{\beta\gamma''}(k'')\Big)
$$

$$
-q\sum_{\phi\psi} J_{\beta\phi}S_{\phi\psi}^{-1}(\vec{q})S_{\psi\gamma''\delta''}^{(3)}(k'',p'')\Bigg]\, g_{\gamma\delta}^{\gamma''\delta''}(\vec{k}''\vec{p}'',\vec{k}\,\vec{p}) \tag{D.1.1}
$$

The calculation of the average $\langle j_\beta^{\mathrm{L}}(\vec{q})|j_{\gamma''}^{\mathrm{L}}(\vec{k}'')\rho_{\delta''}(\vec{p}'')\rangle$ is given as

$$
\langle j_\beta^{\mathrm{L}}(\vec{q})|j_{\gamma''}^{\mathrm{L}}(\vec{k}'')\rho_{\delta''}(\vec{p}'')\rangle = \left\langle \frac{1}{\sqrt{N}}\sum_l \Big(\hat{q}\cdot\vec{v}_l^{\,\beta}\Big)\,\mathrm{e}^{-i\vec{q}\vec{r}_l^{\,\beta}}\frac{1}{\sqrt{N}}\sum_j \Big(\hat{k}''\cdot\vec{v}_j^{\,\gamma''}\Big)\,\mathrm{e}^{i\vec{k}''\vec{r}_j^{\,\gamma''}}\frac{1}{\sqrt{N}}\sum_m \mathrm{e}^{i\vec{p}''\vec{r}_m^{\,\delta''}}\right\rangle\ ,
$$

$$
= \delta_{\beta\gamma''}\left\langle \frac{1}{\sqrt{N}}\sum_l \Big(\hat{q}\cdot\vec{v}_l^{\,\beta}\Big)^2\,\mathrm{e}^{i(\vec{k}''-\vec{q})\vec{r}_l^{\,\beta}}\frac{1}{\sqrt{N}}\sum_m \mathrm{e}^{i\vec{p}''\vec{r}_m^{\,\delta''}}\right\rangle\ ,
$$

$$
= \delta_{\beta\gamma''}\frac{k_{\mathrm{B}}T_\beta}{m_\beta}\left\langle \frac{1}{\sqrt{N}}\sum_l \mathrm{e}^{i(\vec{k}''-\vec{q})\vec{r}_l^{\,\beta}}\frac{1}{N}\sum_l \mathrm{e}^{i\vec{p}''r_l^{\,\beta}}\mathrm{e}^{-i\vec{p}''r_l^{\,\beta}}\frac{1}{\sqrt{N}}\sum_m \mathrm{e}^{i\vec{p}''\vec{r}_m^{\,\delta''}}\right\rangle\ ,
$$

$$
= N\delta_{\beta\gamma''}\frac{\delta(\vec{k}''+\vec{p}'',\vec{q})}{V}\frac{k_{\mathrm{B}}T_\beta}{m_\beta}\left\langle \frac{1}{N\sqrt{N}}\sum_l \mathrm{e}^{-i\vec{p}''r_l^{\,\beta}}\frac{1}{\sqrt{N}}\sum_m \mathrm{e}^{i\vec{p}''\vec{r}_m^{\,\delta''}}\right\rangle\ ,
$$

$$
= \frac{\delta(\vec{k}''+\vec{p}'',\vec{q})}{V}\frac{k_{\mathrm{B}}T_\beta}{m_\beta}S_{\beta\delta''}(\vec{p}'')\delta_{\beta\gamma''} \tag{D.1.2}
$$

Now, use the normalization $g_{\gamma\delta}^{\gamma''\delta''}(\vec{k}''\vec{p}'',\vec{k}\,\vec{p}) = S_{\gamma\gamma''}^{-1}(\vec{k})S_{\delta\delta''}^{-1}(\vec{p})\delta_{\vec{k},\vec{k}''}\delta_{\vec{p},\vec{p}''}$ and the the triple correlation function $S_{\psi\gamma''\delta''}^{(3)}(\vec{k},\vec{p}) = \sum_{\epsilon\sigma\eta} S_{\psi\epsilon}(\vec{q})S_{\gamma''\sigma}(\vec{k})S_{\delta''\eta}(\vec{p})\left(x_\epsilon^{-2}\delta_{\epsilon\sigma}\delta_{\epsilon\eta} + n^2 c_{\epsilon\sigma\eta}^{(3)}(\vec{k}\vec{p})\right)$. We also rewrite the structure factor in terms of the direct correlation function $S_{\alpha\beta}^{-1}(\vec{q}) = \frac{\delta_{\alpha\beta}}{x_\alpha} - nc_{\alpha\beta}(\vec{q})$ and get the vertex

$$
\begin{aligned}
\mathcal{V}_{\beta\gamma\delta}(\vec{q}\vec{k}\vec{p}) = {} & \frac{\delta(\vec{k}+p,\vec{q})}{V}\frac{k_{\mathrm{B}}T_\beta}{m_\beta}\left[(\hat{q}\cdot\vec{k})\delta_{\beta\delta}\left(\frac{\delta_{\beta\gamma}}{x_\beta} - nc_{\beta\gamma}(\vec{k})\right) + (\hat{q}\cdot\vec{p})\delta_{\beta\gamma}\left(\frac{\delta_{\beta\delta}}{x_\beta} - nc_{\beta\delta}(\vec{p})\right)\right. \\
& \left. -qx_\beta\left(x_\beta^{-2}\delta_{\beta\gamma}\delta_{\beta\delta} + n^2 c_{\beta\gamma\delta}^{(3)}(\vec{k}\vec{p})\right)\right] \ .
\end{aligned}
\tag{D.1.3}
$$

Now, we can simplify the left vertex to

$$
\begin{aligned}
\mathcal{V}_{\beta\gamma\delta}(\vec{q}\vec{k}\vec{p}) = {} & \frac{\delta(\vec{k}+p,\vec{q})}{V}\frac{k_{\mathrm{B}}T_\beta}{m_\beta}\left[(\hat{q}\cdot\vec{k})\frac{\delta_{\beta\gamma}\delta_{\beta\delta}}{x_\beta} + (\hat{q}\cdot\vec{p})\frac{\delta_{\beta\gamma}\delta_{\beta\delta}}{x_\beta} + (\hat{q}\cdot\vec{q})\frac{\delta_{\beta\gamma}\delta_{\beta\delta}}{x_\beta}\right. \\
& \left. - (\hat{q}\cdot\vec{k})nc_{\beta\gamma}(\vec{k})\delta_{\beta\delta} - (\hat{q}\cdot\vec{p})nc_{\beta\delta}(\vec{p})\delta_{\beta\gamma} - qx_\beta n^2 c_{\beta\gamma\delta}^{(3)}(\vec{k}\,\vec{p})\right] \ , \\
= {} & \frac{\delta(\vec{k}+p,\vec{q})}{V}\frac{k_{\mathrm{B}}T_\beta}{m_\beta}\frac{\delta_{\beta\gamma}\delta_{\beta\delta}}{x_\beta}\hat{q}(\vec{k}+\vec{p}-\vec{q}) \\
& - \frac{\delta(\vec{k}+p,\vec{q})}{V}\frac{k_{\mathrm{B}}T_\beta}{m_\beta}n\left[(\hat{q}\cdot\vec{k})c_{\beta\gamma}(\vec{k})\delta_{\beta\delta} + (\hat{q}\cdot\vec{p})c_{\beta\delta}(\vec{p})\delta_{\beta\gamma} + qx_\beta nc_{\beta\gamma\delta}^{(3)}(\vec{k}\,\vec{p})\right] \ , \\
= {} & -\frac{\delta(\vec{k}+p,\vec{q})}{V}\frac{k_{\mathrm{B}}T_\beta}{m_\beta}n\left[(\hat{q}\cdot\vec{k})c_{\beta\gamma}(\vec{k})\delta_{\beta\delta} + (\hat{q}\cdot\vec{p})c_{\beta\delta}(\vec{p})\delta_{\beta\gamma} + qx_\beta nc_{\beta\gamma\delta}^{(3)}(\vec{k}\,\vec{p})\right] \ .
\end{aligned}
\tag{D.1.4}
$$

Calculation of the right vertex $\mathcal{W}_{\alpha\beta\gamma}$:

Since we need the Liouville operator explicitly for the right vertex, its calculation is more complex than the left one. Here, I will show a short overview of the calculation. Since it is very technical, I try to comment some parts.

The right vertex is given by:

$$
\begin{aligned}
\mathcal{W}_{\alpha\beta\gamma} &= \sum_{\substack{\alpha'\beta',\\ \vec{k}'\vec{p}'}} \langle \rho_{\alpha'}(\vec{k}')\rho_{\beta'}(\vec{p}')|\mathcal{Q}\mathcal{L}j_\gamma^{\mathrm{L}}(\vec{q})\rangle \, g_{\alpha'\beta'}^{\alpha\beta}(\vec{k}'\vec{p}',\vec{k}\vec{p}) \ , \\
&= \sum_{\substack{\alpha'\beta',\\ \vec{k}'\vec{p}'}} \langle \rho_{\alpha'}(\vec{k}')\rho_{\beta'}(\vec{p}')|(1-\mathcal{P})\mathcal{L}j_\gamma^{\mathrm{L}}(\vec{q})\rangle \, g_{\alpha'\beta'}^{\alpha\beta}(\vec{k}'\vec{p}',\vec{k}\vec{p}) \ , \\
&= \sum_{\substack{\alpha'\beta',\\ \vec{k}'\vec{p}'}} \left[\langle \rho_{\alpha'}(\vec{k}')\rho_{\beta'}(\vec{p}')|\mathcal{L}j_\gamma^{\mathrm{L}}(\vec{q})\rangle - \langle \rho_{\alpha'}(\vec{k}')\rho_{\beta'}(\vec{p}')|\mathcal{P}\mathcal{L}j_\gamma^{\mathrm{L}}(\vec{q})\rangle \right] g_{\alpha'\beta'}^{\alpha\beta}(\vec{k}'\vec{p}',\vec{k}\vec{p})
\end{aligned}
$$

$$\text{(D.1.5)}$$

First we calculte the second term of Eq. D.1.5, $\sum_{\substack{\alpha'\beta',\\ \vec{k}'\vec{p}'}} \langle \rho_{\alpha'}(\vec{k}')\rho_{\beta'}(\vec{p}')|\mathcal{P}\mathcal{L}j_\gamma^{\mathrm{L}}(\vec{q})\rangle$, with the projection operator $\mathcal{P}$:

$$
\mathcal{P} = \sum_{\alpha\beta} |\rho_\alpha(\vec{q})\rangle S_{\alpha\beta}^{-1} \langle \rho_\beta(\vec{q})| + \sum_{\alpha\beta} |j_\alpha^{\mathrm{L}}(\vec{q})\rangle J_{\alpha\beta}^{-1} \langle j_\beta^{\mathrm{L}}(\vec{q})| \ . \tag{D.1.6}
$$

With the triplet correlation function as the average over three densities, the second term gets

$$
\sum_{\substack{\alpha'\beta',\\ \vec{k}'\vec{p}'}} \langle \rho_{\alpha'}(\vec{k}')\rho_{\beta'}(\vec{p}')|\mathcal{P}\mathcal{L}j_\gamma^{\mathrm{L}}(\vec{q})\rangle \, g_{\alpha'\beta'}^{\alpha\beta}(\vec{k}'\vec{p}',\vec{k}\vec{p}) =
$$

$$
\sum_{\substack{\alpha'\beta',\\ \vec{k}'\vec{p}'}} \sum_{\psi\epsilon} \frac{\delta(\vec{k}'+\vec{p}',\vec{q})}{V} S_{\alpha'\beta'\psi}^{(3)}(\vec{k}',\vec{p}') S_{\psi\epsilon}^{-1}(\vec{q}) \langle \rho_\epsilon(\vec{q})|\mathcal{L}j_\gamma^{\mathrm{L}}(\vec{q})\rangle \, g_{\alpha'\beta'}^{\alpha\beta}(\vec{k}'\vec{p}',\vec{k}\vec{p}) \tag{D.1.7}
$$

Now, we have to calculte the matrixelement $\Omega_{\rho j} \propto \langle \rho_\epsilon(\vec{q})|\mathcal{L}j_\gamma^{\mathrm{L}}(\vec{q})\rangle$:

$$
\langle \rho_\epsilon(\vec{q})|\mathcal{L}j_\gamma^{\mathrm{L}}(\vec{q})\rangle = \langle \rho_\epsilon(\vec{q})|\mathcal{L}j_\gamma^{\mathrm{L}}(\vec{q})\rangle = \langle \rho_\epsilon(\vec{q})|(\mathcal{L}_0 + \sum_\chi \sum_{i,j} \mathcal{T}_{ij}^{\chi\gamma})j_\gamma^{\mathrm{L}}(\vec{q})\rangle \ . \tag{D.1.8}
$$

The free streaming part is easy to calculte

$$
\langle \rho_\epsilon(\vec{q}) | \mathcal{L}_0 j_\gamma^{\mathrm{L}}(\vec{q}) \rangle = (-i) \, \langle \rho_\epsilon(\vec{q}) | \frac{1}{\sqrt{N}} \sum_{l,k} \sum_\delta \vec{v}_l^\delta (\hat{q} \cdot \vec{v}_k^\gamma) \vec{\nabla}_l \mathrm{e}^{i \vec{q} \vec{r}_k^\gamma} \rangle \; ,
$$

$$
= (-i) \, \langle \rho_\epsilon(\vec{q}) | \frac{1}{\sqrt{N}} \sum_{l,k} \sum_\delta \delta_{l,k} \delta_{\delta,\gamma} (\hat{q} \cdot \vec{v}_k^\gamma)^2 \hat{q} \, i \, \vec{q} \, \mathrm{e}^{i \vec{q} \vec{r}_k^\gamma} \rangle \; ,
$$

$$
= \langle \rho_\epsilon(\vec{q}) | \frac{1}{\sqrt{N}} \sum_k \mathrm{e}^{i \vec{q} \vec{r}_k^\gamma} \rangle \, q \left(\frac{m_\gamma}{2\pi k_{\mathrm{B}} T} \right)^{3/2} \int \mathrm{d}\phi \int \mathrm{d}\theta \int \mathrm{d}v \, v^4 \sin\theta \cos^2\theta \mathrm{e}^{-\frac{m_\gamma v^2}{2 k_{\mathrm{B}} T}} \; ,
$$

$$
= \langle \rho_\epsilon(\vec{q}) | \frac{1}{\sqrt{N}} \sum_k \mathrm{e}^{i \vec{q} \vec{r}_k^\gamma} \rangle \, q \left(\frac{m_\gamma}{2\pi k_{\mathrm{B}} T} \right)^{3/2} \frac{4\pi}{3} \int \mathrm{d}v \, v^4 \mathrm{e}^{-\frac{m_\gamma v^2}{2 k_{\mathrm{B}} T}} \; ,
$$

$$
= \langle \rho_\epsilon(\vec{q}) | \rho_\gamma(\vec{q}) \rangle \, q \left(\frac{m_\gamma}{2\pi k_{\mathrm{B}} T} \right)^{3/2} \frac{4\pi}{3} 3 \sqrt{\frac{\pi}{2}} \left(\frac{m_\gamma}{k_{\mathrm{B}} T} \right)^{-5/2} \; ,
$$

$$
= S_{\epsilon\gamma}(\vec{q}) \frac{k_{\mathrm{B}} T}{m_\gamma} q \; . \tag{D.1.9}
$$

Now, we need to calculate the interaction part of the Liouville operator

$$
\left\langle \rho_\epsilon(\vec{q}) | \sum_\chi \sum_{i,j} \mathcal{T}_{ij}^{\chi\gamma} j_\gamma^{\mathrm{L}}(\vec{q}) \right\rangle = \left\langle \rho_\epsilon(\vec{q}) | \left(\sum_{\chi\neq\gamma}^{N_\chi} \sum_i^{N_\gamma} \sum_j \mathcal{T}_{ij}^{\chi\gamma} + \sum_{i>j} \mathcal{T}_{ij}^{\gamma\gamma} \right) j_\gamma^{\mathrm{L}}(\vec{q}) \right\rangle \; ,
$$

$$
= \underbrace{\left\langle \rho_\epsilon(\vec{q}) | \sum_{\chi\neq\gamma} \sum_i^{N_\chi} \sum_j^{N_\gamma} \mathcal{T}_{ij}^{\chi\gamma} j_\gamma^{\mathrm{L}}(\vec{q}) \right\rangle}_{I} + \underbrace{\left\langle \rho_\epsilon(\vec{q}) | \sum_{i>j} \mathcal{T}_{ij}^{\gamma\gamma} j_\gamma^{\mathrm{L}}(\vec{q}) \right\rangle}_{II} \; . \tag{D.1.10}
$$

The interaction part is seperated into two different summation, one where all the particles are from the same species and a part where the species of the particles differ.

Here, both averages will be calculate:

$$
\left\langle \rho_\epsilon(\vec{q}) | \sum_{\chi \neq \gamma} \sum_i^{N_\chi} \sum_j^{N_\gamma} \mathcal{T}_{ij}^{\chi\gamma} j_\gamma^{\mathrm{L}}(\vec{q}) \right\rangle = \sum_{\chi \neq \gamma} \frac{N_\chi N_\gamma}{2} \left\langle \rho_\epsilon(\vec{q}) | \mathcal{T}_{11}^{\chi\gamma} j_\gamma^{\mathrm{L}}(\vec{q}) \right\rangle \ ,
$$

$$
= \sum_{\chi \neq \gamma} \frac{N_\chi N_\gamma}{2} \left\langle \rho_\epsilon(\vec{q}) | (\hat{r}_{11}^{\chi\gamma} \cdot \vec{v}_{11}^{\chi\gamma}) \Theta(-\hat{r}_{11}^{\chi\gamma} \cdot \vec{v}_{11}^{\chi\gamma}) \delta(\hat{r}_{11}^{\chi\gamma} - d_{11}^{\chi\gamma})(b_{11}^{\chi\gamma} - 1) j_\gamma^{\mathrm{L}}(\vec{q}) \right\rangle \ ,
$$

$$
= \sum_{\chi \neq \gamma} \frac{N_\chi N_\gamma}{N} \frac{m_\chi}{m_\gamma + m_\chi} \frac{1+\epsilon}{2} \hat{q} \left\langle \sum_i \mathrm{e}^{-i\vec{q}\vec{r}_i^\epsilon} | (\hat{r}_{11}^{\chi\gamma} \cdot \vec{v}_{11}^{\chi\gamma})^2 \hat{r}_{11}^{\chi\gamma} \Theta(-\hat{r}_{11}^{\chi\gamma} \cdot \vec{v}_{11}^{\chi\gamma}) \delta(\hat{r}_{11}^{\chi\gamma} - d_{11}^{\chi\gamma}) \mathrm{e}^{i\vec{q}\vec{r}_1^\gamma} \right\rangle \ ,
$$

$$
= \sum_{\chi \neq \gamma} \frac{N_\chi N_\gamma N_\epsilon}{N} \frac{1+\epsilon}{4} \frac{k_{\mathrm{B}}T}{m_\gamma} \hat{q} \left\langle \hat{r}_{11}^{\chi\gamma} \delta(\hat{r}_{11}^{\chi\gamma} - d_{11}^{\chi\gamma}) \mathrm{e}^{i\vec{q}\vec{r}_{11}^{\gamma\epsilon}} \right\rangle \ . \tag{D.1.11}
$$

Here, we use the YBG-Relation for the spatial average and get

$$
\left\langle \rho_\epsilon(\vec{q}) | \sum_{\chi \neq \gamma} \sum_i^{N_\chi} \sum_j^{N_\gamma} \mathcal{T}_{ij}^{\chi\gamma} j_\gamma^{\mathrm{L}}(\vec{q}) \right\rangle =
$$

$$
- \frac{q}{2} \frac{1+\epsilon}{2} \frac{k_{\mathrm{B}}T}{m_\gamma} \left(S_{\gamma\epsilon}(\vec{q}) - x_\gamma \delta_{\gamma\epsilon} \right)
$$

$$
- \frac{N_\gamma N_\epsilon}{2N} \frac{1+\epsilon}{2} \frac{k_{\mathrm{B}}T}{m_\gamma} \hat{q} \left\langle \hat{r}_{11}^{\gamma\epsilon} \delta(\hat{r}_{11}^{\gamma\epsilon} - d) \mathrm{e}^{i\vec{q}\vec{r}_{11}^{\gamma\epsilon}} \right\rangle
$$

$$
+ \frac{N_\gamma^2 N_\epsilon}{2N} \frac{1+\epsilon}{2} \frac{k_{\mathrm{B}}T}{m_\gamma} \hat{q} \left\langle \hat{r}_{12}^{\gamma\gamma} \delta(\hat{r}_{12}^{\gamma\gamma} - d) \mathrm{e}^{i\vec{q}\vec{r}_{11}^{\gamma\epsilon}} \right\rangle \ . \tag{D.1.12}
$$

The calculation of the second part is equal and easier, and it becomes to

$$
\left\langle \rho_\epsilon(\vec{q}) | \sum_{i>j} \mathcal{T}_{ij}^{\gamma\gamma} j_\gamma^{\mathrm{L}}(\vec{q}) \right\rangle =
$$

$$
- \frac{q}{2} \frac{1+\epsilon}{2} \frac{k_{\mathrm{B}}T}{m_\gamma} \left(S_{\gamma\epsilon}(\vec{q}) - x_\gamma \delta_{\gamma\epsilon} \right)
$$

$$
+ \frac{N_\gamma N_\epsilon}{2N} \frac{1+\epsilon}{2} \frac{k_{\mathrm{B}}T}{m_\gamma} \hat{q} \left\langle \hat{r}_{12}^{\epsilon\gamma} \delta(\hat{r}_{12}^{\epsilon\gamma} - d) \mathrm{e}^{i\vec{q}\vec{r}_{12}^{\epsilon\gamma}} \right\rangle
$$

$$
- \frac{N_\gamma^2 N_\epsilon}{2N} \frac{1+\epsilon}{2} \frac{k_{\mathrm{B}}T}{m_\gamma} \hat{q} \left\langle \hat{r}_{12}^{\gamma\gamma} \delta(\hat{r}_{12}^{\gamma\gamma} - d) \mathrm{e}^{i\vec{q}\vec{r}_{11}^{\gamma\epsilon}} \right\rangle \tag{D.1.13}
$$

So the frequency matrix is

$$\langle \rho_\epsilon(\vec{q}) | \mathcal{L} j_\gamma^{\mathrm{L}}(\vec{q}) \rangle = \frac{k_{\mathrm{B}} T}{2 m_\gamma} q \left[(1 - \epsilon) S_{\gamma \epsilon} + (1 + \epsilon) x_\gamma \delta_{\gamma \epsilon} \right] \qquad (\mathrm{D.1.14})$$

After using the normalization and the definition of the triplet correlation function the first average of the vertex is calculated

$$\sum_{\substack{\alpha' \beta', \\ \vec{k}' \vec{p}'}} \sum_{\psi \epsilon} \frac{\delta(\vec{k}' + \vec{p}', \vec{q})}{V} S_{\alpha' \beta' \psi}^{(3)}(\vec{k}', \vec{p}') S_{\psi \epsilon}^{-1}(\vec{q}) \, \langle \rho_\epsilon(\vec{q}) | \mathcal{L} j_\gamma^{\mathrm{L}}(\vec{q}) \rangle \, g_{\alpha' \beta'}^{\alpha \beta}(\vec{k}' \vec{p}', \vec{k} \vec{p}) =$$

$$\frac{\delta(\vec{k} + \vec{p}, \vec{q})}{V} \frac{k_{\mathrm{B}} T}{2 m_\gamma} q \sum_\epsilon \left(\frac{\delta_{\epsilon \alpha} \delta_{\epsilon \beta}}{x_\epsilon^2} - n^2 c_{\epsilon \alpha \beta}^{(3)}(\vec{k} \vec{p}) \right) \left[(1 - \epsilon) S_{\gamma \epsilon} + (1 + \epsilon) x_\gamma \delta_{\gamma \epsilon} \right] . \qquad (\mathrm{D.1.15})$$

Now, we the three particle average, $\sum_{\substack{\alpha' \beta', \\ \vec{k}' \vec{p}'}} \left\langle \rho_{\alpha'}(\vec{k}') \rho_{\beta'}(\vec{p}') | \mathcal{L} j_\gamma^{\mathrm{L}}(\vec{q}) \right\rangle g_{\alpha \beta}^{\alpha' \beta'}(\vec{k}' \vec{p}', \vec{k} \vec{p})$, should be calculate. The free streaming part, $\mathcal{L}_0$ is done fast

$$\left\langle \rho_{\alpha'}(\vec{k}') \rho_{\beta'}(\vec{p}') | \mathcal{L}_0 j_\gamma^{\mathrm{L}}(\vec{q}) \right\rangle = q \frac{k_{\mathrm{B}} T}{m_\gamma} \frac{\delta(\vec{k}' + \vec{p}', \vec{q})}{V} S_{\alpha' \beta' \gamma}^{(3)}(\vec{k}' \vec{p}') . \qquad (\mathrm{D.1.16})$$

For the particle interaction, the interaction operator $\mathcal{T}$ will be divided into two term, one where all particle are from the same species and one where the species of the interacting particles differ. The $\chi \neq \gamma$ part is given by

$$\left\langle \rho_{\alpha'}(\vec{k}') \rho_{\beta'}(\vec{p}') | \sum_{\chi \neq \gamma} \sum_i^{N_\chi} \sum_j^{N_\gamma} \mathcal{T}_{ij}^{\chi \gamma} j_\gamma^{\mathrm{L}}(\vec{q}) \right\rangle =$$

$$\frac{1}{i} \sum_\chi \frac{N_\chi N_\gamma N_{\alpha'} N_{\beta'}}{\sqrt{N} N} \frac{1 + \epsilon}{4} \frac{k_{\mathrm{B}} T}{m_\gamma} \hat{q} \left\langle \mathrm{e}^{-i \vec{k}' \vec{r}_1^{\alpha'}} \mathrm{e}^{-i \vec{p}' \vec{r}_1^{\beta'}} \hat{r}_{11}^{\gamma \chi} \delta(\hat{r}_{11}^{\gamma \chi} - d_{11}^{\gamma \chi}) \mathrm{e}^{i \vec{q} \vec{r}_1^\gamma} \right\rangle \qquad (\mathrm{D.1.17})$$

The spatial average is explicitly given as

$$\left\langle \mathrm{e}^{-i \vec{k}' \vec{r}_1^{\alpha'}} \mathrm{e}^{-i \vec{p}' \vec{r}_1^{\beta'}} \hat{r}_{11}^{\chi \gamma} \delta(\hat{r}_{11}^{\chi \gamma} - d_{11}^{\chi \gamma}) \mathrm{e}^{i \vec{q} \vec{r}_1^\gamma} \right\rangle =$$

$$\frac{1}{V^4} \int \mathrm{d}^3 r_1^\gamma \int \mathrm{d}^3 r_1^{\alpha'} \int \mathrm{d}^3 r_1^{\beta'} \mathrm{e}^{-i \vec{k}' \vec{r}_1^{\alpha'}} \mathrm{e}^{-i \vec{p}' \vec{r}_1^{\beta'}} \left[\int \mathrm{d}^3 r_1^\chi \hat{r}_{11}^{\chi \gamma} \delta(\hat{r}_{11}^{\chi \gamma} - d_{11}^{\chi \gamma}) g_4(\vec{r}_1^\gamma, \vec{r}_1^\chi, \vec{r}_1^{\alpha'}, \vec{r}_1^{\beta'}) \right] \mathrm{e}^{i \vec{q} \vec{r}_1^\gamma} .$$

$$(\mathrm{D.1.18})$$

For the term in the rectangular brackets we use the YBG-relation:

$$\int \mathrm{d}^3 r_1^\chi \hat{r}_{11}^{\chi\gamma} \delta(\hat{r}_{11}^{\chi\gamma} - d_{11}^{\chi\gamma}) g_4(\vec{r}_1^\gamma, \vec{r}_1^\chi, \vec{r}_1^{\alpha'}, \vec{r}_1^{\beta'}) =$$

$$- \left(\hat{r}_{11}^{\gamma\alpha'} \delta(\hat{r}_{11}^{\gamma\alpha'} - d_{11}^{\gamma\alpha'}) + \hat{r}_{11}^{\gamma\beta'} \delta(\hat{r}_{11}^{\gamma\beta'} - d_{11}^{\gamma\beta'}) \right) g_3(\vec{r}_1^\gamma, \vec{r}_1^{\alpha'}, \vec{r}_1^{\beta'})$$

$$+ \nabla_1^\gamma g(\vec{r}_1^\gamma, \vec{r}_1^{\alpha'}, \vec{r}_1^{\beta'}) - n_\gamma \int \mathrm{d}^3 r_2^\gamma \hat{r}_{12}^{\gamma\gamma} \delta(\hat{r}_{12}^{\gamma\gamma} - d_{12}^{\gamma\gamma}) g_4(\vec{r}_1^\gamma, \vec{r}_2^\gamma, \vec{r}_1^{\alpha'}, \vec{r}_1^{\beta'}) \quad \text{(D.1.19)}$$

So put all the terms together and rewerite some of them as spatial averages the term becomes to

$$\left\langle \rho'_\alpha(\vec{k}') \rho'_\beta(\vec{p}') | \sum_{i,j} \sum_{\chi \neq \gamma} \mathcal{T}_{ij}^{\gamma\chi} j_\gamma^{\mathrm{L}}(\vec{q}) \right\rangle =$$

$$\frac{1}{i} \frac{N_\gamma N_{\alpha'} N_{\beta'}}{2\sqrt{N} N} \frac{1+\epsilon}{2} \frac{k_\mathrm{B} T}{m_\gamma} \hat{q} \frac{\delta(\vec{k}' + \vec{p}', \vec{q})}{V^3 \sqrt{N} N} \int \mathrm{d}^3 r_{11}^{\gamma\alpha'} \int \mathrm{d}^3 r_{11}^{\gamma\beta'} e^{i\vec{k}' \vec{r}_{11}^{\gamma\alpha'}} e^{i\vec{p}' \vec{r}_{11}^{\gamma\beta'}} \nabla_1^\gamma g_3(\vec{r}_{11}^{\gamma\alpha'}, \vec{r}_{11}^{\gamma\beta'})$$

$$- \frac{1}{i} \frac{N_\gamma N_{\alpha'} N_{\beta'}}{2\sqrt{N} N} \frac{1+\epsilon}{2} \frac{k_\mathrm{B} T}{m_\gamma} \hat{q} \frac{\delta(\vec{k}' + \vec{p}', \vec{q})}{V^3 \sqrt{N} N} \left\langle e^{i\vec{k}' \vec{r}_{11}^{\gamma\alpha'}} e^{i\vec{p}' \vec{r}_{11}^{\gamma\beta'}} \hat{r}_{11}^{\gamma\alpha'} \delta(\hat{r}_{11}^{\gamma\alpha'} - d_{11}^{\alpha'}) \right\rangle$$

$$- \frac{1}{i} \frac{N_\gamma N_{\alpha'} N_{\beta'}}{2\sqrt{N} N} \frac{1+\epsilon}{2} \frac{k_\mathrm{B} T}{m_\gamma} \hat{q} \frac{\delta(\vec{k}' + \vec{p}', \vec{q})}{V^3 \sqrt{N} N} \left\langle e^{i\vec{k}' \vec{r}_{11}^{\gamma\alpha'}} e^{i\vec{p}' \vec{r}_{11}^{\gamma\beta'}} \hat{r}_{11}^{\gamma\beta'} \delta(\hat{r}_{11}^{\gamma\beta'} - d_{11}^{\gamma\beta'}) \right\rangle$$

$$- \frac{1}{i} \frac{N_\gamma^2 N_{\alpha'} N_{\beta'}}{2\sqrt{N} N} \frac{1+\epsilon}{2} \frac{k_\mathrm{B} T}{m_\gamma} \hat{q} \left\langle e^{-i\vec{k}' \vec{r}_1^{\alpha'}} e^{-i\vec{p}' \vec{r}_1^{\beta'}} \hat{r}_{12}^{\gamma\gamma} \delta(\hat{r}_{12}^{\gamma\gamma} - d_{12}^{\gamma\gamma}) e^{i\vec{q} \vec{r}_1^\gamma} \right\rangle . \quad \text{(D.1.20)}$$

The same story for the $\chi = \gamma$ part

$$\left\langle \rho'_\alpha(\vec{k}') \rho'_\beta(\vec{p}') | \sum_{i>j} \mathcal{T}_{ij}^{\gamma\gamma} j_\gamma^{\mathrm{L}}(\vec{q}) \right\rangle =$$

$$\frac{1}{i} \frac{N_\gamma^2 N_{\alpha'} N_{\beta'}}{2\sqrt{N} N} \frac{1+\epsilon}{2} \frac{k_\mathrm{B} T}{m_\gamma} \hat{q} \frac{\delta(\vec{k}' + \vec{p}', q)}{V N_\gamma N \sqrt{N}} \int \mathrm{d}^3 r_{11}^{\gamma\alpha'} \int \mathrm{d}^3 r_{11}^{\gamma\beta'} e^{i\vec{k}' \vec{r}_{11}^{\gamma\alpha'}} e^{i\vec{p}' \vec{r}_{11}^{\gamma\beta'}} \nabla_1^\gamma g_3(\vec{r}_1^\gamma, \vec{r}_1^{\alpha'}, \vec{r}_1^{\beta'})$$

$$- \frac{1}{i} \frac{N_\gamma^2 N_{\alpha'} N_{\beta'}}{2\sqrt{N} N} \frac{1+\epsilon}{2} \frac{k_\mathrm{B} T}{m_\gamma} \hat{q} \frac{\delta(\vec{k}' + \vec{p}', q)}{V N_\gamma N \sqrt{N}} \left\langle e^{i\vec{k}' \vec{r}_{11}^{\gamma\alpha'}} e^{i\vec{p}' \vec{r}_{11}^{\gamma\beta'}} \hat{r}_{11}^{\gamma\alpha'} \delta(\hat{r}_{11}^{\gamma\alpha'} - d_{11}^{\gamma\alpha'}) \right\rangle$$

$$- \frac{1}{i} \frac{N_\gamma^2 N_{\alpha'} N_{\beta'}}{2\sqrt{N} N} \frac{1+\epsilon}{2} \frac{k_\mathrm{B} T}{m_\gamma} \hat{q} \frac{\delta(\vec{k}' + \vec{p}', q)}{V N_\gamma N \sqrt{N}} \left\langle e^{i\vec{k}' \vec{r}_{11}^{\gamma\alpha'}} e^{i\vec{p}' \vec{r}_{11}^{\gamma\beta'}} \hat{r}_{11}^{\gamma\beta'} \delta(\hat{r}_{11}^{\gamma\beta'} - d_{11}^{\gamma\beta'}) \right\rangle$$

$$+ \frac{1}{i} \frac{N_\gamma^2 N_{\alpha'} N_{\beta'}}{2\sqrt{N} N} \frac{1+\epsilon}{2} \frac{k_\mathrm{B} T}{m_\gamma} \hat{q} \left\langle e^{-i\vec{k}' \vec{r}_1^{\alpha'}} e^{-i\vec{p}' \vec{r}_1^{\beta'}} \hat{r}_{12}^{\gamma\gamma} \delta(\hat{r}_{12}^{\gamma\gamma} - d_{12}^{\gamma\gamma}) e^{i\vec{q} \vec{r}_1^\gamma} \right\rangle . \quad \text{(D.1.21)}$$

So put both terms together we have

$$
\left\langle \rho_\alpha'(\vec{k}')\rho_\beta'(\vec{p}')| \left(\sum_{\chi \neq \gamma}\sum_{i,j} \mathcal{T}_{ij}^{\gamma\chi} + \sum_{i>j} \mathcal{T}_{ij}^{\gamma\gamma} \right) j_\gamma^{\mathrm{L}}(\vec{q}) \right\rangle =
$$

$$
- \frac{\delta(\vec{k}'+\vec{p}',\vec{q})}{V} x_\gamma x_{\alpha'} x_{\beta'} \frac{1+\epsilon}{2} \frac{k_{\mathrm{B}}T}{m_\gamma} (\hat{q}\cdot\vec{q}) \int \mathrm{d}^3 r_{11}^{\gamma\alpha'} \int \mathrm{d}^3 r_{11}^{\gamma\beta'} \mathrm{e}^{i\vec{k}'\vec{r}_{11}^{\gamma\alpha'}} \mathrm{e}^{i\vec{p}'\vec{r}_{11}^{\gamma\beta'}} g_3(\vec{r}_1^\gamma, \vec{r}_1^{\alpha'}, \vec{r}_1^{\beta'})
$$

$$
- \frac{1}{i} \frac{\delta(\vec{k}'+\vec{p}',\vec{q})}{V} x_\gamma x_{\alpha'} x_{\beta'} \frac{1+\epsilon}{2} \frac{k_{\mathrm{B}}T}{m_\gamma} \hat{q} \left\langle \mathrm{e}^{i\vec{k}'\vec{r}_{11}^{\gamma\alpha'}} \mathrm{e}^{i\vec{p}'\vec{r}_{11}^{\gamma\beta'}} \hat{r}_{11}^{\gamma\alpha'} \delta(\hat{r}_{11}^{\gamma\alpha'} - d_{11}^{\alpha'}) \right\rangle
$$

$$
- \frac{1}{i} \frac{\delta(\vec{k}'+\vec{p}',\vec{q})}{V} x_\gamma x_{\alpha'} x_{\beta'} \frac{1+\epsilon}{2} \frac{k_{\mathrm{B}}T}{m_\gamma} \hat{q} \left\langle \mathrm{e}^{i\vec{k}'\vec{r}_{11}^{\gamma\alpha'}} \mathrm{e}^{i\vec{p}'\vec{r}_{11}^{\gamma\beta'}} \hat{r}_{11}^{\gamma\beta'} \delta(\hat{r}_{11}^{\gamma\beta'} - d_{11}^{\beta'}) \right\rangle . \tag{D.1.22}
$$

This calculation was for the case, that the species α', β' and γ are all different. Now, we have to respect all the different possibilities like $\alpha' = \beta' \neq \gamma$. There are 6 different combinations. Since we show the calculation for one case it is not necessary to write down all the other calculations. I will give the result here for sum over all possibilities and after some more YBG-relations

$$
\left\langle \rho_\alpha'(\vec{k}')\rho_\beta'(\vec{p}')| \left(\sum_{\chi \neq \gamma}\sum_{i,j} \mathcal{T}_{ij}^{\gamma\chi} + \sum_{i>j} \mathcal{T}_{ij}^{\gamma\gamma} \right) j_\gamma^{\mathrm{L}}(\vec{q}) \right\rangle = - \frac{\delta(\vec{k}'+\vec{p}',\vec{q})}{V} \frac{1+\epsilon}{2} \frac{k_{\mathrm{B}}T}{m_\gamma} \left[q S_{\gamma\alpha'\beta'}^{(3)} \right.
$$

$$
- i x_\gamma x_{\alpha'} x_{\beta'} \hat{q} \frac{1}{V^3} \int \mathrm{d}^3 r_1^\gamma \int \mathrm{d}^3 r_1^{\alpha'} \int \mathrm{d}^3 r_1^{\beta'} \mathrm{e}^{i\vec{k}'\vec{r}_{11}^{\gamma\alpha'}} \mathrm{e}^{i\vec{p}'\vec{r}_{11}^{\gamma\beta'}} \nabla_1^\gamma g_3(\vec{r}_1^\gamma, \vec{r}_1^{\alpha'}, \vec{r}_1^{\beta'})
$$

$$
- i \frac{x_\gamma^2 x_\alpha}{2} \hat{q} \frac{1}{V^3} \int \mathrm{d}^3 r_1^\gamma \int \mathrm{d}^3 r_2^\gamma \int \mathrm{d}^3 r_1^{\alpha'} \mathrm{e}^{i\vec{k}'\vec{r}_{11}^{\gamma\alpha'}} \mathrm{e}^{i\vec{p}'\vec{r}_{12}^{\gamma\gamma}} \nabla_1^\gamma g_3(\vec{r}_1^\gamma, \vec{r}_2^\gamma, \vec{r}_1^{\alpha'})
$$

$$
- i \frac{x_\gamma^2 x_\beta}{2} \hat{q} \frac{1}{V^3} \int \mathrm{d}^3 r_1^\gamma \int \mathrm{d}^3 r_2^\gamma \int \mathrm{d}^3 r_1^{\beta'} \mathrm{e}^{i\vec{k}'\vec{r}_{12}^{\gamma\gamma}} \mathrm{e}^{i\vec{p}'\vec{r}_{11}^{\gamma\beta'}} \nabla_1^\gamma g_3(\vec{r}_1^\gamma, \vec{r}_2^\gamma, \vec{r}_1^{\beta'})
$$

$$
- 2i\hat{q} \frac{x_\gamma x_{\alpha'}^2}{2} \frac{1}{V^2} \int \mathrm{d}^3 r_1^\gamma \int \mathrm{d}^3 r_1^{\alpha'} \mathrm{e}^{i\vec{q}\vec{r}_{11}^{\gamma\alpha'}} \nabla_1^\gamma(\vec{r}_1^\gamma, \vec{r}_1^{\alpha'})
$$

$$
- 2i\hat{q} \frac{x_\gamma}{6} \frac{1}{V^2} \int \mathrm{d}^3 r_1^\gamma \int \mathrm{d}^3 r_2^\gamma \mathrm{e}^{i\vec{q}\vec{r}_{12}^{\gamma\gamma}} \nabla_1^\gamma(\vec{r}_1^\gamma, \vec{r}_2^\gamma) . \tag{D.1.23}
$$

In the next step a expression for the triplet correlation function $S^{(3)}_{\alpha\beta\gamma}(\vec{k},\vec{p})$ should be derived:

$$S^{(3)}_{\alpha\beta\gamma}(\vec{k},\vec{p}) = \langle \rho_\alpha(\vec{q}) | \rho_\beta(\vec{k}) \rho_\gamma(\vec{p}) \rangle = \frac{1}{V^3} \frac{1}{N\sqrt{N}} \sum_{l,m,n} \int \mathrm{d}^3 r_l^\alpha \int \mathrm{d}^3 r_m^\beta \int \mathrm{d}^3 r_n^\gamma \mathrm{e}^{-i\vec{q}\vec{r}_l^\alpha} \mathrm{e}^{i\vec{k}\vec{r}_m^\beta} \mathrm{e}^{i\vec{p}\vec{r}_n^\gamma} g_3(\vec{r}_l^\alpha, \vec{r}_m^\beta, \vec{r}_n^\gamma)$$

$$= \frac{1}{V^3} \frac{1}{N\sqrt{N}} \sum_{l,m,n} \int \mathrm{d}^3 r_l^\alpha \int \mathrm{d}^3 r_m^\beta \int \mathrm{d}^3 r_n^\gamma \mathrm{e}^{-i\vec{q}\vec{r}_l^\alpha} \mathrm{e}^{i\vec{k}\vec{r}_l^\alpha} \mathrm{e}^{-i\vec{k}\vec{r}_l^\alpha} \mathrm{e}^{i\vec{k}\vec{r}_m^\beta} \mathrm{e}^{-i\vec{p}\vec{r}_l^\alpha} \mathrm{e}^{-i\vec{p}\vec{r}_l^\alpha} \mathrm{e}^{i\vec{p}\vec{r}_n^\gamma} g_3(\vec{r}_l^\alpha, \vec{r}_m^\beta, \vec{r}_n^\gamma)$$

$$= \frac{1}{V^3} \frac{1}{N\sqrt{N}} \sum_{l,m,n} \int \mathrm{d}^3 r_l^\alpha \int \mathrm{d}^3 r_m^\beta \int \mathrm{d}^3 r_n^\gamma \mathrm{e}^{i(\vec{k}+\vec{p}-\vec{q})\vec{r}_l^\alpha} \mathrm{e}^{-i\vec{k}\vec{r}_{lm}^{\alpha\beta}} \mathrm{e}^{-i\vec{p}\vec{r}_{ln}^{\alpha\gamma}} g_3(\vec{r}_l^\alpha, \vec{r}_m^\beta, \vec{r}_n^\gamma)$$

$$= \frac{1}{V^2} \frac{\delta(\vec{k}+\vec{p},\vec{q})}{N^3} \sum_{l,m,n} \int \mathrm{d}^3 r_{lm}^{\alpha\beta} \int \mathrm{d}^3 r_{ln}^{\alpha\gamma} \mathrm{e}^{-i\vec{k}\vec{r}_{lm}^{\alpha\beta}} \mathrm{e}^{-i\vec{p}\vec{r}_{ln}^{\alpha\gamma}} g_3(\vec{r}_{lm}^{\alpha\beta}, \vec{r}_{ln}^{\alpha\gamma}) \qquad (D.1.24)$$

After respecting all the combinations of l, m and n we get

$$S^{(3)}_{\alpha\beta\gamma}(\vec{k},\vec{p}) =$$

$$= \frac{\delta(\vec{k}+\vec{p},\vec{q})}{V^2} x_\alpha x_\beta x_\gamma \int \mathrm{d}^3 r_{11}^{\alpha\beta} \int \mathrm{d}^3 r_{11}^{\alpha\gamma} \mathrm{e}^{-i\vec{k}\vec{r}_{11}^{\alpha\beta}} \mathrm{e}^{-i\vec{p}\vec{r}_{11}^{\alpha\gamma}} g_3(\vec{r}_{11}^{\alpha\beta}, \vec{r}_{11}^{\alpha\gamma})(1-\delta_{\alpha\beta})(1-\delta_{\alpha\gamma})(1-\delta_{\beta\gamma})$$

$$+ \frac{\delta(\vec{k}+\vec{p},\vec{q})}{V} \left(S_{\alpha\gamma}(\vec{p}) - x_\alpha \delta_{\alpha\gamma} \right) \delta_{\alpha\beta}(1-\delta_{\alpha\gamma})$$

$$+ \frac{\delta(\vec{k}+\vec{p},\vec{q})}{V^2} \frac{x_\alpha^2 x_\gamma}{2} \int \mathrm{d}^3 r_{12}^{\alpha\alpha} \int \mathrm{d}^3 r_{11}^{\alpha\gamma} \mathrm{e}^{-i\vec{k}\vec{r}_{12}^{\alpha\alpha}} \mathrm{e}^{-i\vec{p}\vec{r}_{11}^{\alpha\gamma}} g_3(\vec{r}_{12}^{\alpha\alpha}, \vec{r}_{11}^{\alpha\gamma}) \delta_{\alpha\beta}(1-\delta_{\alpha\gamma})$$

$$+ \frac{\delta(\vec{k}+\vec{p},\vec{q})}{V} \left(S_{\alpha\beta}(\vec{k}) - x_\alpha \delta_{\alpha\beta} \right) \delta_{\alpha\gamma}(1-\delta_{\alpha\beta})$$

$$+ \frac{\delta(\vec{k}+\vec{p},\vec{q})}{V^2} \frac{x_\alpha^2 x_\beta}{2} \int \mathrm{d}^3 r_{11}^{\alpha\beta} \int \mathrm{d}^3 r_{12}^{\alpha\alpha} \mathrm{e}^{-i\vec{k}\vec{r}_{11}^{\alpha\beta}} \mathrm{e}^{-i\vec{p}\vec{r}_{12}^{\alpha\alpha}} g_3(\vec{r}_{11}^{\alpha\beta}, \vec{r}_{12}^{\alpha\alpha}) \delta_{\alpha\gamma}(1-\delta_{\alpha\beta})$$

$$+ \frac{\delta(\vec{k}+\vec{p},\vec{q})}{V^2} \frac{x_\alpha x_\beta^2}{2} \int \mathrm{d}^3 r_{11}^{\alpha\beta} \mathrm{e}^{-i\vec{q}\vec{r}_{11}^{\alpha\beta}} g(\vec{r}_{11}^{\alpha\beta}) \delta_{\beta\gamma}(1-\delta_{\beta\alpha})$$

$$+ \frac{\delta(\vec{k}+\vec{p},\vec{q})}{V^2} \frac{x_\alpha^3}{6} \int \mathrm{d}^3 r_{12}^{\alpha\alpha} \mathrm{e}^{-i\vec{q}\vec{r}_{12}^{\alpha\alpha}} g(\vec{r}_{12}^{\alpha\alpha}) \delta_{\alpha\beta} \delta_{\alpha\gamma} \qquad (D.1.25)$$

Now, rewriting all the ∇g_3-terms with the $S^{(3)}$, the interacting part simplifies to

$$\left\langle \rho_\alpha'(\vec{k}')\rho_\beta'(\vec{p}') \middle| \left(\sum_{\chi \neq \gamma} \sum_{i,j} \mathcal{T}_{ij}^{\gamma\chi} + \sum_{i>j} \mathcal{T}_{ij}^{\gamma\gamma} \right) j_\gamma^{\mathrm{L}}(\vec{q}) \right\rangle =$$

$$-\frac{\delta(\vec{k}'+\vec{p}',\vec{q})}{V} \frac{1+\epsilon}{2} \frac{k_{\mathrm{B}}T}{m_\gamma} \left[q S_{\gamma\alpha'\beta'}^{(3)} - (\hat{q}\cdot\vec{p}')\delta_{\gamma\beta'}S_{\gamma\alpha'}(\vec{k}') - (\hat{q}\cdot\vec{k}')\delta_{\gamma\alpha'}S_{\gamma\beta'}(\vec{p}') \right] \ .$$

(D.1.26)

The triple particle average is

$$\sum_{\substack{\alpha'\beta', \\ \vec{k}'\vec{p}'}} \left\langle \rho_{\alpha'}(\vec{k}')\rho_{\beta'}(\vec{p}') \middle| \mathcal{L} j_\gamma^{\mathrm{L}}(\vec{q}) \right\rangle =$$

$$\sum_{\substack{\alpha'\beta', \\ \vec{k}'\vec{p}'}} \frac{k_{\mathrm{B}}T}{m_\gamma} \frac{\delta(\vec{k}'+\vec{p}',\vec{q})}{V} \left[\frac{1+\epsilon}{2} \left((\hat{q}\cdot\vec{p}')\delta_{\gamma\beta'}S_{\gamma\alpha'}(\vec{k}') + (\hat{q}\cdot\vec{k}')\delta_{\gamma\alpha'}S_{\gamma\beta'}(\vec{p}')) \right) + \frac{1-\epsilon}{2} q S_{\alpha'\beta'\gamma}^{(3)}(\vec{k}'\vec{p}') \right] \ .$$

(D.1.27)

In the end with the use of the normalization, the convolution approximation for $S^{(3)}$ and the direct correlation function for the structure factors we get the right vertex

$$\mathcal{W}_{\alpha\beta\gamma} = -\frac{\delta(\vec{k}+\vec{p},\vec{q})}{V} \frac{k_{\mathrm{B}}T}{m_\gamma} n \frac{1+\epsilon}{2} \left[(\hat{q}\cdot\vec{k})\delta_{\gamma\beta}c_{\gamma\alpha}(\vec{k}) + (\hat{q}\cdot\vec{p})\delta_{\gamma\alpha}c_{\gamma\beta}(\vec{p}) + qnx_\gamma c_{\gamma\alpha\beta}^{(3)}(\vec{k},\vec{p}) \right] \ .$$

(D.1.28)

We have the following relation between both vertices:

$$\mathcal{W}_{\alpha\beta\gamma} = \frac{1+\epsilon}{2} \mathcal{V}_{\alpha\beta\gamma}$$

(D.1.29)

E YBG-Relation

The pair correlation function $g(\vec{r})$ for binary systems is defined as:

$$\frac{g(r_1^{\alpha_1}, r_2^{\alpha_2})}{V^2} = \frac{1}{Z_N} \int d^3 r_2^{\alpha_1} .... \int d^3 r_{N_{\alpha_1}}^{\alpha_1} \int d^3 r_1^{\alpha_2} \int d^3 r_3^{\alpha_2} .... \int d^3 r_{N_{\alpha_2}}^{\alpha_2}$$

$$\prod_{i>2} \int d^3 r_1^{\alpha_i} .... d^3 r_{N_{\alpha_i}}^{\alpha_i} \exp\left[-\beta \sum_{\substack{i<j \\ k,l}} U(r_{ij}^{\alpha_k \alpha_l}) - \beta \sum_{\substack{i=j \\ k \neq l}} U(r_{ij}^{\alpha_k \alpha_l})\right].$$

(E.1.1)

with the potential U, the inverse temperature β and the partition function Z. Rewrite $g(\vec{r})$ and look at the derivative with respect to $r_1^{\alpha_1}$:

$$\nabla_1^{\alpha_1} g(r_1^{\alpha_1}, r_2^{\alpha_2}) = -\beta \frac{V^2}{Z_N} \int d^3 r_2^{\alpha_1} .... \int d^3 r_{N_{\alpha_1}}^{\alpha_1} \int d^3 r_1^{\alpha_2} \int d^3 r_3^{\alpha_2} .... \int d^3 r_{N_{\alpha_2}}^{\alpha_2} \prod_{i>2} \int d^3 r_1^{\alpha_i} .... d^3 r_{N_{\alpha_i}}^{\alpha_i}$$

$$\left[\sum_{\substack{1<i \\ l}} \nabla^{\alpha_1} U(r_{1i}^{\alpha_1 \alpha_l}) + \sum_{\substack{i=1 \\ l>1}} \nabla^{\alpha_1} U(r_{1i}^{\alpha_1 \alpha_l})\right] \exp\left[-\beta \sum_{\substack{i<j \\ k,l}} U(r_{ij}^{\alpha_k \alpha_l}) - \beta \sum_{\substack{i=j \\ k \neq l}} U(r_{ij}^{\alpha_k \alpha_l})\right]$$

$$= -\beta \frac{V^2}{Z_N} \int d^3 r_2^{\alpha_1} .... \int d^3 r_{N_{\alpha_1}}^{\alpha_1} \int d^3 r_1^{\alpha_2} \int d^3 r_3^{\alpha_2} .... \int d^3 r_{N_{\alpha_2}}^{\alpha_2} \prod_{i>2} \int d^3 r_1^{\alpha_i} .... d^3 r_{N_{\alpha_i}}^{\alpha_i}$$

$$\left[\nabla U(r_{12}^{\alpha_1 \alpha_2}) + \sum_{\substack{2<i \\ l}} \nabla U(r_{1i}^{\alpha_1 \alpha_l}) + \sum_{\substack{i=2 \\ l \neq 2}} \nabla U(r_{1i}^{\alpha_1 \alpha_l}) + \sum_{\substack{i=1 \\ l>2}} \nabla U(r_{1i}^{\alpha_1 \alpha_l})\right] \exp\left[-\beta \sum_{\Gamma} U(r_{ij}^{\alpha_k \alpha_l})\right]$$

(E.1.2)

Now we simplify the expression with the use of the special canonical distribution function

$$\nabla_1^{\alpha_1} g(r_1^{\alpha_1}, r_2^{\alpha_2}) = -\beta \left[\nabla_1^{\alpha_1} U(r_{12}^{\alpha_1 \alpha_2})\right] g(r_1^{\alpha_1}, r_2^{\alpha_2}) - \beta n_{\alpha_3} \int d^3 r_3^{\alpha_3} \nabla U(r_{13}^{\alpha_1 \alpha_3}) g_3(r_1^{\alpha_1}, r_2^{\alpha_2}, r_3^{\alpha_3})$$

$$- \beta \sum_{i \neq 3} n_{\alpha_i} \int d^3 r_3^{\alpha_i} \nabla U(r_{13}^{\alpha_1 \alpha_i}) g_3(r_1^{\alpha_1}, r_2^{\alpha_2}, r_3^{\alpha_i})$$

(E.1.3)

with $n_{\alpha_i} = N_{\alpha_i}/V$.

F   Velocity Integration of Binary Mixture

$$\langle (\hat{r}_{12} \cdot \vec{v}_{12})^2 \, \Theta(-\hat{r}_{12} \cdot \vec{v}_{12}) \rangle =$$

$$\left(\frac{m_\gamma}{2\pi k_B T_\gamma} \right)^{\frac{3}{2}} \left(\frac{m_\chi}{2\pi k_B T_\chi} \right)^{\frac{3}{2}} \int d^3 v_1 \int d^3 v_2 (\hat{r}_{12} \cdot \vec{v}_{12})^2 \, \Theta(-\hat{r}_{12} \cdot \vec{v}_{12}) e^{-\frac{m_\gamma v_1^2}{2k_B T_\gamma}} e^{-\frac{m_\chi v_2^2}{2k_B T_\chi}}$$

$$\text{(F.1.1)}$$

Substitute the variables:

$$v_{12} = \frac{v_1 - v_2}{\sqrt{2}} \quad \text{and} \quad V = \frac{v_1 + v_2}{\sqrt{2}}$$

$$dv_1 = \sqrt{2} dv_{12} \quad \text{and} \quad dv_2 = \sqrt{2} dV$$

with $\mathcal{N}_i = \left(\frac{m_i}{2\pi k_B T_i} \right)^{\frac{3}{2}}$ the normalization we get

$$= 2\mathcal{N}_\gamma \mathcal{N}_\chi \int d^3 v_{12} \int d^3 V (\hat{r}_{12} \cdot \vec{v}_{12})^2 \, \Theta(-\hat{r}_{12} \cdot \vec{v}_{12}) \exp\left\{ -\frac{1}{4k_B} \left(\frac{m_\gamma}{T_\gamma}(v_{12} + V)^2 + \frac{m_\chi}{T_\chi}(v_{12} - V)^2 \right) \right\} =$$

$$2\mathcal{N}_\gamma \mathcal{N}_\chi \int_0^{2\pi} d\phi_{v_{12}} \int_0^\pi d\vartheta_{v_{12}} \int_0^\infty dv_{12} \int_0^{2\pi} d\phi_V \int_0^\pi d\vartheta_V \int_0^\infty dV \, v_{12}^2 \sin\vartheta_{v_{12}} V^2 \sin\vartheta_V$$

$$|\hat{r}_{12}|^2 |v_{12}|^2 \cos^2\vartheta_{v_{12}} \Theta(-|\hat{r}_{12}||v_{12}|\cos\vartheta_{v_{12}}) \exp\left\{ -\frac{v_{12}^2}{4k_B} \left(\frac{m_\gamma}{T_\gamma} + \frac{m_\chi}{T_\chi} \right) \right\} \exp\left\{ -\frac{V^2}{4k_B} \left(\frac{m_\gamma}{T_\gamma} + \frac{m_\chi}{T_\chi} \right) \right\}$$

$$\text{(F.1.2)}$$

$$\exp\left\{ -\frac{|\vec{V}||\vec{v}_{12}|\cos\vartheta_V}{2k_B} \left(\frac{m_\gamma}{T_\gamma} - \frac{m_\chi}{T_\chi} \right) \right\}$$

$$= \frac{8\pi^2}{3} \mathcal{N}_\gamma \mathcal{N}_\chi \int_0^\infty dv_{12} \int_0^\pi d\vartheta_V \int_0^\infty dV \, v_{12}^4 V^2 \sin\vartheta_V$$

$$\exp\left\{ -\frac{v_{12}^2}{4k_B} \left(\frac{m_\gamma}{T_\gamma} + \frac{m_\chi}{T_\chi} \right) \right\} \exp\left\{ -\frac{V^2}{4k_B} \left(\frac{m_\gamma}{T_\gamma} + \frac{m_\chi}{T_\chi} \right) \right\} \exp\left\{ -\frac{V v_{12} \cos\vartheta_V}{2k_B} \left(\frac{m_\gamma}{T_\gamma} - \frac{m_\chi}{T_\chi} \right) \right\}$$

$$= \frac{k_B}{2} * \frac{\left(\frac{m_\gamma}{T_\gamma} \right)^{\frac{3}{2}} \left(\frac{m_\chi}{T_\chi} \right)^{\frac{3}{2}}}{\left(\frac{m_\gamma T_\chi + m_\chi T_\gamma}{T_\gamma T_\chi} \right)^{\frac{3}{2}} \left(\frac{m_\gamma m_\chi}{m_\gamma T_\chi + m_\chi T_\gamma} \right)^{\frac{5}{2}}} = \frac{k_B}{2} \frac{m_\gamma T_\chi + m_\chi T_\gamma}{m_\gamma m_\chi}$$

$$= \frac{k_B T}{m} \quad \text{for } m_\gamma = m_\chi = m \text{ and } T_\gamma = T_\chi = T$$

$$\text{(F.1.3)}$$

G Frequency Ω of the Spin Model

Here, the analytical calculation of the frequency Ω will be represent. We start with the definition in eq. 4.3.11

$$
\begin{aligned}
\Omega &= - \langle \eta_{\sigma_i}(0)|\hat{H}|\eta_{\sigma_i}(0)\rangle = \langle \eta_{\sigma_i}(0)|P_{\text{eq}}^{-1/2}(\{\sigma\}_\alpha)\underline{\Omega}P_{\text{eq}}^{1/2}(\{\sigma\}_\alpha)|\eta_{\sigma_i}(0)\rangle \ , \\
&= - \sum_\alpha \langle \eta_{\sigma_i}(0)|P_{\text{eq}}^{-1/2}(\{\sigma\}_\alpha)(\hat{S}_\alpha - 1)\omega(\{\sigma\}_\alpha)P_{\text{eq}}^{1/2}(\{\sigma\}_\alpha)|\eta_{\sigma_i}(0)\rangle \ , \\
&= - \underbrace{\langle \eta_{\sigma_i}(0)|P_{\text{eq}}^{-1/2}(\{\sigma\})\omega(\{-\sigma\})P_{\text{eq}}^{1/2}(\{-\sigma\})|\eta_{-\sigma_i}(0)\rangle}_{\text{parity}\to 0} + \sum_\alpha \langle \eta_{\sigma_i}(0)|\omega(\{\sigma\}_\alpha)|\eta_{\sigma_i}(0)\rangle \ , \\
&= \sum_\alpha \frac{\omega_0}{N}\delta_{1,\sigma_\alpha}\left[1 - \langle \Theta^{k,f}(x)\rangle\right] \ , \\
&= \omega_0 p\left[1 - \langle \Theta^{k,f}(x)\rangle\right] \ .
\end{aligned}
\tag{G.1.1}
$$

The average of the theta function is given as

$$
\begin{aligned}
\left\langle \Theta\left(\sum_{j\in\mathcal{K}} n_j(0) - k + f - 1\right)\right\rangle &= \frac{\sum_{M_1=0,1}\cdots\sum_{M_K=0,1}\Theta\left(\sum_{j\in\mathcal{K}} n_j(0) - k + f - 1\right)e^{-\beta\sum_\alpha n_\alpha}}{\sum_{M_1=0,1}\cdots\sum_{M_N=0,1}e^{-\beta\sum_\alpha n_\alpha}} \ , \\
&= \frac{\sum_{i=0}^{f-1}\binom{k}{i}e^{-(k-i)\beta}}{(1 + e^{-\beta})^k}
\end{aligned}
\tag{G.1.2}
$$

so

$$
\Omega = \omega_0 p\left(1 - \frac{\sum_{i=0}^{f-1}\binom{k}{i}e^{-(k-i)\beta}}{(1 + e^{-\beta})^k}\right) \ .
\tag{G.1.3}
$$

For $k = 3$ and $f = 2$ we have:

$$
\left\langle \Theta\left(\sum_{j\in\mathcal{K}} n_j(0) - k + f - 1\right)\right\rangle = \frac{e^{-3\beta} + 3e^{-2\beta}}{(1 + e^{-\beta})^3}
\tag{G.1.4}
$$

and

$$
\Omega = \omega_0 p\left(1 - \frac{e^{-3\beta} + 3e^{-2\beta}}{(1 + e^{-\beta})^3}\right) \ .
\tag{G.1.5}
$$

H   Different path for data fitting

In this appendix I want to show the data fit of the different paths in the F_{12}-model which can be seen in Fig. 7.5.1.

As a comparison I put the same figure as in chapter 7, here the first Fig. H.1.1. The perpendicular path, $v_2 = v_2^c$ and v_1 varies is in Fig. H.1.2. In the respective inserts the different paths are shown
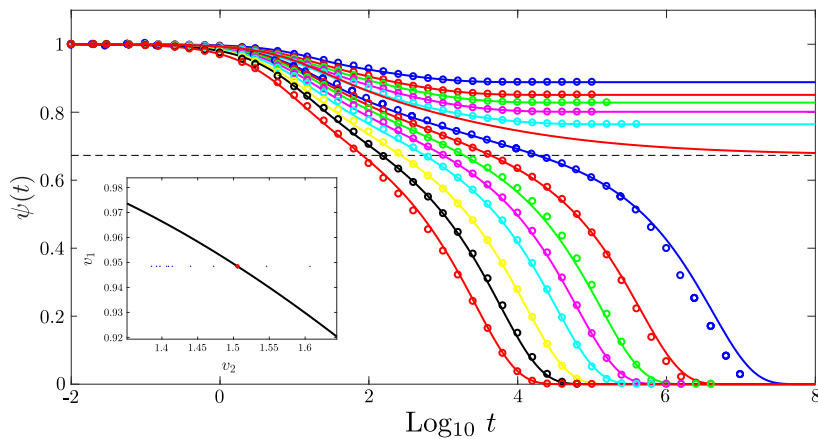
Figure H.1.1: Fitting the simulation data for $v_1 = v_1^c$
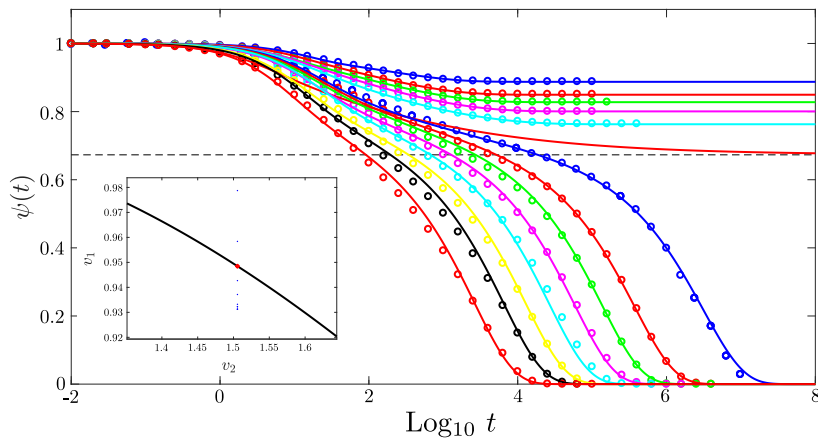
Figure H.1.2: Fitting the simulation data for $v_2 = v_2^c$

In the upcoming figures, Fig. H.1.3 and Fig H.1.4, I express one of the control parameter as a function of the other one, $v_1 = \alpha v_2$, where α is the slope of the line.   For all the
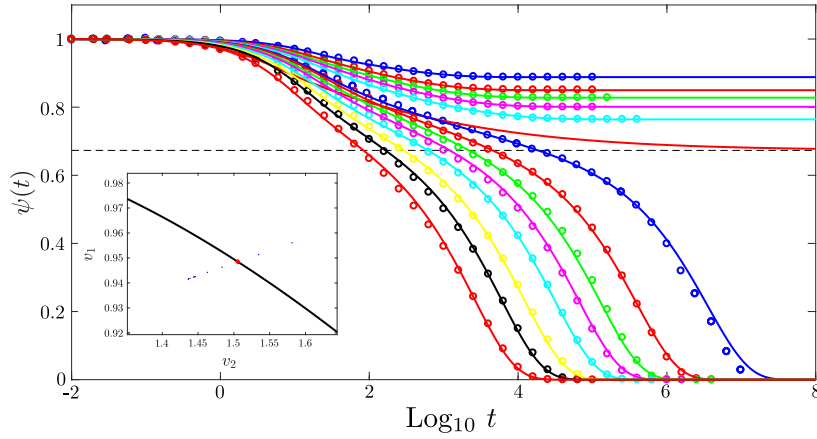
Figure H.1.3: Fitting the simulation data for $\alpha = 0.1$
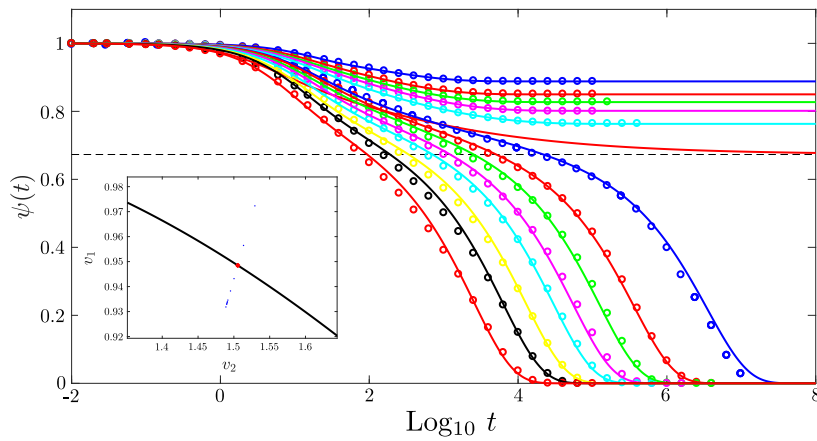
Figure H.1.4: Fitting the simulation data for $\alpha = 1$

paths we used the fitted exponent parameter, $\lambda_S = 0.815$, and one can see that the simulation data are in a good agreement with the schematic model.

List of Figures

Danksagung

Eidesstattliche Versicherung

Ich versichere, dass ich die von mir vorgelegte Dissertation selbstständig angefertigt, die benutzten Quellen und Hilfsmittel vollständig angegeben und die Stellen der Arbeit – einschließlich Tabellen, Karten und Abbildungen –, die anderen Werken im Wortlaut oder dem Sinn nach entnommen sind, in jedem Einzelfall als Entlehnung kenntlich gemacht habe; dass diese Dissertation noch keiner anderen Fakultät oder Universität zur Prüfung vorgelegen hat; dass sie – abgesehen von unten angegebenen Teilpublikationen – noch nicht veröffentlicht worden ist sowie, dass ich eine solche Veröffentlichung vor Abschluss des Promotionsverfahrens nicht vornehmen werde.

Die Bestimmungen dieser Promotionsordnung sind mir bekannt. Die von mir vorgelegte Dissertation ist von Prof. Dr. Matthias Sperl betreut worden.

☒   Teilpublikationen liegen nicht vor.
☐   Nachfolgend genannte Teilpublikationen liegen vor:

Promotionsbeginn: 01.Juli 2016
(Beginn der praktischen Arbeit)

Promotionsende:
(Monat der mündlichen Prüfung)   September 2019

Ich versichere, dass ich alle Angaben wahrheitsgemäß nach bestem Wissen und Gewissen gemacht habe und verpflichte mich, jedmögliche, die obigen Angaben betreffenden Veränderungen, dem Dekanat unverzüglich mitzuteilen.

_____   _____
Datum   Unterschrift

Lebenslauf

Persönliche Daten

Name	Koray Önder
Geburtsdatum	29. April 1991
Geburtsort	49393 Lohne
Staatsbürgerschaft	Deutsch

Ausbildung

07/2016 – heute	**Promotion in der Physik (Dr. rer. nat.)**, Universität zu Köln, Promotionsschwerpunkt: Theoretische- und statistische Festkörperphysik. Tag der mündlichen Prüfung: 20.09.2019
09/2014 – 04/2016	**Studium der Physik (Master of Science)**, Technische Universität Dortmund, Studienschwerpunkte: Theoretische Festkörperphysik. **Abschluss:** Master of Science
10/2011 – 09/2014	**Studium der Physik (Bachelor of Science)**, Technische Universität Dortmund, Studienschwerpunkte: Oberflächenanalyse mit Hilfe von Röntgenstrahlung. **Abschluss:** Bachelor of Science
07/2011	**Abitur**, Gymnasium Lohne.

Berufspraktische Erfahrungen

2013 –2016	**Studentische Hilfskraft**, *TU Dortmund*, Betreuung von Studierenden in Übungsgruppen der Fakultät Physik.

Sprachen

Türkisch	Muttersprache
Deutsch	Zweitsprache
Englisch	gute Kenntnisse
Latein	Grundkenntnisse